Isolation, Purification and Characterization of Photosynthetic Membrane Proteins from *Galdieria sulphuraria* and *Chlamydomonas reinhardtii*

by

Balakumar Thangaraj

A Dissertation Presented in Partial Fulfillment
of the Requirements for the Degree
Doctor of Philosophy

Approved November 2010 by the
Graduate Supervisory Committee:

Petra Fromme, Chair
Everett Shock
Julian Chen

ARIZONA STATE UNIVERSITY

December 2010

ABSTRACT

In oxygenic photosynthesis, Photosystem I (PSI) and Photosystem II (PSII) are two transmembrane protein complexes that catalyze the main step of energy conversion; the light induced charge separation that drives an electron transfer reaction across the thylakoid membrane. Current knowledge of the structure of PSI and PSII is based on three structures: PSI and PSII from the thermophilic cyanobacterium *Thermosynechococcus elonagatus* and the PSI/light harvesting complex I (PSI-LHCI) of the plant, *Pisum sativum*. To improve the knowledge of these important membrane protein complexes from a wider spectrum of photosynthetic organisms, photosynthetic apparatus of the thermo-acidophilic red alga, *Galdieria sulphuraria* and the green alga, *Chlamydomonas reinhardtii* were studied.

Galdieria sulphuraria grows in extreme habitats such as hot sulfur springs with pH values from 0 to 4 and temperatures up to 56°C. In this study, both membrane protein complexes, PSI and PSII were isolated from this organism and characterized. Ultra-fast fluorescence spectroscopy and electron microscopy studies of PSI-LHCI supercomplexes illustrate how this organism has adapted to low light environmental conditions by tightly coupling PSI and LHC, which have not been observed in any organism so far. This result highlights the importance of structure-function relationships in different ecosystems. *Galdieria sulphuraria* PSII was used as a model protein to show the amenability of integral membrane proteins to top-down mass spectrometry. *G.sulphuraria* PSII has been characterized with unprecedented detail with identification of post translational

modification of all the PSII subunits. This study is a technology advancement paving the way for the usage of top-down mass spectrometry for characterization of other large integral membrane proteins.

The green alga, *Chlamydomonas reinhardtii* is widely used as a model for eukaryotic photosynthesis and results from this organism can be extrapolated to other eukaryotes, especially agricultural crops. Structural and functional studies on the PSI-LHCI complex of *C.reinhardtii* grown under high salt conditions were studied using ultra-fast fluorescence spectroscopy, circular dichroism and MALDI-TOF. Results revealed that pigment-pigment interactions in light harvesting complexes are disrupted and the acceptor side (ferredoxin docking side) is damaged under high salt conditions.

To my beloved parents, Saroja and Thanagaraj
To my lovable and supportive wife Kaviya

ACKNOWLEDGEMENTS

This work would not have been possible without the assistance of a number of people at Arizona State University and elsewhere. I would like to express my gratitude to all those who assisted and supported me during my doctoral studies. First and foremost, I would like to thank my advisor, Dr. Petra Fromme for the opportunity to conduct my doctorial study under her, for the encouragement, guidance, understanding, patience and support she has given, and for freely sharing her knowledge and wisdom with me. Her mentorship was paramount in providing me a well rounded experience consistent with my long-term career goals. She encouraged me to not only grow as an experimentalist but also as an independent thinker. She has been a great mentor and above all, a great human being.

To my committee members, Drs. Everett Shock and Julian Chen, for their advice, knowledge, expertise and approval of this document.

To Dr. Raimund Fromme, for knowledge sharing and it's great fun to work with.

To Dr. Ingo Grotjohann, for always so accessible and provide guidance.

To Drs. Rajagopal Subramanyam, Devendra Chauhan and Christopher Vanselow for their advice, colloboration and friendship.

To the entire Fromme group, for the camaraderie, support, help and the environment.

To Dr. Craig Jolley, Dr. Iosifina Sarrou and Mike Vaughn, for their scientific knowledge, help and support.

To Dr. Julian Whitelegge, for his support, mentiorship, advice and encouragement.

To National Institutes of Health, for financial support (NIH 01 GM71619-01) of this work.

TABLE OF CONTENTS

Page

LIST OF TABLES

LIST OF FIGURES

LIST OF ABBREVIATIONS

Å	Angstrom
Abs	Absorbance
ADP	Adenosine diphosphate
Arabidopsis	Arabidopsis thaliana
ATP	Adenosine triphosphate
AU	Absorbance units
β-DDM	n-dodecyl-β-D-maltoside
BLAST	Basic Local Alignment and Search Tool
Car	Carotenoid
CAD	Collision activated dissociation
CD	Circular dichroism
Chlamydomonas	*Chlamydomonas reinhardtii*
Cyt b_6f	Cytochrome b_6f
Cyt c_6	Cytochrome c_6
Da	Dalton
DOLOP	Database of bacterial lipoproteins
ECD	Electron capture dissociation
EM	Electron microscopy
ETC	Electron transfer chain
ETD	Electron transfer dissociation
ExPASy	Expert protein analysis system
F_A	Iron sulfur cluster A

F_b	Iron sulfur cluster B
F_X	Iron sulfur cluster X
FDAS	Fluorescence decay associated spectra
FNR	Ferredoxin: $NADP^+$ reductase
FPLC	Fast performance liquid chromatography
FT-ICR	Fourier transform ion cyclotron resonance
FT-MS	Fourier transform mass spectrometry
Galdieria	*Galdieria sulphuraria*
HCD	High energy colliosional dissociation
HEPES	4-(2-hydroxyethyl)-1-piperazineethanesulfonic acid
HPLC	High performance liquid chromatography
hν	Light
IMT	Intact mass tags
IsiA	Iron stress induced A protein
kDa	Kilodalton
LC-MS+	Liquid chromatography/mass spectrometry with fraction Collector
LC-MS/MS	Liquid chromatography with tandem mass spectrometry
LHCI	Light harvesting complex I
LHCII	Light harvesting complex II
LHCr	Light harvesting complex of red algae
LMM	Low molecular mass
LTQ	Linear trap quadropole

MALDI-TOF	Matriz assisted laster desorption ionization-time of flight
MES	2-(N-morphiline) ethanesulfonic acid
MS	Mass spectroscopy
NADP	Nicotinamide adenine dinucleotide phosphate
OD	Optical density
ORF	Open reading frame
PAGE	Polyacrylamide gel electrophoresis
PC	Plastocyanin
Pea	*Pisum sativum*
PDB	Protein data bank
PSI	Photosystem I
PSII	Photosystem II
RC	Reaction center
ROS	Reactive oxygen species
SDS	Sodium dodecyl sulfate
SOD	Superoxide dismutase
Spinach	*Spinach oleracia*
SRCD	Synchotron radiation circular dichroism
TCSPC	Time-correlated single photon counting
T.elongatus	*Thermosynechococcus elongatus*
TMH	Transmembrane helices
TMPD	N,N,N,N-tetramethyl-*p*-phenylenediaminedihydrochloride

CHAPTER 1 INTRODUCTION

PHOTOSYNTHESIS

Photosynthesis is one of the most important energy converting biological process on the Earth (1). By this process, cyanobacteria, algae and plants harvest light energy from the sun and convert it to chemical energy and this sustains nearly all living matter. The light energy is captured by pigments (chlorophylls and carotenoids) and is used to convert water and carbon dioxide into energy-rich organic compounds (simple and complex sugars) with oxygen as a by-product (1). Hence it is of utmost importance to investigate the basic photosynthetic processes as they occur in nature.

The overall reaction of photosynthesis can be written as,

$$6H_2O + 6CO_2 \Longrightarrow C_6H_{12}O_6 + 6O_2$$

Light (oxygenic photosynthesis) and dark (Calvin cycle) reactions

Harvesting and conversion of light energy to chemical energy takes place in thylakoid membranes of bacteria, algae or plant cells, through an interaction of several membrane intrinsic and soluble proteins (1). In algae and higher plants, the thylakoid membranes are located in the chloroplast (2) (Fig. 1-1). The thylakoid membranes can be divided into stacks of membranes called granal regions and non-stacked membranes called stroma lamellae. The fluid compartment that surrounds the thylakoids is known as the stroma, and the space inside the thylakoids is known as the lumen (2). Cyanobacteria are photosynthetic prokaryotes; hence the thylakoid membranes are located directly in the cytoplasmic space. According to the endosymbiosis hypothesis explaining the

origin of chloroplasts, an ancestor of cyanobacteria was engulfed by a eukaryotic cell, which subsequently led to the formation of chloroplasts (2).

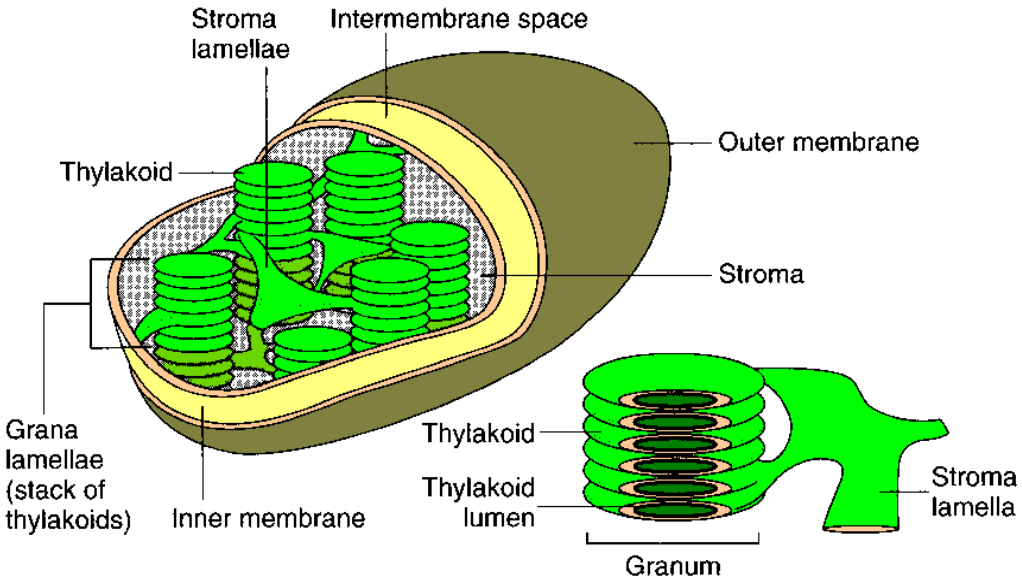

FIGURE 1-1 Diagram of a chloroplast. Figure adapted from (2)

Photosynthetic process consists of a number of photochemical and enzymatic reactions. It occurs in two distinct stages, the light reactions (oxygenic photosynthesis) which convert light energy to ATP and NADPH; and the dark reactions, which convert CO_2 to carbohydrate using ATP and NADPH (2). Both reactions occur in chloroplasts. During the light-dependent stage, chlorophyll and carotenoids absorb light energy, which excite the pigment molecules to higher energy levels. The energy is transferred from the antenna pigments to the reaction center cores of photosystem I (PSI) and photosystem II (PSII), where charge separation takes place (2). The electrons for this process are provided by PSII by oxidation of water to O_2, electrons and protons. The final products of the light

reactions are the high energy molecules NADPH and ATP and O_2 is released as a by-product.

NADPH and ATP produced during the light reaction, drive the second stage of reaction, called dark reaction or Calvin cycle, and these reactions does not require light. During this dark reaction, carbon dioxide reduction to carbohydrates is fuelled by ATP and NADPH.

$6CO_2 + 12NADPH + 18ATP \Longrightarrow C_6H_{12}O_6 + 12NADP + 18ADP + 6H_2O + 18P_i$

Origin of photosynthesis

It is generally agreed that anoxygenic photosynthesis evolved prior to oxygenic photosynthesis, approximately 3.8 billion years ago (3). Anoxygenic photosynthetic bacteria descendants still can be found today and these include the purple bacteria, the green sulfur bacteria, the green nonsulfur bacteria and the heliobacteria. The early anoxygenic photosynthetic organisms might have utilized easy to oxidize electron sources, such as H_2 and H_2S (3, 4). However, these electron sources are limited, such as H_2S was available only in environments near volcanoes. So, photosynthetic organisms had to look for an unlimited, ubiquitous and stable source of electrons: water. This led to evolution of oxygenic photosynthesis. The development of oxygenic photosynthesis by current cyanobacterial ancestors nearly 2.5 billion years ago was one of the significant events in evolutionary history that would alter the early Earth's reducing atmosphere to an oxygenic atmosphere. The first traces of cyanobacterial ancestors are found in the form of 2.5 billion year old stromatolites, and the

oxygen was present in the atmosphere in significant quantities around 2.2 billion years ago (5-7). Early traces of photosynthetic activity can be detected by the fact that photosynthetic carbon fixation is slightly more efficient for lighter isotope. This means that ^{13}C (which accounts for ~ 1% of carbon on Earth) is incorporated in organic material at a lower rate than the more abundant ^{12}C, and this depletion of ^{13}C can be taken as an indicator of biological activity (2).

Reaction center types

The photosynthetic reaction centers of photosynthetic organisms may be classified according to the nature of the final electron acceptors (2): Type I reaction centers, use iron-sulfur clusters, whereas type II reaction centers utilize quinone as a final electron acceptor. Purple bacteria and green non sulfur (green filamentous) bacteria contain type II reaction center. Green sulfur bacteria and heliobacteria contain a type I reaction center. Cyanobacteria harbor both a type I reaction center (photoystem I) and a type II reaction center (photosystem II). Only cyanobacteria, containing both types of RC's, are capable of photosynthetic oxygen evolution and all other photosynthetic prokaryotes only conduct anoxgenic photosynthesis. As mentioned before, red algae, green algae and higher plants have chloroplasts, which evolved by engulfment of precursor cyanobacteria (endosymbiosis) into a non-photosynthetic eukaryotic host. So they are capable of performing oxygenic photosynthesis.

Oxygenic photosynthesis

Oxygenic photosynthesis is catalyzed by four large membrane protein complexes: photosystem II (PSII), the cytochrome b_6f complex (Cyt b_6f), photosystem I (PSI)

and the ATP synthase (1). Except for an X-ray structure of a complete ATP synthase which is still lacking, X-ray structures from PSII, PSI and Cyt b_6f complex have been published in recent years (Fig. 1-2).

In oxygenic photosynthesis, PSII uses light energy to extract electrons from water releasing O_2 and protons (8). Plastoquinone (PQ) is the final electron acceptor in PSII. Upon double reduction it takes up two H^+ at the stromal side and leaves PSII as plastoquinol, migrates in the lipid bilayer, and transfer the electrons to another membrane bound protein complex, the cytochrome b_6f complex, resulting in the release of two protons into the lumen. In the Cyt b_6f complex, the two-electron oxidation of a reduced quinone (PQH_2) does not follow the same path once they arrive (8). The first electron moves through the high-potential transfer chain, the Rieske Iron-sulfur protein and Cytochrome f, which are located on the lumenal side and they mediate this transfer. The second electron move via the "Q" cycle to to reduce a quinone that is bound at the stromal Q_i site. Following a second reduction event at the Q_i site, the two protons are taken up from the stroma at this site and the reduced quinone is released into the lipid layer to join the reduced quinone pool. The electron from the Cytochrome f in the Cyt b_6f complex is passed on to PSI by the small soluble electron carrier, plastocyanin or cytochrome c_6 (Cyt c_6). Plants use only plastocyanin as the lumenal electron carrier, while cyanobacteria can also use cytochrome c_6 as an electron carrier (9). Cytochrome c_6 represents the more ancient electron carrier and there is evidence that the Cu^{2+} containing plastocyanin has replaced Cyt c_6
as a response to iron limitation in the ocean. The organism *Galdieria sulphuraria*

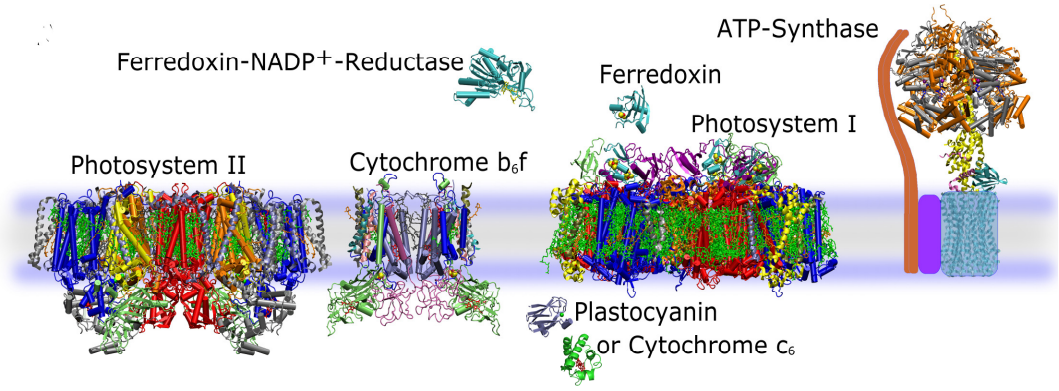

FIGURE 1-2 Oxygenic photosynthesis apparatus in thylakoid membrane. The proteins shown and the pdb files used are photosystem II from *Thermosynechococcus elongatus* (2AXT)(10), the dimer of cytochrome b_6f from *Mastigocladus laminosus* (IVF5)(11), the soluble protein plastocyanin from *Synechococcus sp. Pcc7942* (1BXV)(12), cytochrome c_6 from *Arthrospira maxima* (1F1F)(13), the trimeric complex of photosystem I from *Thermosynechococcus elongatus* (1JB0)(14), the soluble protein ferredoxin from *Anabaena Pcc7119* (1CZP) (15)and the ferredoxin:$NADP^+$ reductase from *Anabaena Pcc7119* (1QUE)(16, 17). The final protein, the ATP synthase, is not directly part of the electron transfer chain, but produces ATP from ADP and phosphate using the electrochemical proton gradient generated during electron transfer. Whereas all the other models have been derived from cyanobacterial sources, we used the model of the bovine mitochondrial F_1-ATPase (1H8E) (18) as placeholder for the membrane-extrinsic CF_1 part of the protein. The membrane intrinsic F_0 part is even less well characterized, which is indicated by the cartoons. Color coding of cofactors: All chlorophylls are depicted in green, pheophytins in yellow, carotenoids in orange, hemes in red, lipids in brown, FeS clusters, S in yellow, Fe in red. Figure adapted from (1).

the red algae, used in this study has only Cyt c_6, as the sole electron carrier. It does not contain a gene for plastocyanin (9).

PSI catalyzes the second step of the light reactions by capturing light energy with a large antenna system of 96 *Chl a* and 22 carotene molecules, funneling the exciton to two chlorophylls in the center of the complex, P700 (14). The excitation energy is used to drive electrons against a potential gradient through a series of redox carriers from the inner (lumenal) side of the thylakoid

membrane to ferredoxin/flavodoxin on the cytoplasmic (stromal) side. Ferredoxin transfers electrons to FNR (ferredoxin: NADP+oxidoreductase), which in turn reduces $NADP^+$ to NADPH (nicotinamide adenine dinucleotide phosphate). The electron transfer reactions are coupled to the transfer of protons from the stromal to lumenal side of the membrane and electrochemical potential drives the synthesis of ATP by ATP synthase.

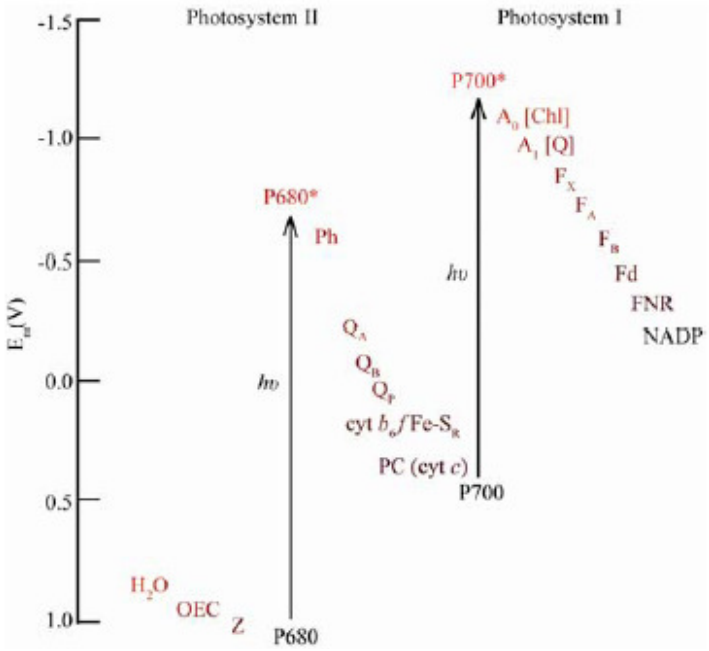

FIGURE 1-3 The "Z-scheme" of oxygenic photosynthesis. Electrons transfer is driven by light excitation of P680 and P700 of PSI and PSII, respectively; other transfer steps involve a decrease in energy and are spontaneous. The electron transfer chain in PSII consist of the oxygen evolving complex (OEC), a tyrosine reside (Z), the primary donor P680, a pheophytin (Ph), and two quinones (Q_A and Q_B). The mobile plastoquinone (Q_p) upon double reduction carries the electron to cytochrome b_6f (cyt b_6f Fe-S_R), from where it is delivered to plastocyanin (PC) or Cytochrome c_6 (Cyt c). In PSI, the charge separation is driven by P700 excitation and the electron is transferred to Chlorophyll A_0, plastoquinone A_1 and three iron-sulfur clusters (F_x, F_A and F_B) are shown. The electron is passed to ferredoxin (Fd) from F_B upon subsequent docking of 2 F_d molecules, then to ferredoxin-$NADP^+$ reductase (FNR) and finally to $NADP^+$. Figure adapted from (2).

A summary of the sequence of these events in oxygenic photosynthesis is referred to as the "Z" scheme, because of its characteristics sideways "Z"-shape (Fig. 1-3). Vertical increase in redox potential is associated with the light-driven steps, whereas the other electron transfer steps involve a decrease in redox potential and occur spontaneously.

PHOTOSYSTEM II

Photosystem II component of the chloroplast/cyanobacterial photosynthetic apparatus is a large transmembrane protein/cofactor complex that utilizes light energy to oxidize water to molecular oxygen and to reduce membrane diffusible plastoquinone to plastoquinol. The latest crystal structure of PSII from *Thermosynechoccoccus elonagatus* reveals that each PSII monomer consists of 20 protein subunits, 35 chlorophyll a molecules, 12 beta-carotene molecules, 2 pheophytin molecules, 3 plastoquinone, 2 heme, 1 bi-carbonate, 25 lipids and a Mn_4CaCl cluster (Figs. 1-4 and 1-5).

The architectural core of PSII consists of a dimer of membrane-spanning proteins D1 (PsbA) and D2 (PsbD) for PSII, each with five transmembrane α-helices with a pseudo C_2 symmentry axis in the center of each monomer (Fig. 1-4). The core resembles the purple bacteria reaction center. The primary electron/proton transfer cofactors are bound to these two proteins. Additionally, D1 provides ligands to the catalytic site of water oxidation, consisting of four manganeses, one calcium and one chloride ion. The D1 protein has to be replaced every 30 minutes in plants in bright sunlight. This is caused by the cationic radical

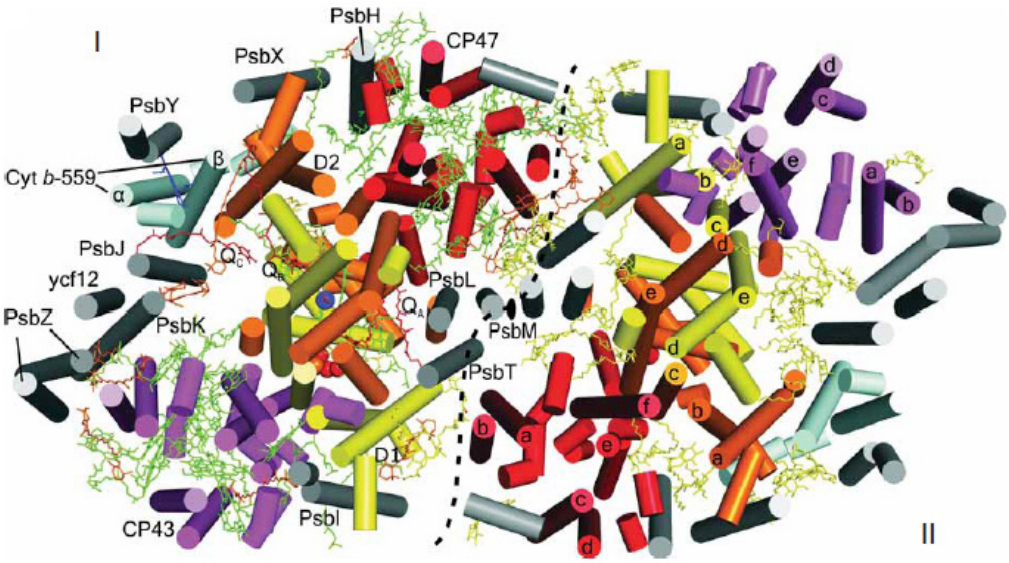

FIGURE 1-4. Structure of PSII with assignment of protein subunits and cofactors with transmembrane helices indicated from the stromal side. The monomer-monomer interface is indicated by a black dashed line and the noncystallographic C2 axis relating the two monomers as a black ellipse (center). Helical parts are shown as cylinders and the subunits D1/PsbA (yellow), D2/PsbD (orange), CP43/PsbC (magenta), CP47/PsbB (red), cyt b-559 (cyan, subunits a/PsbE and b/PsbF) and the remaining eleven small subunits (gray) are labeled in monomer I. In monomer II, the five TMHs of D1 and D2 are labeled a to e and the six TMHs in CP43 and CP47 are labeled a to f. Cofactors are shown in stick mode; monomer I shows Chl*a* (green), Car (orange), heme (blue), Pheo (yellow), PQ (red), the Mn4Ca cluster (red and orange spheres; barely visible) and non-heme iron (blue sphere). Monomer II shows lipids and detergents (yellow). Figure adapted from (19).

$P680^{+\bullet}$, which has the high redox potential of +1.1 V (2). Photodamage might occur by direct oxidation of the protein by $P680^{+\bullet}$ or by the formation of the $^{3}P680$ triplet and highly reactive singlet oxygen, which would lead to irreversible damage to D1 protein (2). Three genes (PsbA1, PsbA2 and PsbA3) for D1 have been found in cyanobacterial genomes, and are supposed to be expressed under different growth conditions (2).

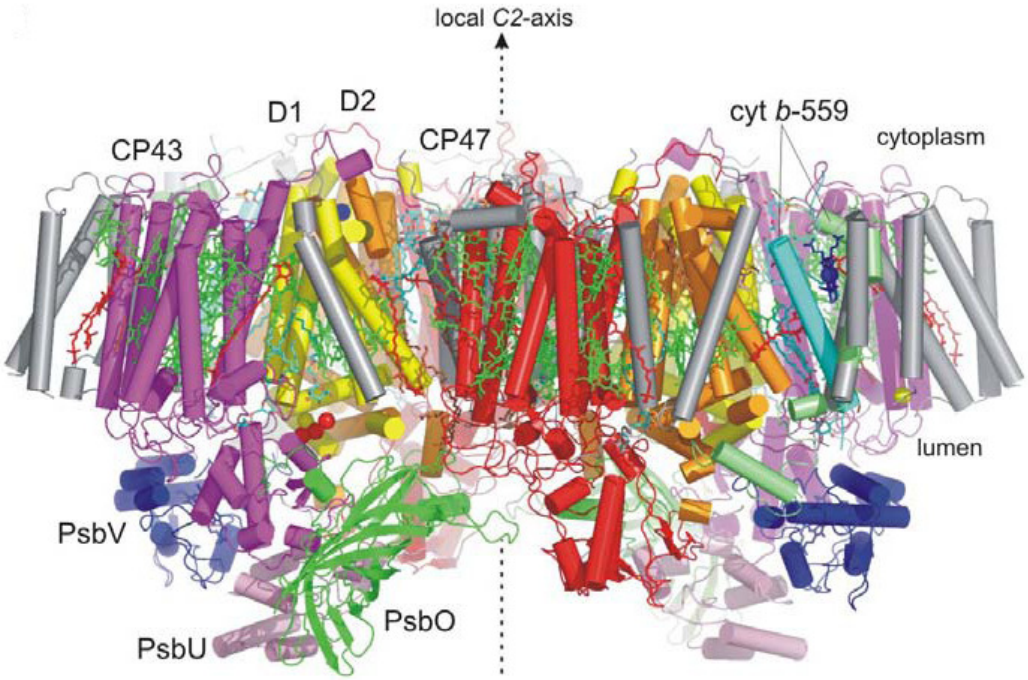

FIGURE 1-5 Crystal structure of cyanobacterial PSII dimer (side view along the membrane plane). The two monomers are separated by a dashed black line. Reaction center subunits D1 (yellow) and D2 (orange), antenna subunits CP43 (magenta) and CP47 (red), α- and β-chain of cyt b-559 (green and cyan), low molecular subunits (grey). Membrane extrinsic subunits, PsbO (green), PsbU (pink) and PsbV (blue). Cofactors in green (Chla), yellow (Pheo), red (Carotenoids), blue (haem), violet (quinone). Figure adapted from (10)

The flanking transmembrane proteins bind additional light harvest chlorophyll pigments and are named CP43 (PsbC) and CP47 (PsbB), respectively (Fig. 1-4). Both subunits have six transmembrane helices (TMH), and their cofactors (chlorophylls and carotenoids) capture light energy and transfer the exciton energy to the reaction center. Both proteins have exceptionally large lumenal loops between TMH 5 and 6, the loop of CP43 provides one ligand for coordination of the Mn cluster (19). The membrane intrinsic hetero-oligomeric

cytochrome b_{559} has two subunits, α (PsbE) and β (PsbF). Each subunit has one single TMH each providing its single histidine as ligand to the heme group of the cytochrome.

Apart from these subunits, PSII consist of several small subunits called low molecular mass (LMM) subunits (PsbH, PsbI, PsbJ, PsbK, PsbL, PsbM, PsbN, PsbT, PsbX, PsbY and PsbZ) (Fig. 1-4). Most of the LMM subunits consist of one single transmembrane spanning α-helix and are located peripheral to the central core. The sequences for these small subunits are only moderately conserved among photosynthetic organisms (20). Deletion mutations of these LMM subunits from both prokaryotic and eukaryotic model systems are compared in order to understand the function of these subunits. From these comparisons, it seems that the majority are involved in stabilization, assembly or dimerization of the PSII complex. These small subunits may facilitate fast dynamic conformational changes that the PSII complex needs to perform an optimal photosynthetic activity and they facilitate during D1 repair (20).

Of the 20 subunits present in cyanobacterial PSII, three subunits (PsbO, PsbU, and PsbV) are located outside the membrane, on the lumenal side of PSII (Fig. 1-5). The extrinsic subunits stabilize the lumenal hump of PSII. PsbO subunit is present in PSII of all photosynthetic organisms. In the PSII X-ray structures, PsbO was identified as a β-barrel structure and is involved in the stabilization of the Mn-cluster (1). Other extrinsic subunits of cyanobacteria are PsbU and PsbV. The subunit PsbU is located at the periphery of the lumenal hump and may further stabilize the complex. PsbV (Cyt c_{550}) is located at the side

of the lumenal hump and it contains a heme whose function is not known at this time. However, because of the strong sequence homology between PsbV and cytochrome c_6, a lumenal electron donor to photosystem I in cyanobacteria and some algae, it is possible that Cyt c_{550} may be the original ancestor electron donor to the nonoxygenic ancestor of PSII that has been trapped and made an extrinsic subunit of PSII for the stabilization of the oxygen evolving complex (21).

In higher plants and green algae, PsbU and PsbV subunits are replaced by PsbP and PsbQ (1). However, in red algae, the extrinsic subunits composition is heterogenous. They contain a combination of subunits present in both cyanobacteria and higher plants and extrinsic subunit compositions differ between individual species of red algae. For example, *Cyanidium caldarium* has extrinsic subunits PsbO, PsbU and PsbV. Along with these subunits, there is special subunit, PsbQ′ which is known to be present only in this organism (22). Similarly, *Cyanidioschzyom merolae* has extrinsic subunits, PsbO, PsbU, PsbP and PsbQ (22). It will be of great interest to know the extrinsic subunits in other red algae and it is a current hot topic of research.

Electron transfer chain

The electron transfer chain of PSII consists of four chlorophyll a (*Chla*), two pheophytins, two PQs, one redox active tyrosine Tyr_Z and the Mn cluster (Fig. 1-6). During photosynthesis, the harvested light is transferred to the center of the PSII where it excites the P680 (termed as P_{680} for the maximum absorbance change at 680 nm) to $P680^*$, inducing $P680^*$ to transfer the electron to pheophytin, leaving P680 as a radical, $P680^{\bullet+}$ (1). This radical is one of the most

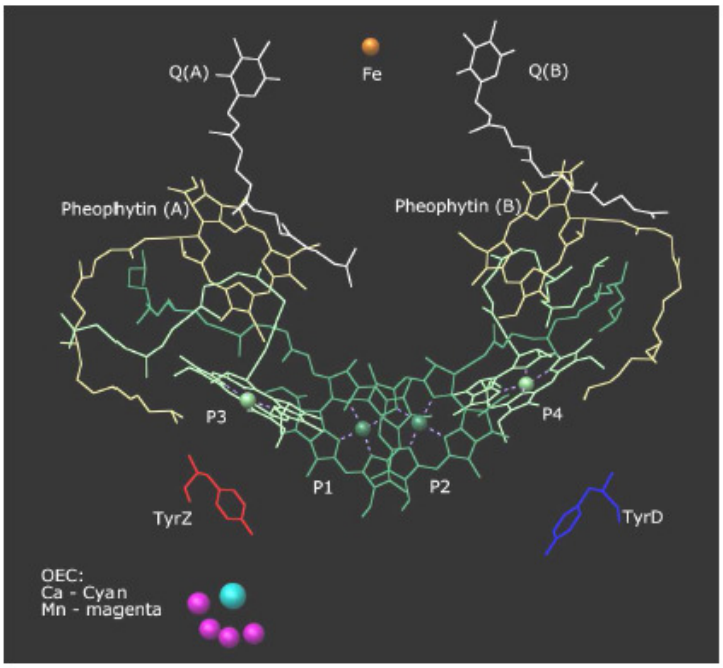

FIGURE 1-6 The electron transfer chain (ETC) of cyanobacterial photosystem II (PSII). Chlorophylls are shown in dark green, pheophytins in yellow, and plastoquinones in white. The redox-active Tyrz is drawn in red, while the symmetrically related, non-redox-active Tyr_D is drawn in blue. Within the Oxygen-evolving complex (OEC), Calcium is drawn in cyan, while the 4 Mn atoms are shown in magenta. It is not clear at this time whether only P1 and P2 or also P3 and P4 participate in formation of the $P680^{\bullet+}$ state. However, spectroscopic evidence suggests that the various oxidation states of the primary donor may be predominantly localized on different chlorophyll molecules. Although $P680^{*}$ may be distributed over all 4 chlorophylls, the triplet state $^{3}P680$ may be located on P3(23), and P680, and the cationic radical $P680^{\cdot +}$ is suggested by evidence to be localized to P1. Drawn using Chimera, using coordinates from the deposited structure 2AXT(10).

oxidizing species found in nature. A nearby tyrosine residue, the redox-active Tyr_Z, rereduces, $P680^{\bullet+}$ and is itself re-reduced by an electron from the OEC, which has been extracted by the OEC from water (1). From the D1 bound pheophytin, the electron is passed to PQ_A, and then to PQ_B which subsequently leaves PSII as PQH_2 (plastoquinol) after two electron transfer events and the

uptake of two protons from the stromal side of the membrane. The resulting plastoquinol molecule is then released into a membrane-diffusing plastoquinol pool that feeds electrons into a separate membrane protein the cytochrome b_6f complex. An oxidized plastoquinone from the PQ pool enters the PQ_B binding site to begin a new 2 electron 'acceptor side" cycle. Although there is little doubt in the electron transfer chain and the co-factors involved in it, the structural information on the Mn cluster is not sufficient enough to determine the exact position of Mn ions and the water splitting mechanism, which is under active investigation.

Light harvesting antenna - phycobilisomes

Along with the internal chlorophyll antenna system for light harvesting, cyanobacterial PSII uses a membrane extrinsic anternna, the phycobilisomes for light harvesting (Fig. 1-7).

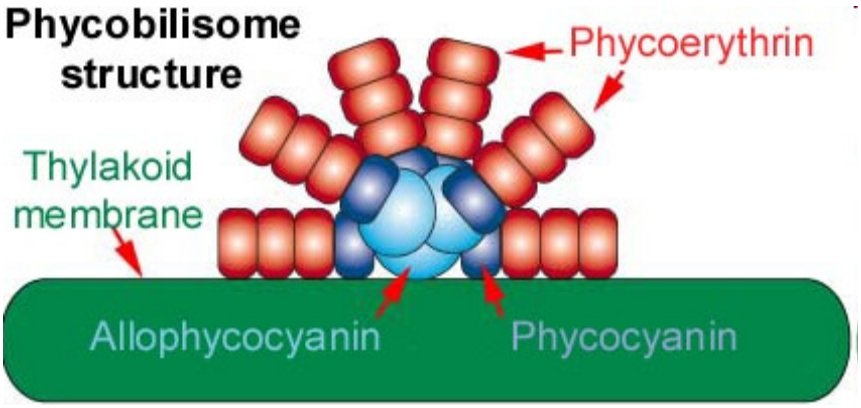

FIGURE 1-7 Phycobilisome model showing the arrangement of different phycobiliproteins: The core is made of allophycyanin from which several rods are originating made of disks of phycocyanin and phycoerythrin proteins. Note that most cyanobacteria and the red algae, *Galdieria sulphuraria* used in this study do not contain phycoerythrin. Figure adapted from (2)

The phycobilisomes are extra-membraneous antenna complexes located on the stromal side of PSII. They are hemispheric or hemivoid shape and are present in cyanobacteria and red algae (2). This complex contains two or three types of pigment-proteins known as biliproteins, and these proteins are linked together by linker proteins. Phycoerythrin, phycocyanin and allophycocyanin are the different types of biliproteins and they differ in protein identity, chromophore type and attachment and also in their relative location in the phycobilisome complex. The phycobilisome absorbs light across the ~ 590 – 650 nm range of the solar

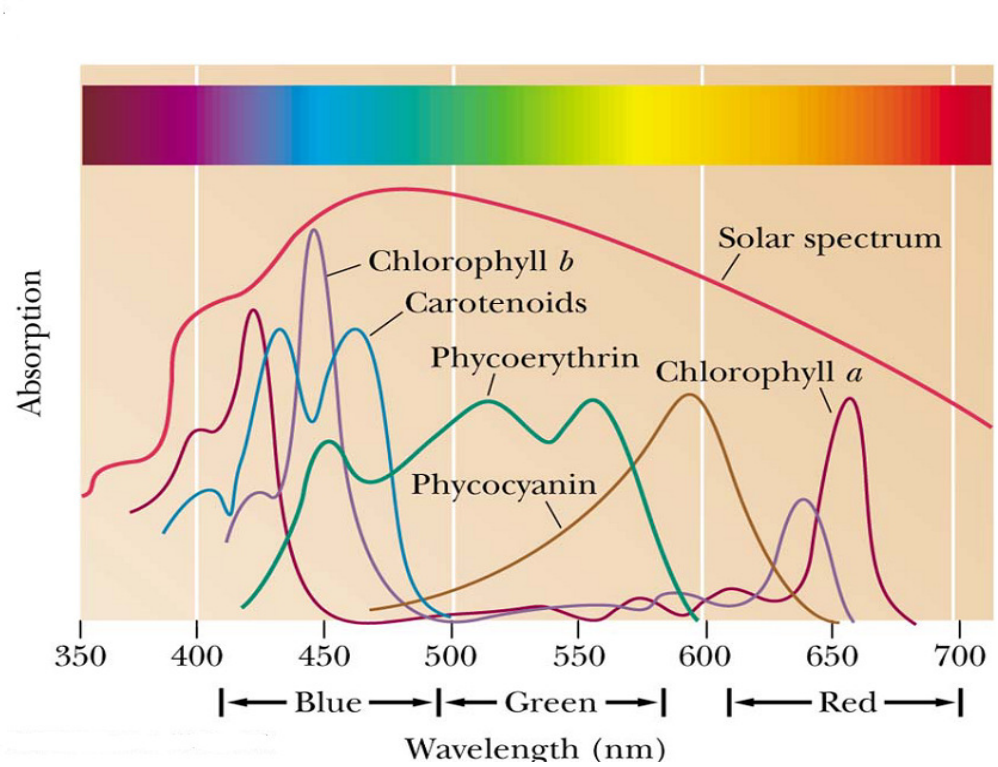

FIGURE 1-8 The absorption spectrum of photosynthetic pigments. Adapted from (24)

spectrum a region neither chlorophyll nor carotenoids are capable of absorbing light (Fig. 1-8). An organism with phycobilisome has greater accessibility to usable light within the visible spectrum and hence greater adaptability and light capturing capacity (2).

PHOTOSYSTEM I

Photosystem I catalyzes the electron transfer from plastocyanin/Cyt c_6 on the lumenal side of the thylakoid membrane to ferredoxin/flavodoxin on the stromal side by a chain of electron carriers (1). It is the largest and most complex membrane protein for which a structure has been determined. The 2.5 Å structure of cyanobacteria PSI-trimer reveals that each PSI monomer consists of 12 protein subunits, to which 127 cofactors are non-covalently bound: one functional unit of PSI contains 96 chlorophyll-a molecules, 22 carotenoids, 3 Fe_4-S_4 clusters and 2 phylloquinones (Fig. 1-9).

The membrane-intrinsic part of PSI has two large dominant subunits, PsaA and PsaB (Fig. 1-10). These subunits coordinate the organic cofactors of the ETC and the majority of PSI's light harvesting pigments. PsaA and PsaB are characterized by a very similar eleven-transmembrane helix topology and their sequences are ~ 44% identical. It is generally assumed that PSI evolved from a homodimeric reaction center as seen in green sulfur bacteria or heliobacteria (2). The remains of the original homodimeric organization can be seen in the similarity of PsaA and PsaB, especially in the components of the ETC (Fig. 1-12).

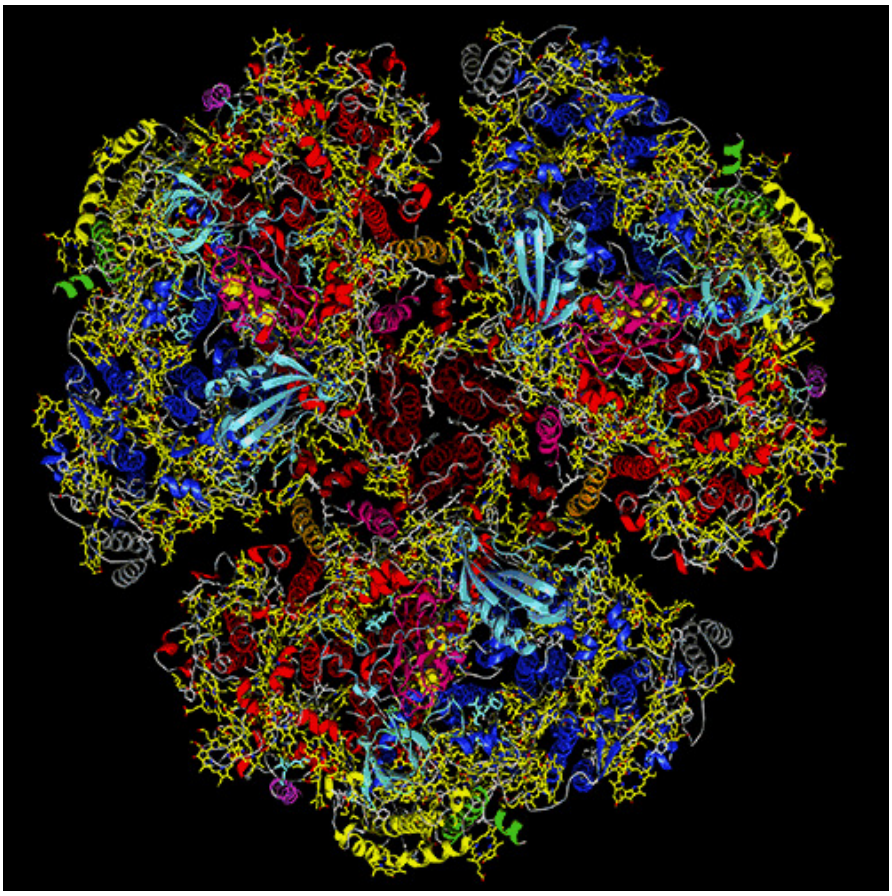

FIGURE 1-9 Crystal structure of trimeric PSI from thermophilic cyanobacterium *Thermosynechococcus elongatus* at 2.5 Å resolution Color code of extrinsic subunits, PsaC- Magenta; PsaD-Light blue; PsaE – turquoise. (view from the stromal side). Figure adapted from (14)

Some of the subunits of PSI, peripheral to the core subunits PsaA/B play an important structural role. The subunit, PsaL helps in the formation the trimerization of PSI monomers (Fig. 1-10). This region of PSI is significantly changed in eukaryotic PSI, which does not form trimers (Fig. 1-13). PsaF is thought to interact with peripheral light-harvesting proteins in both cyanobacteria and plants. Other smaller membrane-intrinsic subunits, PsaI (magenta), PsaJ (green), PsaK (grey), PsaM (orange) and PsaX (pink) coordinate pigments and stabilize the antenna complexes of PSI.

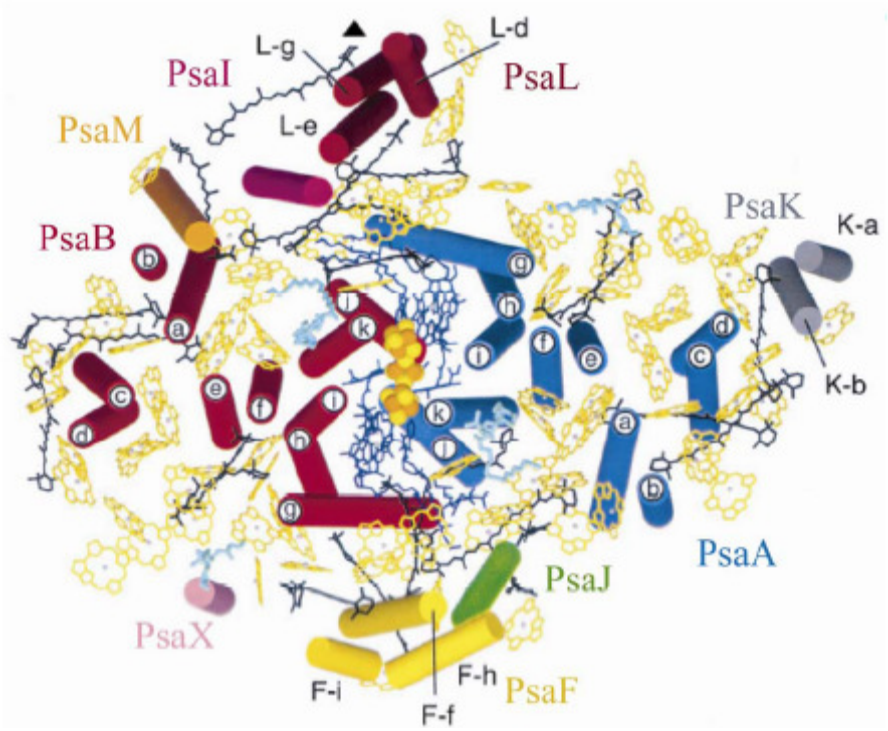

FIGURE 1-10 Cyanobacterial PSI monomer view from the stromal side (top view). Alpha helices are shown as cylinders. Solvent exposed loops have been omitted as well as the extrinsic subunits. Protein is color-coded by subunit; TM helices of PsaA and PsaB are labeled with letters a through j. Organic cofactors of the ETC are sulfur clusters of the ETC are depicted in dark blue (6 chlorophylls and 2 phylooquinone), orange sphere (Fe) and yellow sphere (S). Anternna chlorophyll – yellow, only chlorine head group is shown, phytl chain omitted for clarity; Carotenoids – black; Lipids – light blue. The trimerization axis is marked with a black triangle. Figure adapted from (25).

The three subunits of cyanobacterial PSI - PsaC, PsaD and PsaE are located outside of the membrane plane, and are referred as the stromal hump (Fig. 1-11). PsaC coordinates the two terminal iron-sulfur clusters F_A and F_B and its interactions with the membrane-intrinsic portions of PSI are stabilized by PsaD and PsaE.

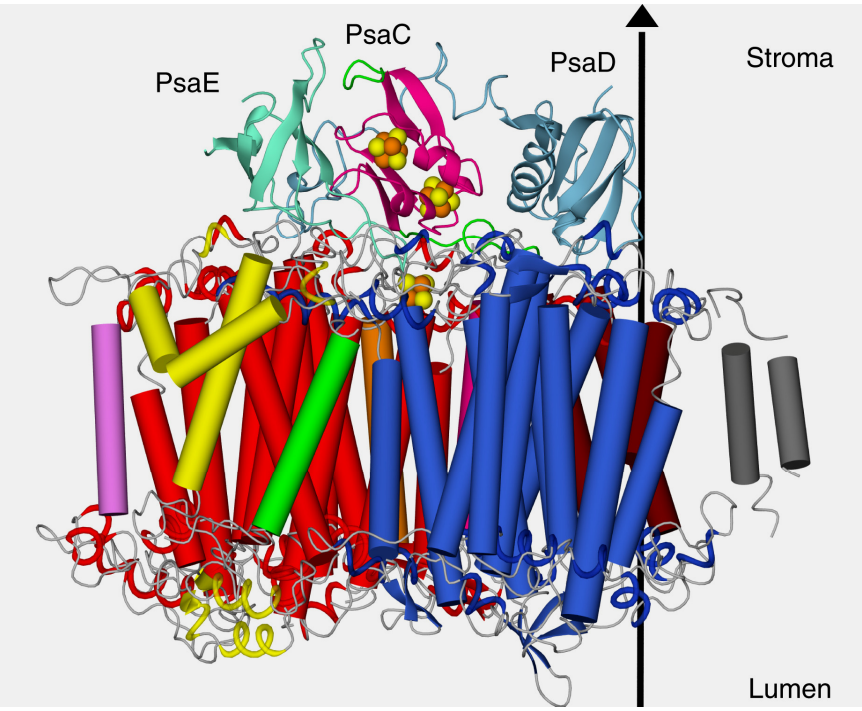

FIGURE 1-11 Side view of a PSI monomer: PsaA (red); PsaB (blue); PsaL (brown);PsaF(yellow); PsaX(violet); PsaJ (green); PsaI(orange);PsaK (grey) & PsaM (dark red). Three stromal subunits PsaC (purple), PsaD (light blue) & PsaE (Turquiose) and 3 Fe_4-S_4 clusters F_x, F_A and F_B (Chlorphylls and carotenoids are omitted for clarity). Membrane intrinsic subunits are colored as in Figure 11. The trimerization axis is marked with a black arrow. Figure reproduced from(25).

Electron transport chain

Electron transport chain of PSI is shown in Fig. 1-12. Two chlorophyll molecules, centrally located on the lumenal side of PSI, may represent as P700. It is called P700 because of the decrease in absorption at 700 nm, observed upon its oxidation (1). Older literature sometimes refers to P700, as the “special pair”. During photosynthesis, excitation from light harvested by the antenna system chlorophylls is funneled to the reaction center, where it is used to excite P700 to $P700^*$. Charge separation occurs, and $P700^*$ ejects an electron, leaving behind $P700^{\bullet+}$ (Fig. 1-12).

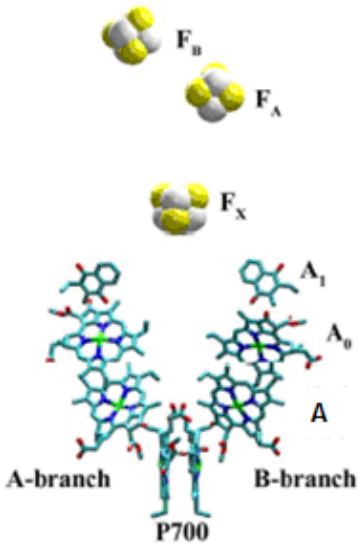

FIGURE 1-12 The electron transfer chain of PSI. Charge separation begins when an exciton is trapped at P700 to $P700^*$. From $P700^*$ electron often travel through one of the branches of the electron transfer chain, eventually reaching the terminal iron-sulfur clusters, forming F_AF_B. Finally, $P\ 700^{+\bullet}$ is re-reduced by plastocyanin/cytochrome c_6 and F_B^- is re-oxidized by ferredoxin. Phytol chain from chlorphyll and phylloquinone are omitted for clarity.Figure adapted from (14)

The electron is then transferred up one of the ETC branches to F_X, then to F_A and F_B and subsequently, from F_B out of PSI and on to Ferredoxin. $P700^{+\bullet}$ is re-reduced by accepting an electron from a lumenal electron carrier.

EUKARYOTIC PSI

The structure and architecture of the core of photosystem I are highly conserved between cyanobacteria, algae and higher plants. Eukaryotic PSI exists as a functional monomer instead of as a trimer, as seen in cyanobacteria (26) (Fig. 1-13). A commonly prevailing idea is that the ancestor of both plants and cyanobacteria possessed a monomeric reaction center – with cyanobacteria subsequently forming the trimerized photosystem for greater light harvesting

efficiency, whereas in algae and higher plants evolving the attached LHCI complexes (1). The plant PSI structure shows four LHCI proteins (Lhca1 through Lhca4) bound to the PSI core. The external antenna system in plants is asymmentric and heterogenous, and is strongly modified under changing environmental conditions (e.g. light intensity, light wavelength, environmental stress). One of the short-term adaptive processes that helps the eukaryotic photosynthetic machinery respond effectively to changing environmental conditions is known as state transitions where LHCII moves between PSI and PSII (2).

The recent structure of the plant PSI-LHCI supercomplex at 3.4 Å resolution was a significant breakthrough in understanding plant photosynthesis and also an achievement for structural biology (26, 27) (Fig. 1-13). Crystallized PSI-LHCI complex (~ 600 kDa) contains 13 protein subunits that traverse the thylakoid membrane (PsaA, PsaB, PsaF, PsaG, PsaI, PsaJ, PsaK, PsaL and Lhca 1-4) comprising 45 transmembrane helices, 3 stroma exposed subunits (PsaC, PsaD and PsaE) and 1 lumenal subunit (PsaN). In the structure, 168 chlorophylls, three Fe_4S_4 clusters, two phylloquinones and five caroteonids were modeled (27). Plant PSI-LHCI has a core complex similar to cyanobacteria, but more than a billion years of separate evolution has shaped some key modifications.

Comparisons between the plant PSI-LHCI structure and cyanobacterial PSI structure reveals some key differences (28) (Fig. 1-13). Plant PSI lacks PsaM, which is located at the monomer-monomer interface and PsaX, (present mainly in thermophilic cyanobacteria), but possesses additional subunits: four LHCI

proteins; PsaG, acts as a template for assembly of light harvesting proteins; and PsaH to prevent trimer formation and interact with light harvesting complex II (LHCII). Additional subunits, PsaO and PsaP were identified in plants, but they are not present in the current structure. Other crucial difference exists in the subunit PsaF. Both in plants and cyanobacteria, PsaF has a fold that is unique among transmembrane proteins. In addition to its single transmembrane helix, there is a V-shaped structure formed by a helix that begins at the stromal side, extends halfway through the membrane, then forms a kink and emerges again on the stromal side. Given its location on the complex, this V-shaped domain is probably involved in the interactions between PSI and its external light harvesting complex I. PsaF posseses a membrane extrinsic region of the lumenal side of PSI. In cyanobacteria, the N-terminal loop of the PsaF is relatively short, while in plants this loop is extended by 21 residues (28). In plants, the extended PsaF contains several positively charged amino acid residues, which matches well with an acidic patch on plastocyanin, leading to the formation of a more stable PSI-plastocyanin complex in plants.

The functional significance of the PSI monomer in plants is that the PsaL interface, which is involved in trimer-maintaining interactions in cyanobacteria, provides a vital interface for interactions between plant PSI and an additional light harvesting antenna complex, the LHC II in processes of state transition (28). Recruiting of LHCII (flexible antenna systems) in higher organisms is vital for regulating photosynthetic machinery. Plants are exposed to high light intensities

on land surfaces in comparison with light-limited environment of shallow water cyanobacterial habitats (28).

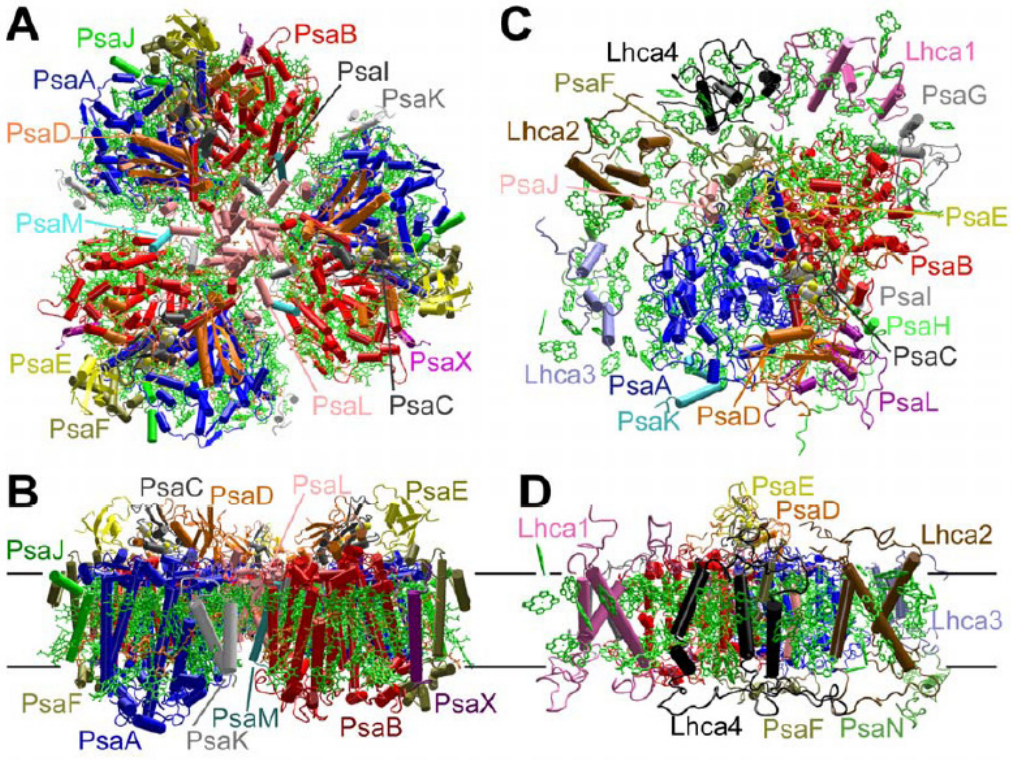

FIGURE 1-13 Comparison of cyanobacterial and plant PSI-LHCI structures. (A) Stromal view of the cyanobacterial PSI trimer from the 2.5 Å crystal structure(14). Chlorophyll is shown in green, β-carotene in orange, iron-sulfur clusters in gray and yellow, and proteins are color-coded by subunit. (B) View along the membrane plane of the cyanobacterial PSI trimer. (C) Stromal view of the plant PSI monomer, from the 3.4 Å crystal structure (27) (D) View along the membrane of plant PSI-LHCI. In B and D membrane plane is indicated by black lines.

Several studies have shown that the mobile pool of LHCII switch back and forth between two photosytems for balancing the excitation energy. In plants, single LHCII trimer was proposed to interact with the PsaH/L side of PSI (29). But for green algae, *Chlamydomonas*, it was suggested that two LHCII trimers interact

with PSI-LHCI through three phosphorylated protein linkers (30). So, it is essential for plant/green algae PSI to adopt a monomeric structure to allow LHCII to form a proper membrane-mediated interaction with PSI.

THE RED ALGAE, GALDIERIA SULPHURARIA

Red algae are unicellular eukaryotes that are capable of oxygenic photosynthesis. *Galdieria sulphuraria* is a thermo-acidophilic red microalga that inhabits extreme environments (31). It belongs to an ancient group of algae, called the Cyanidiales (31). Cyanidiales are the principle photosynthetic organisms in hot acid environments. Prokaryotic cyanobacteria are frequently found in hot environments such as hot springs. However, cyanobacteria never occur at pH < 4.0. These acidic environments are dominated by eukaryotic red micro-algae, the Cyanidiales and these organisms can also grow 3 cm below the rock surface (31) (Fig. 1-14) . Based on the current taxonomy, Cyanidiales comprises of three genera (Cyanidium, Cyanidioschyzon and Galdieria) and six species have been characterized so far: *Galdieria sulphuraria*, *Galdieria partita*, *Galdieria daedala*, *Galdieria maxima*, *Cyanidium caldarium* and *Cyanidioschyzon merolae* (31). Among the Cyanidiales, *Galdieria sulphuraria* is unique, as this alga grows autotrophically, as well as mixo-./-heterotrophically on a broad range of organic substrates (50 different carbon sources), propagate by endospores and is tolerant to high concentration of toxic metal ions (cadmium, mercury, aluminium and nickel) (32).

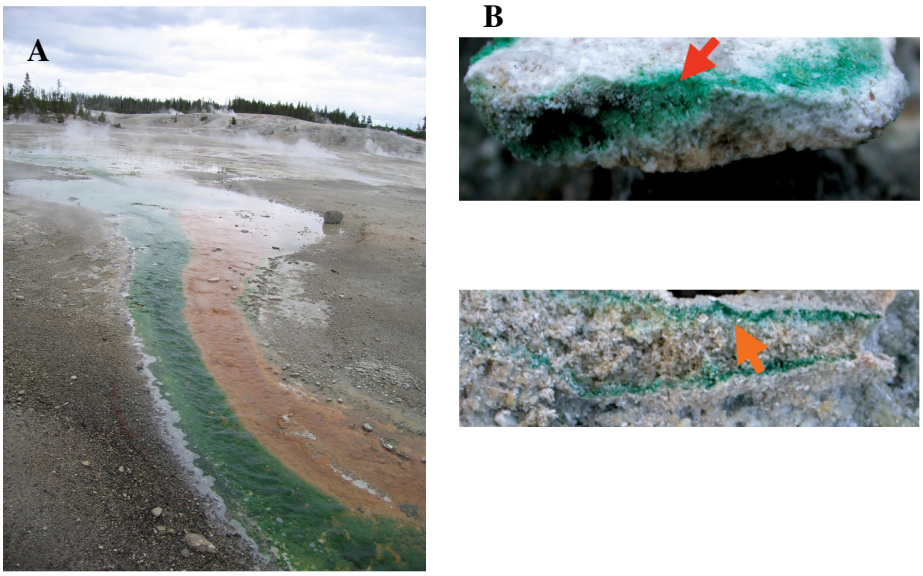

FIGURE 1-14 *Galdieria sulphuraria* habitats (A) in acidic geothermal habitats (B) *Galdieria sulphuraria* growth below the rock surface. Figure adapted from (33)

Galdieria sulphuraria (hereafter referred as *Galdieria* in this chapter and other chapters) has a rigid cell wall enriched with proteins and low amounts of cellulose, which are useful for their survival under biotic and abiotic stresses (32). It has been reported that *Galdieria* was able to survive at pH 2 for several years in an environment lacking light and organic carbon (34). Due to an increase in attention to this micro red alga, the genome project of *Galdieria* was initiated and completed recently and the draft genome is publicly available (32). *Galdieria* genome analysis revealed unique properties and 30 % of *Galdieria* sequences have no paralogs in other Cyanidiales. It also showed the presence of a large number of putative monosaccharide transporters, phosphate translocators and photorespiratory pathway which are essential for their survival under extreme conditions (33). In recent years, several studies focusing on *Galdieria* enzyme

regulation and its metabolic transporters have been published (34, 35). These studies used *Galdieria* as a model organism for rhodophyta and investigated the position of *Galdieria* in the scheme of eukaryotic evolution. Because of its metabolic flexibility and the extreme conditions in which this organism performs oxygenic photosynthesis, *Galdieria* would be a highly interesting or a model candidate for biochemical, structural, functional and evolutionary studies on photosynthetic proteins. Also, the conditions which *Galdieria* carries out photosynthesis are at the high end of the range of this process, making *Galdieria sulphuraria* a valuable model for biochemical and biophysical studies on the photosynthetic apparatus (32).

To start to explore the potential of *Galdieria* and for gaining deeper understanding of its photosynthetic machinery, I have initiated the culture of *Galdieria* in our lab and isolated the photosynthetic membrane proteins (PSI and PSII). Most of the work presented in this dissertation in various chapters, focuses Galdieria *sulphuraria* and its photosystems, except for chapter 5, which focuses on PSI-LHCI complex of green algae, *Chlamydomonas reinhardtii*.

In Chapter 2, growth, isolation and purification of PSI-LHCI and PSII from the red alga, *Galdieria sulphuraria* is presented. In chapter 3, the efficient light harvesting of *Galdieria* in their dark and acidic habitat, is discussed more extensively. In Chapter 4, PSII isolated from *Galdieria*, is characterized by top-down mass spectrometry. Post-translational modifications for individual PSII subunits are identified and are discussed. Chapter 5 deals with the isolation of

PSI-LHCI complexes from green algae, *Chlamydomonas reinhardtii*, and their response to high salt stress conditions.

CHAPTER 2 ISOLATION, PURIFICATION AND CHARACTERIZATION OF PHOTOSYSTEM I AND PHOTOSYSTEM II FROM *GALDIERIA SULPHURARIA*

INTRODUCTION

In an evolutionary perspective, the photosynthetic red algae (Rhodophyta) are one of the most primitive eukaryotic algae, phylogenetically related to prokaryotic cyanobacteria (31). In red algae, the photosynthetic apparatus appears to be in a transitional state between cyanobacteria and higher plants (36). Red algal chloroplasts has an ultrastructure similar to cyanobacteria, however, there is no differentiation into stacked and unstacked regions as noted in green algae and higher plants. In terms of photosynthetic membrane proteins they are transitional: both cyanobacteria and red algae, contain phycobilisomes, as a peripheral light harvesting antenna for photosystem II (PSII); red algal photosystem I (PSI) has an intrinsic light harvesting antenna as noted in green algae and higher plant PSI (refer to chapter 1 for more details).

In *Cyanidium caldarium* and *Cyanidioschyzon merolae,* the relative species of *Galdieria*, both photosystems (PSI and PSII) have been isolated and characterized (36-38). In case of *Galdieria*, there are no experimental studies on both photosystems.

Photosystem I

In prokaryotes and eukaryotes, the PSI core is similar and has been conserved over millions of years of evolution (1). However, the system differ significantly in the oligomeric organization, subunit composition and peripheral antenna systems.

Cyanobacterial PSI is a trimer and each monomer consists of 12 highly conserved subunits (1): PsaA, PsaB, PsaC, PsaD, PsaE, PsaF, PsaI, PsaJ, PsaK, PsaL, PsaM and PsaX. In green algae and higher plants, PSI is a monomer and contains peripheral light-harvesting chlorophyll a/b complexes (LHCI), and these light harvesting complexes are not found in cyanobacteria. PSI is monomeric in green algae and higher plants and it consist of 13 subunits (1): PsaA, PsaB, PsaC, PsaD, PsaE, PsaF, PsaG, PsaH, PsaI, PsaJ, PsaK, PsaL, PsaN, PsaO and PsaP. However, the number of light harvesting proteins between green algae and higher plants differs: Higher plants (*Pisum sativum*) has four light harvesting proteins (Lhca 1-4), whereas in green algae (*Chlamydomonas reinhardtii*) nine distinctive lhc proteins are proposed to form the PSI-LHCI supercomplex (28).

Our current knowledge of PSI from *Galdieria*, depends on a genetic analysis study in which they analyzed the genes encoding PSI proteins in *Galdieria* and compared them to the cyanobacterial and eukayotic PSI complexes (9). A total of 13 subunits (PsaA, PsaB, PsaC, PsaD, PsaE, PsaF, PsaI, PsaJ, PsaK, PsaL, PsaM, PsaN and PsaO) have been identified in the *Galdieria sulphuraria* genome. This includes the cyanobacterial specific, PsaM subunit as well as the green algae and higher plant specific subunits, PsaN and PsaO. Along with subunit identification, this study concluded that *Galdieria* PSI may represent a common ancestor of PSI from cyanobacteria, green algae and plants (9). From an another study, five light harvesting proteins (lhcr1-lhcr5) genes have been reported to be present in *Galdieria* genome, of which (lhcr4) has been confirmed by N-terminal sequencing (39). To confirm the identification of the *Galdieria*

PSI-LHCI subunits and for biochemical and biophysical characterization of this evolutionary ancestoral PSI-LHCI complex, we purified the PSI-LHCI complex from *Galdieria sulphuraria*. Results of our study might provide some insight about the evolutionary position of this organism in the development of photosynthetic eukaryotes.

Photosystem II

Photosysem II (PS II) is one of the important enzymes on earth, as this enzyme has changed our earth atmosphere 2.5 billion years ago from an anoxygenic state to oxygenic state (1) (refer to chapter 1 for more details).

The extrinsic subunit PsbO (33 kDa) is a common subunit conserved among cyanobacteria, red algae, green algae and higher plants(1). Apart from PsbO subunit, plants and green algae contains the PsbP (23 kDa) and PsbQ (17 kDa) extrinsic subunits. In cyanobacteria and red algae, PsbP and PsbQ are replaced by PsbV cyt c_{550} (16 kDa) and PsbU (12 kDa) (22). In addition to these, red algae contains a fourth extrinsic subunit PsbQ$'$ (20 kDa), with their sequence highly homologous with the PsbQ protein present in green algae and higher plants. Cross-reconstitution studies demonstrated that the PsbQ$'$ protein from *Cyanidium caldarium* is functional in place of PsbQ in green algae and higher plants, with complete restoration of oxygen evolution (40). In another reconstitution study, the extrinsic subunits of red algae *Cyanidium caldarium* partially restored oxygen evolution in both cyanobacteria and higher plants (41). Altogether, these studies imply that extrinsic subunits of PSII in red algae might

occupy an intermediate position during the evolutionary process of PSII from cyanobacteria to higher plants (22).

Different genera in Cyanidiales have different extrinsic PSII subunits. *Cyanidium caldarium* has PsbO, PsbU, PsbV and PsbQ′ as their extrinsic subunits, while *Cyaniodioschyzon merolae* has four different extrinsic subunits - PsbO, PsbU, PsbP and PsbQ (22). However there is no knowledge about the extrinsic subunits of PSII in *Galdieria*. Considering the unique position of *Galdieria* among other Cyanidiales, a detailed study on PSII membrane subunits in general and extrinsic subunits in particular might provide some answers about the evolution of extrinsic subunits in PSII and would provide a more complete picture of the PSII extrinsic subunits of all the genera under Cyanidiales.

In the past ten years, there are several articles published on isolation of PSI and PSII from several photosynthetic organisms (36-38, 42-45). In some of those articles, procedures are outlined for isolation of partially pure PSI and PSII membrane proteins, but they involve complex and time consuming sucrose density gradient centrifugation method, a method not suitable for large scale purification, an essential prerequisite for protein crystallization studies. Also, more than one detergent was employed for isolation of these photosynthetic membrane complexes, which is not favorable for crystallization and structural studies. In this work, we developed a simple, fast and large scale purification method, an essential criteria for obtaining large amounts of PSI and PSII for biochemical, biophysical and crystallization experiments. The method we have developed, address these issues, by using only one detergent β-DDM (n-dodecyl-

β-D-maltoside) and feature a fast performance liquid chromatography for PSI and PSII purification. Using this method both PSI and PSII are separated by the anion exchange chromatography step with further purification of PSI and PSII by separate runs using size exclusion chromatography.

MATERIALS AND METHODS

Galdieria cell culture

Galdieria sulphuraria cells were grown at 42^0 C in 11 L capacity flasks containing 1X (see appendix A) medium at pH 2, with a constant supply of air, air and 2% CO_2 and illumination at 25 μmol photon m^{-2} s^{-1} (Li-cor, model LI-189) (Fig. 2-1).

FIGURE 2-1 *Galdieria* cell culture in 11 L flasks**.**

Cells were monitored frequently by taking absorption spectra of cells (400-800 nm) and optical density of the cells was measured at 730 nm. Light intensity was increased accordingly with an increase in cell density. The cell cultures were started either from a cell stock frozen at -80^0C or by using fresh cells from the

previous cell culture. Cells were harvested at regular intervals after they had reached an optical density of between 1.0 and 1.2 in 12 to 14 days. Cells were harvested by centrifugation in a Sorvall SLA-1500 rotor (Dupont, Wilmington, DE) at 2500 rpm (950 x g) for 2 min at 25^0 C.

Isolation and purification of PSI and PSII

Harvested cells were homogenized in MMCM buffer (20 mM MES pH 6.0, 10 mM $CaCl_2$, 10 mM $MgCl_2$ & 500 mM mannitol) and protease inhibitors (1 mM PMSF and 1 mM Benzamidine) were added before breaking of cells. For thylakoid preparation, cells were disrupted by using glass beads (0.5 mm dia) in beadbeater cell homogenizer (BioSpec products, Inc., OK, USA) (Fig. 2-2). The beater was spun for for 30 sec for 14 times with a break time of 1 min in between. Cell suspension along with glass beads were washed with MCM buffer (20 mM MES pH 6.0, 10 mM $CaCl_2$, 10 mM $MgCl_2$), followed by centrifugation in a Sorvall SLA-1500 rotor (Dupont, Wilmington, DE) at 14,000 rpm (29806 x g) for 10 min at 4^0C to remove unbroken cells and glass beads. Thylakoid membranes were homogenized with MMGCM buffer (MMCM + 20 % glycerol) (glycerol was added for the stabilization of PSII) and solubilized in the same buffer using 1.25 % n-dodecyl–β-D–maltoside (β- DDM) in dark for 20 minutes at room temperature. The solubilized membrane protein detergent complexes was separated from membrane portions by ultracentrifugation in a 70Ti rotor (Beckman Coulter Inc., Fullerton, CA) at 50,800 rpm (265145 x g) for 90 minutes at 4^0C.

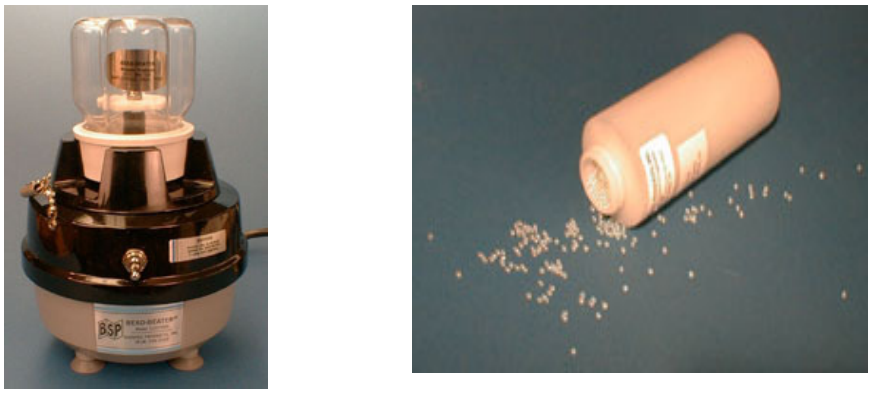

FIGURE 2-2 Bead beater and beads.

All column and chromatography column run was performed under green light at 4^0C: Buffer A (20 mM MES pH 6.0, 10 mM $CaCl_2$, 10 mM $MgCl_2$, 20 % glycerol and 0.02% β-DDM; Buffer B (buffer A + 125 mM $MgSO_4$). The supernatant obtained from ultracentrifugation was loaded on anion exchange column (XK26/20, GE health care, NJ, USA) packed with Q-sepharose high performance (GE health care, NJ, USA), pre equilibrated with 96% buffer A and 4 % buffer B. The column was run at a flow rate of 6 ml/min. After the sample has been loaded in the column, it was washed with 4 % buffer B to remove phycobiliproteins in an isocratic mode for 8 min (0.5 column volume), followed by an increase in salt concentration from 4 to 14 % B in 30 seconds to elude PSI. A washing step with 14% B was performed for 35 minutes (2.3 column volumes), PSI was completely eluded of the column and PSI fractions were collected. After completely washing PSI of the column with 14 % B, the salt concentration was increased with a second step gradient from 14 % to 27 % B in 30 seconds followed by an isocratic step at 27% for 30 minutes (2 column volumes) to elude PSII. Fractions of both PSI and PSII were individually pooled and concentrated

using Amicon ultra-15 ultra concentrator (Millipore Corporation, MA) in a centrifuge (Allegra 25R, Beckman Coulter Inc., Fullerton, CA) in a TS-5.1-500 swinging bucket rotor at 4000 rpm (3401 x g) at 4^0C. The concentrated samples of PSI and PSII were further purified separately by size exclusion chromatography column (XK16/70, GE health care, NJ, USA) filled with Superose 6 material (Amersham Biosciences, USA). PSI was purified using AKTA FPLC system (GE healthcare, NJ, USA), whereas PSII was purified using Waters 600E-system controller (Waters Corporation, Milford, MA) with a flow rate of 1 ml/min. In the size exclusion column, Buffer C1 (20 mM MES pH 6.0, 10 mM $CaCl_2$, 10 mM $MgCl_2$, 20 % glycerol and 0.02% β-DDM and 17.5 mM $MgSO_4$) & Buffer C2 (20 mM MES pH 6.0, 10 mM $CaCl_2$, 10 mM $MgCl_2$, 20 % glycerol and 0.02% β-DDM and 33.75 mM $MgSO_4$) were used for removing impurities of PSI and PSII, respectively. PSI and PSII fractions were concentrated in Amicon ultra-15, as mentioned before. Purified proteins were either used directly for experiments or they are stored in the same buffer in liquid nitrogen for future experiments.

Visible spectrum

Visible spectra of *galdieria* cells and purified photosystems (PSI and PSII) were determined at room termperature in a DU 640 spectrophotometer (Beckman Coulter Inc., Fullerton, CA). Visible spectra were recorded with 0.5 nm step size, 600 nm/min scan speed. The Chl*a* concentration of both photosystem preparations were determined at room temperature after extraction of chlorophylls in 80% (v/v) acetone using $\varepsilon_{(664 - 700)}$ = 76.8 $mM^{-1}cm^{-1}$ and measuring absorptions at 664 and 700 nm as described in (46).

Galdieria PSI SDS-PAGE

A SDS 10% tricine gel was ran in a Bio-Rad cell (Mini Protean Tetra) to determine protein composition and purity of the *Galdieria* PSI-LHCI preparation, according to the procedure outlined in (47). Briefly, the anode running buffer consists of 100 mM tris base (pH 8.9) and the cathode running buffer consists of 100 mM tris base, 100 mM tricine and 1.0% SDS with no pH adjustment. The gel contains two parts each with a different density. One was 4% acrylamide (stacking gel) which is where the samples were loaded while the second was 10% acrylamide (separating gel). The separating gel is polymerized first and then the stacking gel is polymerized on top of the separating gel. Purified *Galdieria* PSI-LHCI samples were mixed with 3µL of 4x SDS sample buffer (26.7% SDS, 4 mL H_2O, 133 mM Tris pH 8.0, β-mercaptoethanol, 26.7% glycerol, and 133µM Bromophenol Blue) and denatured on an incubator at 56°C for 15 minutes. As a reference, PSI crystals from the cyanobacteria *Thermosynechococcus elongatus* were also loaded. For this 3µL of crystal suspension was added to 9µL of water. 9µL of this suspension was added to 9 µL of SDS sample buffer. Samples were then loaded into the wells and run at 50 volts for 30 minutes to cross the stacking gel. The voltage was increased to 150 volts in order to cross the more dense stacking gel at for one hour and stained with Coomassie Blue. *Galdieria* PSI-LHCI from three different preparations was loaded on to the gel. Precision plus protein standards (Bio-Rad Laboratories, Inc., CA, USA) were used for determining the apparent molecular masses.

Synchotron radiation CD spectrum of PSI

Circular dichroism (CD) spectroscopy is a valuable tool for secondary structure analysis of proteins. In recent years, its has been possible to use synchrotrons as light sources for CD, with the technique being known as Synchrotron Radiation Circular Dichroism (SRCD) (48). In comparison with conventional CD, SRCD have several advantages: the flux from a synchrotron light source remains higher at lower wavelength (which are more sensitive to secondary structure differences), higher signal to noise ratio (small amounts of material) and less signal averaging (stronger signal) (49). Synchotron radiation CD spectra (SRCD) spectra were collected on beamline CD1 at the ISA facility, University of Aarhus, Denmark. Instrument parameters were set as follows: step size 1nm, averaging time 2s, wavelength range 280 - 170 nm and temperature 20^{o}C. Samples were loaded into demountable Quartz SUPRACIL cells (Hellma UK LTD) with optical pathlengths of 9μm for *G. sulphuraria* PS I (3mg/ml) and 100 μm for *T. elongatus* PS I (0.83 mg/ml). Three replicate scans were averaged and subtracted from 3 replicate scans of the buffer baseline and the final spectra were calibrated using a spectrum of camphorsuphonic acid obtained after each beam fill (50). Data processing was carried out using the CDTool software and the spectra were analyzed using the DICHROWEB server (51, 52). The final values are the averaged results from the different secondary structure prediction algorithms CONTINLL (53) SELCON3 (54) and CDDSTR (55) using dataset SP175 (56).

Galdieria PSII SDS-PAGE

Sodium dodecylsulfate polyacrylamide gel electrophoresis (SDS-PAGE) was done with a SDS-PAGE, Pharmacia Phast system (GE healthcare, NJ, USA) using precast SDS-HD gels (GE healthcare, NJ, USA). *Galdieria* PSII samples were mixed with sample buffer (20 mM Tris/HCl, pH 6.8, 2 mM EDTA, 5 % SDS, 0.2 % DTT) resulting in a Chl*a* concentration of 20 to 60 µM. After incubating the sample at 56^{o}C for 15 min, 1 µL of the sample was applied per lane. Precision plus protein standards (Bio-Rad Laboratories, Inc., CA, USA) were used for determining the apparent molecular masses. After the gel is finished running, it was rinsed with water and transferred to a setting solution (12.5 % glutaraldehyde) and allow it to equilibrate in a rocker for 60 minutes. After 60 minutes, the gel was rinsed with water for 5 minutes and transferred to the silver staining solution (1 % silver nitrate) and equilibrate for 60 minutes in a rocker. As the solution is light sensitive, the container along with the gel and silver stain solution is covered with aluminium foil. The gel was washed with water for 5 minutes and transferred to the developer solution (0.25 % formaldehyde, 6.25 % sodium carbonate). After the appearance of bands and gel is developed sufficiently, transfer the gel immediately to fixing solution (10 % glycerol, 10 % acetic acid), so that the gel does not become overdeveloped.

Galdieria PSII oxygen evolving activity

The intactness of manganese cluster can be determined by measuring the oxygen evolving activity of the isolated PSII from *Galdieria*. Oxygen evolution measurements were conducted at room temperature using oxygen electrode

(Hansatech Instruments, UK). The electrode was calibrated using air-saturated and nitrogen saturated water. For oxygen evolution, sample was illuminated with 36 red light emitting diodes. The buffer used contained 100 mM PIPES-NaoH, pH 7.0, 5 mM $CaCl_2$ & 0.03 % β-DDM and sample concentration was diluted to a chlorophyll concentration of 20 to 50 µM. Artificial electron acceptor (250 mM benzoquinone in 100 % DMSO) and donor (10 mM potassium ferricyanide in water) were added along with buffers, for continuous occurrence of water-splitting reaction. The oxygen activity increased with each stage of PSII purification and the oxygen activity of the crystals is higher than the published result, indicating a higher intactness of the Mn cluster in crystals.

RESULTS AND DISCUSSION

Cell growth and isolation of PSI and PSII

Using the current cell growth set up, a cell density of 1.2 OD was obtained within 10 to 12 days and about 60 to 80 g of cells could be harvested from 10 L of culture (Fig. 2-3).

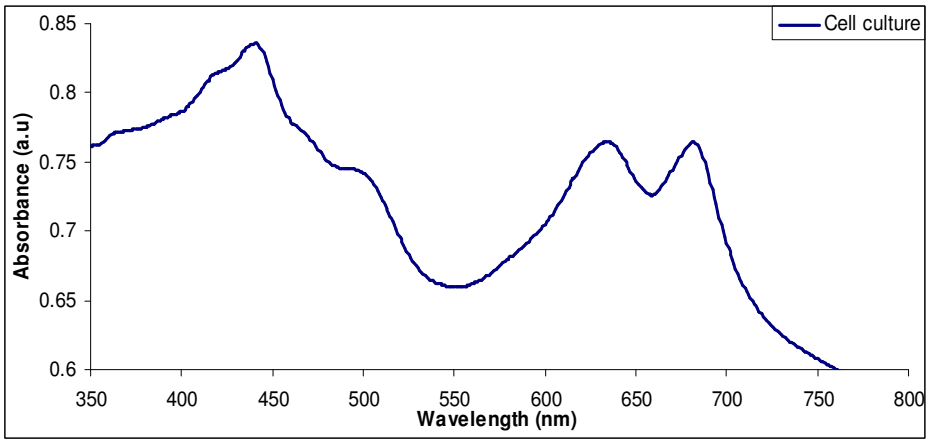

FIGURE 2-3 Absorption spectra of *Galdieria* cell culture.

Similar high cell densities and harvest have been reported previously for *Galdieria* cell cultures(57). In comparison with *T.elongatus* cultures (0.8 g/L), ten times more cell yield can be obtained (8 g/L) from *Galdieria*.

The detailed procedure developed for solubilising and purifying PSI and PSII is described in the materials and methods section. Briefly, thylakoid membranes were solubilized with 1.25 % β-DDM and the solubilized protein-detergent complexes were separated from thylakoid membranes by ultra-centrifugation. *Galdieria* PSI and PSII were purified by a chromatographic procedure using Q-sepharose (anion-exchange) in the first step and Superose 6 (size exclusion) in the second step to remove impurities (Figs. 2-4 to 2-6). With the procedure we had developed, we are able to purify active photosystems within 10 hours starting from the cell breakage.

After extensive optimization, we had developed a step gradient, where PSI eludes first and PSII eludes second in the same anion exchange column run. In this procedure, phycobilisomes do not bind to the column and they elude without contaminating PSI or PSII. Initially, we had thought that the PSI of *Galdieria* might not have light harvesting complexes attached to it. But SDS-tricine gel of purified *Galdieria* PSI confirmed the presence of LHCI proteins in *Galdieria* PSI (Fig. 2-7) (see chapter 3, for ultra-fast fluorescence spectroscopy and mass spectrometry results of *Galdieria* PSI-LHCI). Both PSI and PSII was purified separately by s second column run in a size exclusion chromatography column. Figure 2-5, shows the size exclusion chromatogram of PSI–LHCI supercomplex. In the chromatogram there are two peaks: the first peak which eludes at ~ 60

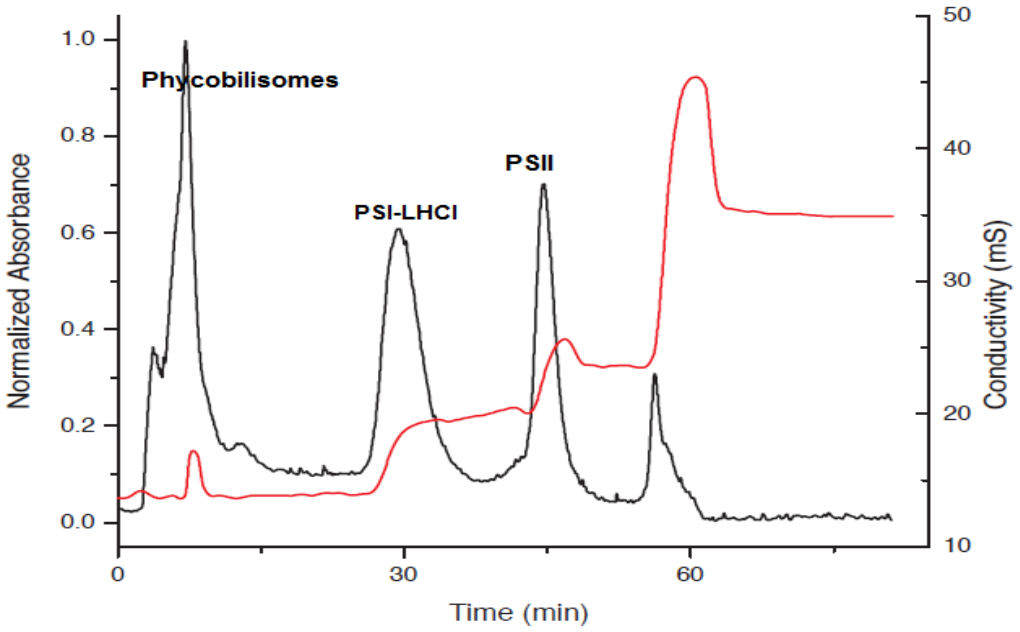

FIGURE 2-4 Anion exchange chromatography of PSI-LHCI and PSII. Black solid line: Absorption at 280 nm; Red solid line: conductivity.

minutes of the column run is the pure *Galdieria* PSI-LHCI superomplex and the second peak which eludes at ~ 80 minutes contains partially disassembled PSI-LHCI supercomplex.

PSI-LHCI supercomplex of green algae (see chapter 5) are not purified by strong anion exchange chromatography and they are generally purified by sucrose gradient ultra-centrifugation, a mild and a gentle purification procedure. This is because the LHCI proteins of green algae are not tightly bound to the PSI core and they fall apart during a chromatography (anion exchange and size exclusion) run. But in *Galdieria*, PSI-LHCI supercomplex are extremely stable and intact even after one anion exchange and two size exclusion chromatography runs. This clearly shows that LHCI proteins of *Galdieria* are tightly bound to the PSI core (see chapter 3, for more details).

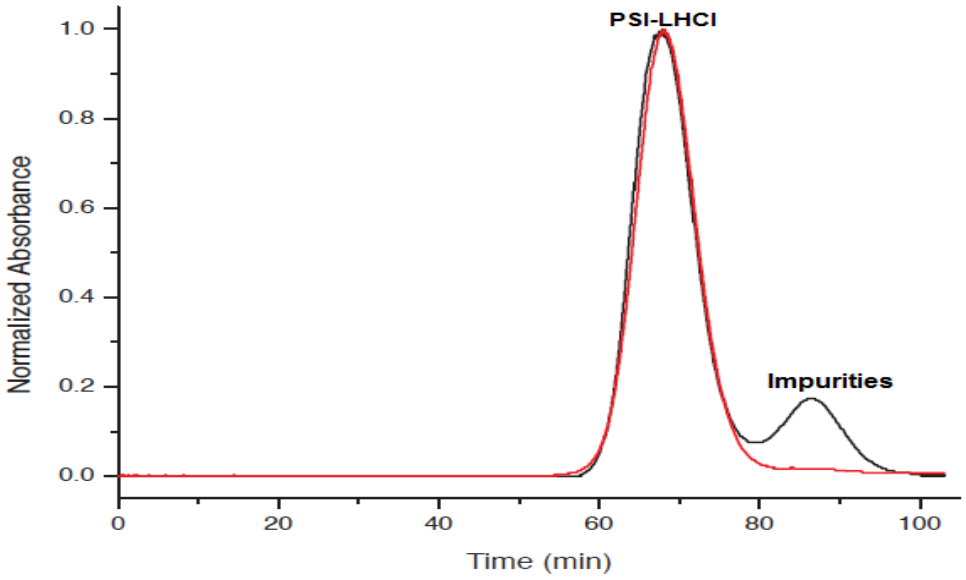

FIGURE 2-5 Size exclusion chromatography of PSI-LHCI with absorption at 280 nm. Black solid line: First size exclusion chromatography of the concentrated PSI from anion exchange chromatography; Red solid line: second size exclusion chromatography of the concentrated PSI fraction from the first size exclusion chromatography.

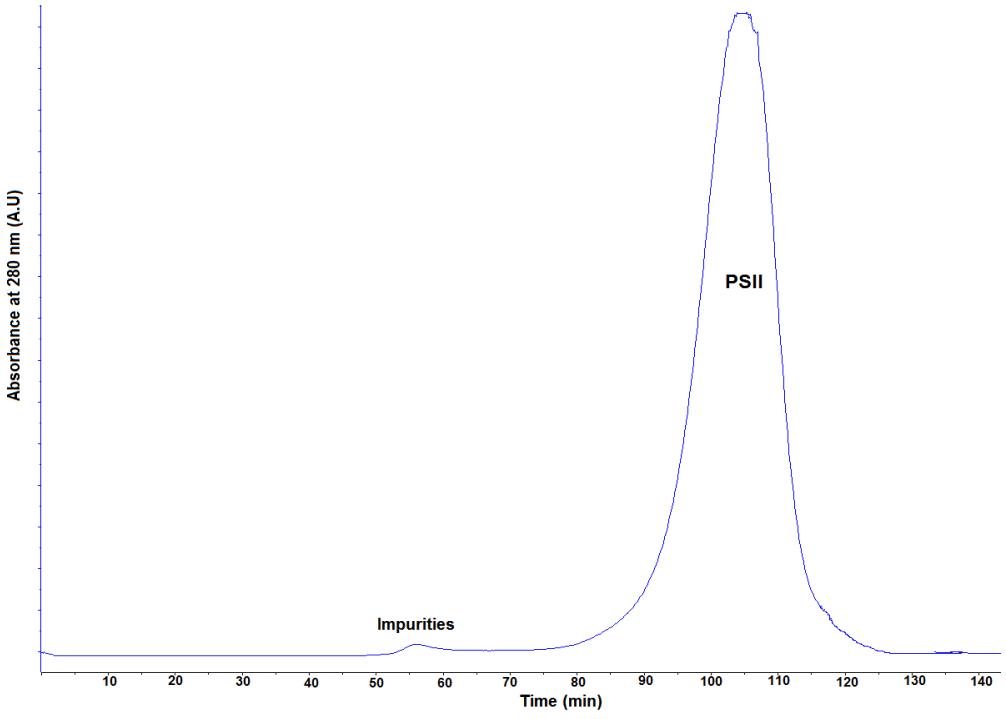

FIGURE 2-6 Size exclusion chromatrography of PSII with absorption at 280 nm

Visible spectrum

The visible spectrum of both purified PSI-LHCI and PSII is shown in Fig 2-7. The spectrum shows characteristics of PSI and PSII absorption. PSI-LHCI spectra shows absorption maxima at 678 nm with the peak tilted towards the blue region. PSI-LHCI absorbs above 700 nm due to the presence of red chlorophylls (see chapter 3). PSII spectra shows a absorption maxima at 674 nm, with the peak tilted towards the blue region, with no absorption above 700 nm and a characteristic shoulder peak around 410 nm due to the presence of pheophytin in PSII.

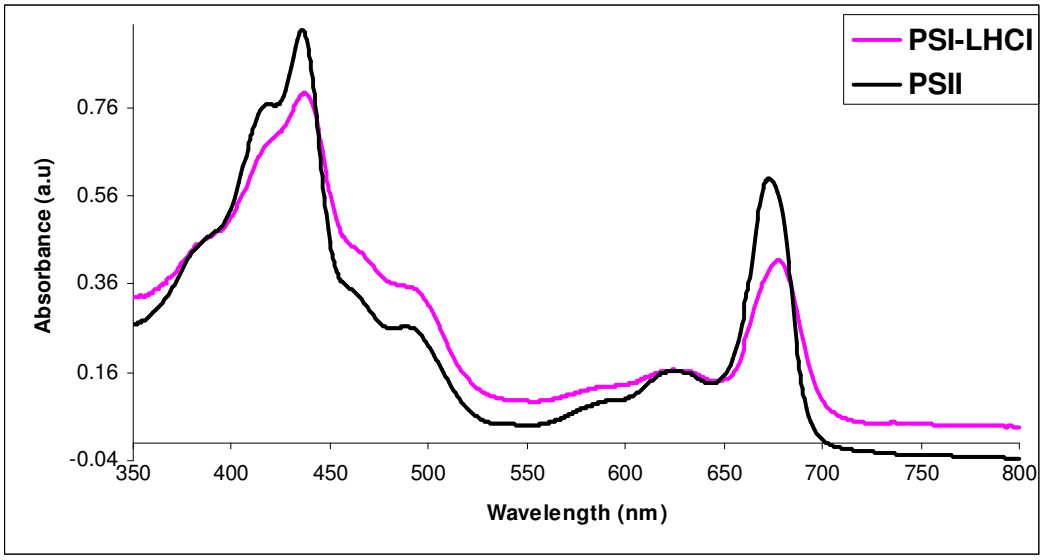

FIGURE 2-7 Absorption spectra of *Galdieria* PSI-LHCI and PSII at room temperature

***Galdieria* PSI SDS-PAGE**

For further characterization, SDS-PAGE was carried out on purified PSI-LHCI samples to know its molecular composition (Fig. 2-8). Comparison of *Galdieria*

PSI–LHCI lanes with *T.elongatus* PSI lane clearly showed the presence of light harvesting proteins (lhcr) in *Galdieria*. Five genes for lhcr proteins were identified in *Galdieria* genome: Lhcr1 has a molecular weight of 29 kDa and the other lhcr proteins (lhcr 2 to 5) has an apparent molecular weight of ~20kDa and several strong bands were seen in the *Galdieria* PSI lanes around 20 kDa.

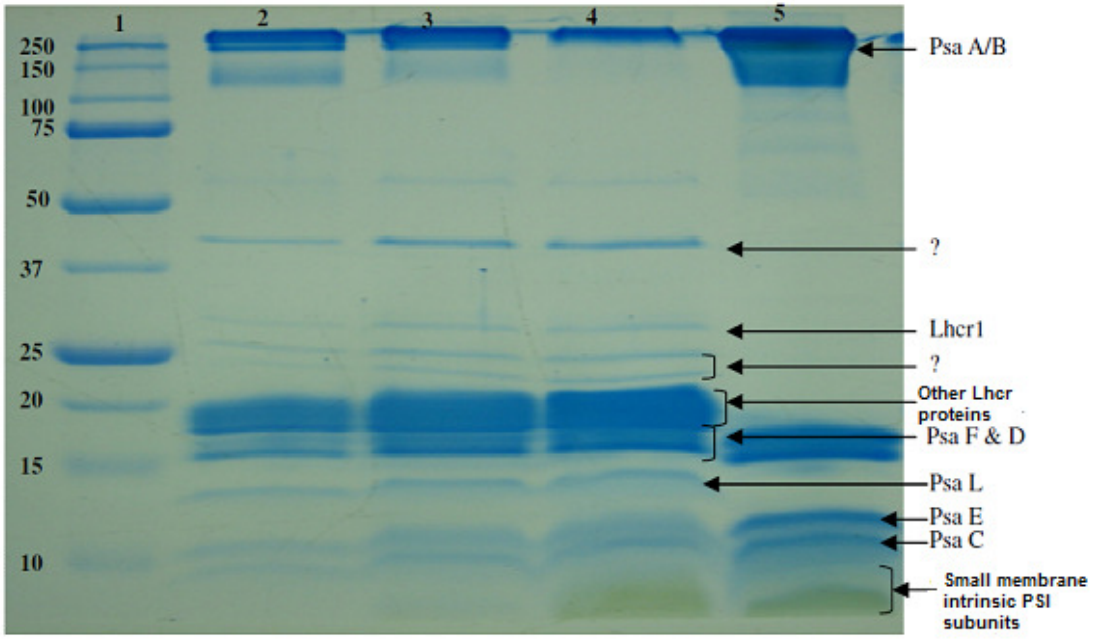

FIGURE 2-8 10 % SDS-tricine gel of *Galdieria* PSI-LHCI. Lane 1: Molecular weight markers; Lane 2: *Galdieria* PSI-LHCI; Lane 3: *Galdieria* PSI-LHCI; Lane 4: *Galdieria* PSI-LHCI; Lane 5: PSI crystals of *Thermosynechococcus elongatus*. *Galdieria* PSI-LHCI from different preparations are loaded in lanes from 2 to 4. ? represents unidentified subunits in *Galdieria* PSI.

T.elongatus PSI has no lhc proteins and correspondingly there are no bands around 20 kDa. From the gel, PsaA, PsaB, PsaF, PsaD, PsaL, PsaE, PsaC and other smaller PSI subunits were visible in *Galdieria* PSI-LHCI. Subunit, PsaL stained stronger in *Galdieria* PSI-LHCI than *T.elongatus* PSI. In addition to the known subunits, *Galdieria* PSI-LHCI contains additional subunits that so far have

not been identified. These bands could represent small impurities or potential new subunits of the PSI-LHCI complex from *Galdieria* (~30% of the genome is unique).

Galdieria PSI synchrotron CD spectrum

To investigate the secondary structure of *Galdieria* PSI-LHCI complex, far-UV Circular Dichroism (CD) was recorded (see materials and methods). For comparison, *T.elongatus* PSI was used as the X-ray structure has been determined for this membrane protein.

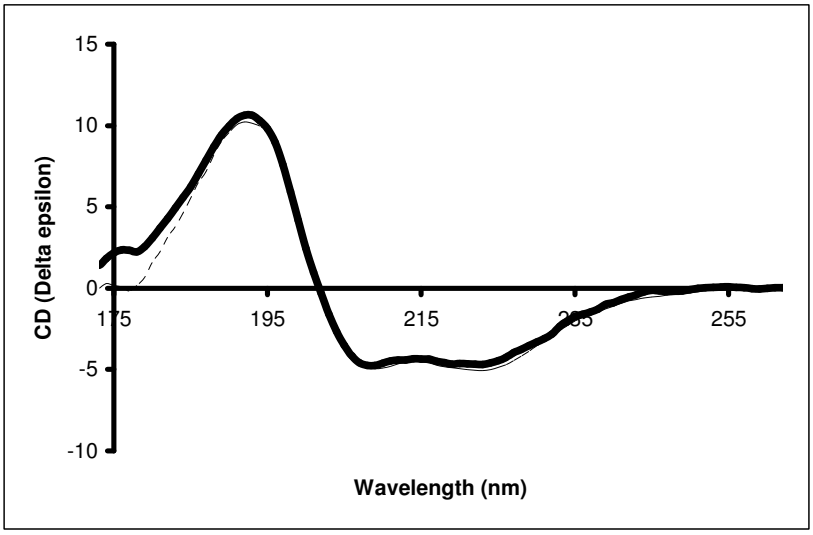

FIGURE 2-9 Synchotron CD spectra of *Galdieria* PSI-LHCI and *Thermosynechococcus elongatus* PSI. Dashed line: PSI *T. elongates*; Thick solid line: PSI-LHCI *G. sulphuraria*

CD spectra from both PSI looks similar and has a major positive peak around 190 nm and negative peaks around 208 nm and 220 nm, indicating that majority of the secondary structure is α-helical (Fig. 2-9). Secondary structure analysis using different programs showed that 50 % of the structure is α-helical, followed by β-

sheets and random coil (Table 1). As *Galdieria* PSI contains LHCI proteins (LHC proteins are not present in *T.elongatus*), we expected that *Galdieria* should have a higher α-helical % than *T.elongatus*. In contrast to our hypothesis, secondary structural analysis results showed that α-helical % is higher in *T.elongatus* PSI than *Galdieria* PSI. Secondary structure predicted for both photosystems is within the error range of each other. LHCI proteins are made of α-helical structure. This result clearly shows that even SRCD was not able to resolve the secondary structural differences between the two PSI membrane proteins.

TABLE 2-1 Secondary structural analysis of PSI

Sample	% α-helix	% β-sheet	% random
T.elongatus PSI	50 ± 3	10 ± 3	28 ± 2
G. sulphuraria PSI-LHCI	48 ± 3	13 ± 2	28 ± 2

***Galdieria* PSII SDS-PAGE**

PSII fractions from size exclusion chromatography were concentrated and molecular composition of the sample was identified using SDS-PAGE (see materials and methods) (Fig. 2-10). In the SDS-PAGE analysis of *Galdieria* PSII, CP47, CP43, PsbO, D1, D2, PsbU, PsbV , PsbE, PsbF, Psb27 and Psb28 subunits were identified. Comparison of lanes (1 to 3) with lane (5) clearly showed that *Galdieria* PSII subunit compositions might be different than *T.elongatus* PSII. From the gel, it is hard to confirm or identify the PSII subunits of *Galdieria*, and further work is needed to reveal the identity of different bands and PSII subunit

composition is described in chapter 4. Subunits Psb27 and Psb28 were not identified initially, but high resolution mass spectrometry data helped in the identification of these subunits.

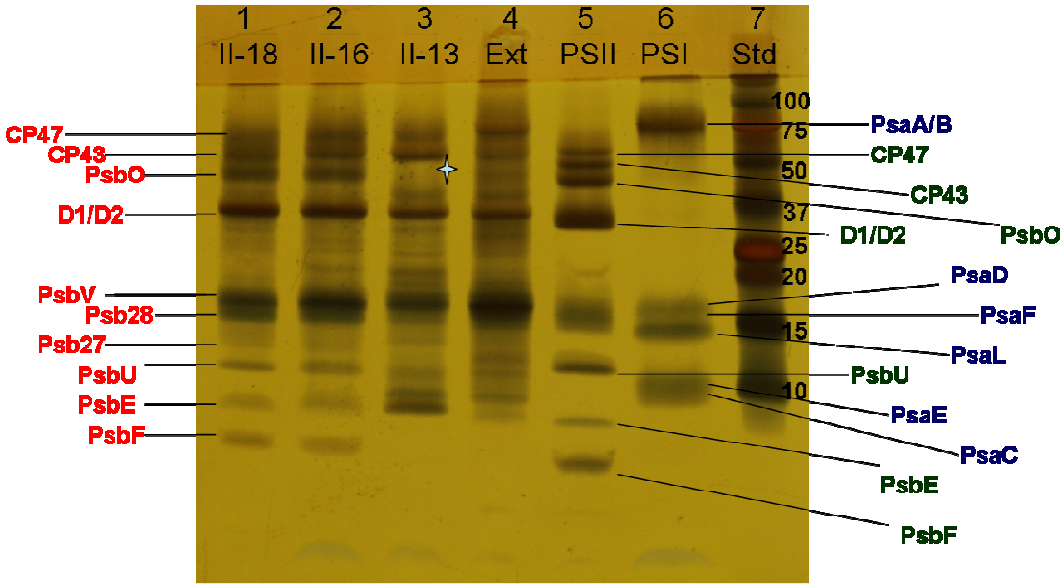

FIGURE 2-10 SDS-PAGE of *Galdieria* PSII. Lanes 1 to 3: *Galdieria* PSII from different preparations; Lane 4: *Galdieria* thylakoid extract; Lane 5 *Thermosynechococcus elongatus* PSII crystals; Lane 6: *Thermosynechococcus elongatus* PSI crystals; Lane 8: Molecular weight standard. Color code – red represents the PSII subunits from *Galdieria*; Blue represents the PSI subunits of *Thermosynechococcus elongatus*; Green represents the PSII subunits of *Thermosynechococcus elongatus*.Star in lane 3, indicates the loss of PsbO subunit in early PSII preparation, but present in later *Galdieria* preparations after optimization of isolation conditions.

Galdieria PSII oxygen evolving activity

To know the water splitting activity of isolated *Galdieria* PSII, oxygen evolution was measured under continuous light. The values are obtained at different stages of PSII isolation are shown in Table 2. For comparative purpose, PSII sample from *Thermosynechococcus elongatus* was used.

TABLE 2-2 Oxygen evolution activity (μmol O_2/mg Chla hr) of photosystem II

Sample	Organism	
	Thermosynechococcus elongatus	*Galdieria sulphuraria*
Thylakoid extract	185 - 250	115 - 182
Purified PSII	1280 - 1450	850 - 1220

Values are ranges obtained from at least three independent measurements for each sample type from different PSII preparations.

Both thylakoid extract and purified PSII from *Galdieria* has oxygen evolving activity much less than the *Thermosynechococcus elongatus* PSII. But the oxygen evolving activity for *Galdieria* is similar or slightly lower than the PSII oxygen evolving activity from other organisms (43, 45, 58).

In *Thermosynechococcus elongatus* PSII preparation, crystallization was used as a tool for purification and no size exclusion chromatography was involved. In case of *Galdieria* preparation, we focused on rapid purification of both PSI-LHCI and PSII membrane proteins involving size exclusion chromatography, a possible reason for low oxygen evolving activity of *Galdieria* PSII. This result shows that further optimization is required for isolation of PSII from *Galdieria*. The oxygen evolving activity measurements are from the PSII samples isolated from early PSII preparations. Figure 2-10 clearly showed that in early preparations (lane 3 in Fig. 2-10), PsbO subunit was lost. But after optimization of PSII isolation, PsbO was present in later preparations (lane 1 and

2), which would improve the oxygen evolving activity of isolated PSII from *Galdieria*. Additionally, we are yet to identify the crystallization conditions of *Galdieria* PSII. Once we had identified the crystallization condition, we can use crystallization as a tool for purification (in place of size exclusion chromatography), similar to PSII purification from *Thermosynechococcus elongatus*. This might improve the oxygen evolving activity of *Galdieria* PSII.

CONCLUSION

The cultivation of *Galdieria sulphuraria* was optimized for maximum yield of photosystem I and II. The method described here allows rapid purification of photochemically active PSI-LHCI and PSII membrane protein complexes from the thermo-acidophilic redalga, *Galdieria sulphuraria* in the same anion exchange column run. The isolated *Galdieria* PSI-LHCI supercomplex was stable and intact (after one anion exchange column run and two size exclusion column runs) in comparison with other eukaryotic PSI-LHCI supercomplexes (see chapter 3). For *Galdieria* PSII, further optimization of the isolation conditions are required. By using only one detergent (β-DDM) throughout the whole purification procedure, the formation of uniform micelles of known composition was ensured providing a homogenous starting material for further experiments (see chapter 3 and 4).

CHAPTER 3 EFFICIENT LIGHT HARVESTING IN A DARK, HOT, ACIDIC ENVIRONMENT: THE STRUCTURE AND FUNCTION OF PSI-LHCI FROM GALDIERIA SULPHURARIA

INTRODUCTION

Photosynthetic eukaryotes have light-harvesting complexes (LHCI and LHCII), which absorb light energy and transfer it to the reaction center of photosystems (PSI and PSII). Light harvesting proteins are nuclear encoded and in most cases they consist of membrane intrinsic proteins with three transmembrane helices. Light harvesting proteins bind different types of chlorophyll (Chl) and carotenoid, depending upon the organism. Despite our extensive knowledge of PSI-LHC supercomplexes from other eukaroyotes, relatively little is known about the PSI-LHC of rhodophytes (red algae). It has been proposed that *Galdieria* and its relatives belong to a line of red algae that diverged early from main lineage. So this chapter focuses on the structure and composition of PSI-LHCI supercomplexes from *Galdieria* by electron microscopy (EM) and liquid chromatography with tandem mass spectrometry (LC-MS/MS) and also to interrogate their light-harvesting function by ultrafast optical spectroscopy published in Thangaraj et al. (November 2010) in Biophysical journal.

A more detailed introduction introduction on photosynthesis, photosystems *and Galdieria sulphuraria* were described in chapter 1. Briefly, our current knowledge of the photosystems of *Galdieria sulphuraria* is minimal, and is mostly inferred from studies of other Cyanidiales. A recent study analyzed the

genes encoding PSI proteins in *Galdieria* and compared them to the cyanobacterial and eukaryotic PSI complexes (9), concluding that *Galdieria* PSI might be similar to a common ancestor of PSI from cyanobacteria, green algae and plants. Five *lhc* (*lhcr1-lhcr5*) genes have been reported to be present in the *Galdieria* genome, of which one (*lhcr4*) has been confirmed by N-terminal sequencing (39). Results from this study have shown that Lhcr4 has a transit peptide of 44 amino acids, with a molecular mass of 20574 Da for the mature protein (185 amino acids).

MATERIALS AND METHODS

Cell culture, PSI-LHCI isolation and characterization

Galdieria sulphuraria cells were grown at 42°C in 11 L flasks containing a 10X medium at pH 2.0, with a constant supply of air and 2% CO_2 and illumination at 25 µmol photon m^{-2} s^{-1} (Li-cor, model LI-189) (57). A more detailed description of the isolation and purification of PSI-LHCI from *Galdieria sulphuraria* is mentioned in Chapter 2. Briefly, cells were harvested by centrifugation at 2500 rpm for 2 min at 25°C. Harvested cells were homogenized in MM buffer (20 mM MES pH 6.0, 10 mM $CaCl_2$, 10 mM $MgCl_2$ & 500 mM mannitol) and 1 mM PMSF was added before cells were broken. Following cell lysis using a bead beater (Biospec products Inc., OK) and washing, the thylakoid membranes were solubilized by 1.25 % n-dodecyl–β-D–maltoside (β-DDM) at room temperature. Thylakoid membranes were centrifuged at 58,000 rpm for 90 minutes and the detergent-solubilized PSI-LHCI was further purified from the thylakoid extract by anion exchange chromatography with a step gradient, followed by size exclusion

chromatography as described in (18). PSI (crystals) of *Thermosynechococcus elongatus* used in this study for comparative purposes were isolated and purified as described in Fromme and Witt (59). Similarly, PSI-LHCI of *Chlamydomonas reinhardtii* used in this study for comparative purposes is described in detail in chapter 5.

Low temperature fluorescence emission spectra

PSI samples were adjusted to 10 μM Chl with Tris buffer (pH 7.5) containing 60 % glycerol and 0.02 % β-DDM and the emission spectra was measured at 77 K with a FLUOROMAX-3 spectrofluorometer between 600 and 800 nm using excitation at 468 nm.

Differential extinction co-efficient of *Galdieria* P700

We determined the differential extinction coefficient of P700 by flash-induced absorption changes of P700 due to a redox reaction with N,N,N,N-tetramethyl-*p*-phenylenediaminedihydrochloride (TMPD) using the method published previously (60). PSI complexes were diluted to a final chlorophyll concentration of 40 μM in a buffer containing 100 mM Tricine (pH 8), 10 mM $CaCl_2$, 10 mM $MgCl_2$, 0.02% β-DDM and 800 μM TMPD. The reaction of PSI with $TMPD^+$ was performed in an anaerobic cuvette with a 1 cm path length. Before the measurements, the buffer was degassed and the sample loaded, in an anaerobic chamber. The flash induced absorbance difference spectra of P700 and TMPD were recorded at room temperature using JTS-10 LED kinetic spectrometer (Bio-Logic, Grenoble, France). The sample was excited by actinic light (650 nm), intensity 3000μE/m^2/s duration 10 ms. We used interference filters at 703 nm and

573 nm for P700 and $TMPD^+$ accordingly. Since we measure at 703 nm, for the calculation of the extinction coefficient at 700 nm the absorption was normalized based on the dual beam spectrophotometer readings. As a control, the same method was applied to *T. elongatus* PSI samples. Extinction coefficient values of between 10.6 and 12 mM^{-1} cm^{-1} (60, 61) have been published for oxidized TMPD, so an extinction coefficient range was given for *Galdieria* PSI-LHCI complex and *T. elongatus* PSI. Chlorophyll (Chl a) concentrations were determined after extraction with acetone/water (4:1, v/v), by using an extinction coefficient of 76.79 mM^{-1} cm^{-1} at the Q_y maximum of 664 nm (46).

Dual-beam spectrophotometer

The Chl *a*/P700 ratio of *T. elongatus* PSI and *Galdieria* PSI-LHCI supercomplexes was determined by measuring P700 oxidation. The proteins were suspended in a buffer containing 20 mM MES, pH 6.4, 100mM $MgSO_4$ and 0.02% β-DDM. The sample (4 ml) was equally divided between two glass cuvettes (2 ml each). 10 µl ascorbate (0.5M) was added to one cuvette and 10 µl potassium ferricyanide (0.1 M) was added to the other. The absorption difference spectrum (reduction-oxidation) was measured between 650-850 nm using a Cary dual beam spectrophotometer. The differential extinction co-efficients obtained for *Galdieria* PSI-LHCI was employed for quantitation of the Chl *a*/P700 ratio (62) .

Mass-spectrometry and data analysis

Galdieria PSI samples were precipitated with cold acetone (-20°C) to remove lipids, detergents chlorophyll and other cofactors. The precipitated protein was

recovered by centrifugation (10,000×g) and the supernatant removed. The protein pellet was dissolved in 90% formic acid for immediate injection into an HPLC system prepared for reversed phase chromatography. column preparation, fraction collection, mass spectrometry instrumentation set up for intact proteins and data analysis for those was performed as described elsewhere (63, 64). Selected fractions from LC-MS+ were trypsin digested, analyzed by nano LC-MS/MS and the obtained mass spectrometry data were analyzed by Mascot software (Matrix Sciences, London, UK) as described previously (64).

Electron microscopy and single particle analysis

Samples of purified PSI-LHCI complex were diluted with buffer (20 mM MES pH 6.4, 100 mM Mg_2SO_4, 10 mM $CaCl_2$ and 0.03% β-DDM) to a final concentration of ~6 μM and negatively stained with 2% uranyl acetate on glow-discharged carbon-coated copper grids. Electron microscopy was performed on a Philips CM120 electron microscope equipped with a LaB6 tip, operated at 120 kV. In total, 925 electron micrographs were recorded with a Gatan 4K slow-scan CCD camera at 130,600× magnification with a pixel size (after binning the images) of 2.3 Å at the specimen level. GRACE software was used for semi-automated specimen selection and data acquisition (65). The 38,859 single particle projections (128 × 128 pixel frame) were subjected to multi-reference alignment and reference-free alignment procedures, multivariate statistical analysis and hierarchical ascendant classification, all routines within the GRoningen Image Processing (GRIP) software package (66). The final two-dimensional projection maps of the presented PSI views were calculated from the

best-resolved classes using the correlation coefficient determined in the alignment step as a criterion. The final sums were made by summing about 30% of the class members, with the correlation coefficient in the alignment step as a parameter.

Ultrafast fluorescence spectroscopy

Fluorescence decay kinetics were measured using an ultrafast streak camera, as described previously (67-69). Briefly, the sample was illuminated by 130 fs pulses from a mode-locked Ti:S laser (Mira 900, Coherent Laser Inc., Santa Clara, CA) pumped by a frequency-doubled Nd:YVO_4 laser (Verdi, Coherent Laser Inc.). The repetition rate was reduced to 4.75 MHz using a pulse picker (Model 9200, Coherent Laser Inc.) and the excitation light was frequency-doubled to 400 nm. To avoid singlet-singlet annihilation, the pulse energy was reduced to ~0.1 nJ using a neutral density filter. Fluorescence data were collected at a right angle to the excitation beam and focused on the entrance slit of a Chromex 250IS spectrograph coupled to a Hamamatsu C5680 streak camera with a M56757 sweep unit. Time-intensity surfaces were recorded at time scales of 0.8, 1.4, and 2 ns on a Hamamatsu C4742 CCD camera. The FWHM of the overall instrument response function (IRF) was ~6 ps at the 0.8 ns timescale, ~12 ps at the 1.4 ns timescale, and ~20ps at the 2 ns timescale. Global analysis was carried out using ASUFIT (URL: www.public.asu.edu/~laserweb/asufit/asufit.html). Experiments at room temperature were carried out in a 3×3 mm glass cuvette (Starna Cells, Inc.). Measurements at 77K used a 1.0×0.5 cm plastic cuvette in an N_2-cooled cryostat (Oxford Instruments). Samples used at 77K were diluted in 66% glycerol to ensure freezing as a transparent glass.

Time-correlated single photon counting

Fluorescence decay kinetics were also measured using the time-correlated single-photon counting (TCSPC) technique. Excitation pulses of 130 fs at 400 nm, operated at 4 MHz were obtained from a Ti:S laser coupled to a frequency doubler and pulse selector (Spectra Physics, Millennia pumped Tsunami, and pulse selector Model 3980) Fluorescence emission was collected at 90° and detected using a double-grating monochromator (Jobin-Yvon, Gemini-180) and a microchannel plate photomultiplier tube (Hamamatsu R3809U-50). The polarization of the emission was 54.7° relative to that of the excitation. Data acquisition was done using a single photon counting card (Becker-Hickl, SPC-830). The IRF had a FWHM of 45 ps, measured from the scattering of sample at 400 nm. The excitation power was kept below 100 μW to avoid singlet-singlet annihilation. The data was fitted with a sum of exponential decay model globally or at a single wavelength using ASUFIT.

RESULTS

Biochemical analysis of the isolated *Galdieria* PSI-LHCI clearly shows that the sample is of high purity with minor contaminations from phycobiliproteins. Fluorescence emission spectra of *Galdieria* PSI-LHCI supercomplexes measured at 77 K showed two shoulder peaks at 685 and 690 nm indicative of fluorescence emission from LHCI complex and a dominant peak at 723 nm a typical region of fluorescence emission from PSI (Fig. 3-1).

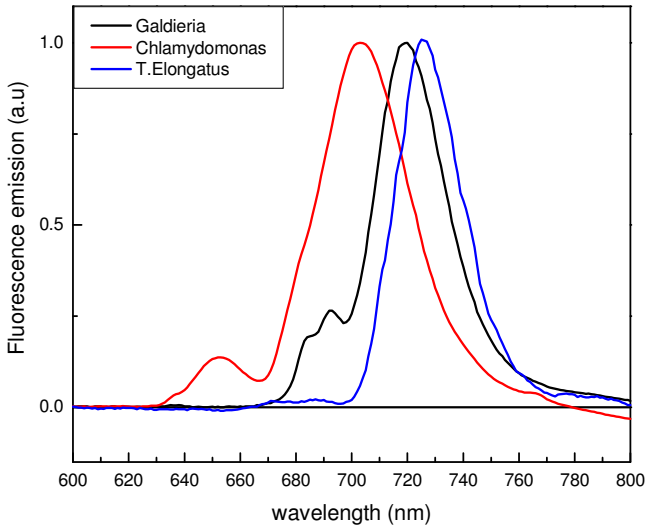

FIGURE 3-1 Low temperature flourescence emission spectra. PSI-LHCI supercomplex of red alga, *Galdieria sulphuraria* (black) and the green alga, *Chlamydomonas reinhardtii* (red), and the trimeric PSI of cyanobacteria, *Thermosynechococcus elongatus*. These samples were excited with an actinic light at 468 nm.

The spectra show no peaks at 650 nm and 660 nm, the region of fluorescence for phycobiliproteins (phycocyanin and allophycocyanin), an indication that the *Galdieria* PSI-LHCI sample does not contain significant impurities from phycobilisomes. Emission spectra from *Chlamydomonas* exhibit a major peak at 705 nm, due to fluorescence emission from PSI and a minor peak at 650 nm from Chl *b*. For *T. elongatus*, the single peak at 730 nm corresponds to a typical emission band from PSI. This figure clearly indicates that *Galdieria* PSI-LHCI has red chlorophyll pool almost similar to *T. elongatus*, with significantly more red emission than *Chlamydomonas*.

Depending upon the extinction co-efficient of TMPD used (see materials

and methods) a molar extinction coefficient of 115±5 mM^{-1} cm^{-1} was obtained for *Galdieria* PSI-LHCI complexes at 700 nm (Fig. 3-2). For *T. elongatus* PSI, an extinction coefficient of 65±5 mM^{-1} cm^{-1} was obtained.

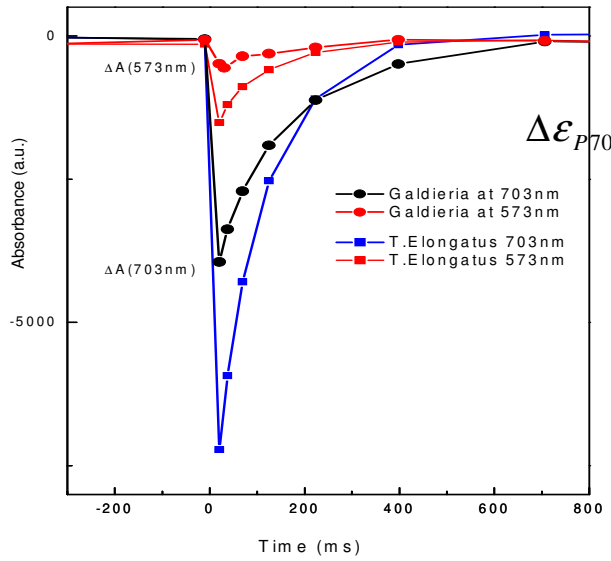

$$\Delta\varepsilon_{P700} = \Delta\varepsilon_{TMPD} \cdot \frac{\Delta A(703nm}{\Delta A(573nm}$$

FIGURE 3-2 P700 extinction co-efficient. The flash induced absorbance difference spectra of P700 and TMPD for *Galdieria* and *T.elongatus*. Each trace is an average of 3 different scans. The calculation of the extinction coefficient for P700 was based in the redox reaction of P700 with TMPD, using above mentioned formula.

The chemically oxidized-minus-reduced spectra of P700 for PSI-LHCI complexes of *Galdieria* and PSI trimer for *T. elongatus* are shown in Fig. 3-3. With the extinction coefficient value range obtained for *Galdieria* PSI-LHCI, the Chl *a*/P700 ratio range of 237±7 was determined for *Galdieria*, and a range of 102±7 was obtained for PSI *T .elongatus*. The Chl *a*/P700 value obtained for PSI *T. elongatus* agrees well with previous reports and the X-ray structure (70). The ratio obtained for *Galdieria*, however, is higher than the ratios reported for other red alga, *Porphyridium purpureum* (136±20) and *Cyanidium caldarium* (103±10) (71). Similar Chl *a*/P700 ratio was deduced for PSI-LHCI of the green alga *C.*

reinhardtii (217±6).

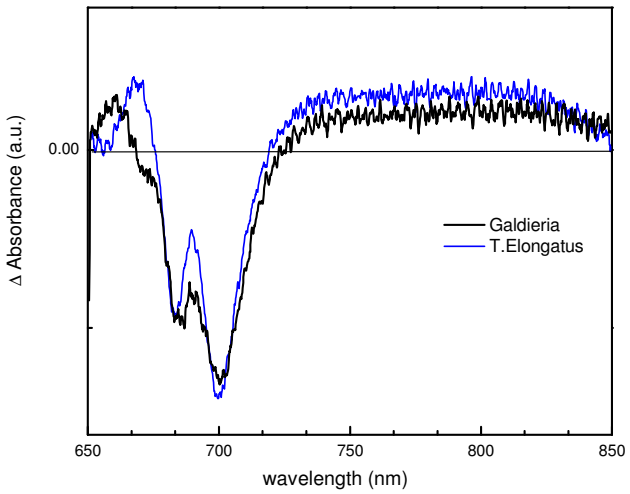

FIGURE 3-3 Oxidized minus reduced spectra of P700. Samples of *Galdieria* PSI-LHCI and *T.elongatus* PSI were suspended in 20 mM MES (pH 6.4), 100 mM $MgSO_4$ and 0.02 % β-DDM. Each trace is an average of three scans and the spectra were recorded at room temperature.

Low-resolution intact protein mass spectrometry analysis revealed the presence of all the PSI subunits (except PsaM and PsaN) and all five of the light harvesting complexes (LHCr1 – LHCr5) with different post translational modifications (data not shown). Furthermore, mass spectrometry data analysis of trypsin-digested fractions revealed the presence of at least 4 different Lhcr peptides from four of the five different light harvesting complexes identified in *Galdieria sulphuraria* (Table 3-1, Appendix B). The single LHCI peptide missing from Table 1, LHCr4, has been identified by N-terminal sequencing (39). Therefore we assume that all the five LHCr proteins are present.

TABLE 3-1 LHCr peptides of *Galdieria* identified by LC-MS analysis

Identity	Swiss – Prot database number	Accession number	Peptide	Position	P-score
LHCr1	Q9M441	CAB 75583	K.VPPVLAHDVYVK.T	198-209	56
LHCr2	Q8RW55	CAC 87422	R.EPGYFGFDPLGLGK.N	159-172	62
LHCr3	Q9FEM1	CAC 87419	R.EPGYFGFDPLGLAK.D	166-179	84
LHCr5	Q9FEMO	CAC 87421/CAC 10534	R.LDESMPGYAGFDPLGF SDKFDVK.F	56-78	71

Electron microscopy

Single particle analysis was performed on a set of ~39,000 top-view projections of *Galdieria sulphuraria* PSI particles. The complex appears to have an oval shape in the membrane plane projection with overall dimensions of 19.6×18.5 nm (Fig. 3-4). The most prominent inner feature is an L-shaped ridge in the centre, with the corner at the upper left side; the dotted block arc shape (Fig. 3-4A-C) indicates the PsaE, PsaC and PsaD subunits of the stromal hump. Classification shows, however, that the projection maps have a slight variation in size. The map of frame A represents the largest, most abundant type of projection; the maps of frames B-C show projections with slightly smaller widths, although they share same overall shape and inner features. This is clear from the distance of the edge (see white arrowhead) to the ridge, between maps of Fig. 3-4A and 3-4B the difference is about 0.1 nm. Nevertheless, because all maps show the same prominent L-shaped inner feature and overall oval circumference, the difference

in width between maps in Fig. 3-4, A-D is likely not structure-related, but caused by a gradual tilt of particles attached to the carbon support film of the EM specimens. Indeed it is known that the roughness of the carbon support film may cause some particle tilting and a clear example is the previously analyzed cyanobacterial PSI (72). Because cyanobacterial PSI forms trimers, loss of three-fold symmetry in the top view projection directly indicates tilting. In a non-symmetric particle, such as the *Galdieria sulphuraria* PSI-LHCI complex, a possible tilt is more difficult to identify. The particles presented in Fig. 3-4, E and F have dimensions of about 17×14 nm and 16×12.4 nm, corresponding to smaller particles with a lower LHCr content.

Electron microscopy images clearly show that *Galdieria* PSI-LHCI is a monomer with a dense belt of LHC antenna proteins closely surrounding PSI. This result is the experimental proof of the hypothesis raised by genetic analysis that *Galdieria* PSI may contain plant-type monomeric PSI-LHCI (9). *Galdieria* PSI-LHCI also differs significantly from the complexes in higher plants and green algae; the LHCs in *Galdieria* are more functionally tightly coupled to the PSI core than in higher plants and green algae. This functional tight coupling is shown by the ultrafast spectroscopy and TCSPC result that follows.

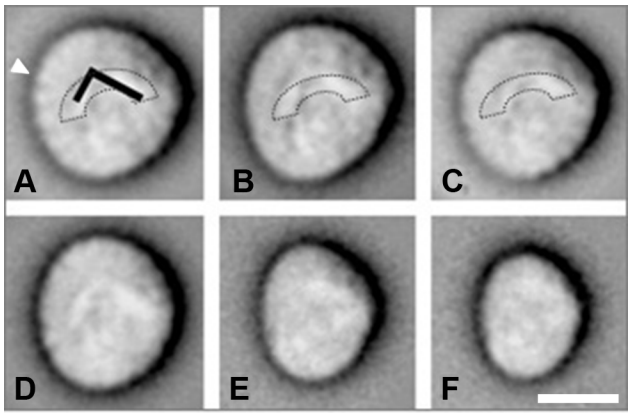

FIGURE 3-4 *Galdieria sulphuraria* PSI-LHCI single particle images. Image analyses of ~39,000 top view projections of *G. sulphuraria* PSI particles. (A-D) Most abundant particle classes observed in projection maps. (E,F) Smaller, less-abundant particle classes. The numbers of averaged particles are from A to F: 2657, 3771, 3300, 2797, 882 and 948, respectively. The scale bar is 10 nm. The position of a ridge at the core moiety is indicated by an L; the block arc shape indicates the PsaE, PsaC and PsaD subunits of stromal hump; the white arrowhead marks the side where projection map of (A) is wider than (B).

Fluorescence decay kinetics

Room-temperature fluorescence decay data were collected at timescales of 800 ps, 1.4 ns, and 2 ns; all three data sets could be satisfactorily described by three components with lifetimes of 6-13 ps, 48-50 ps, and 400-850 ps. Spectral shapes obtained from global analysis at the three timescales were very similar, and a consensus FDAS could be constructed by averaging the fitting results (Fig. 3-5A). The 6-13 ps component shows a positive peak centered at ~690 nm, representing fluorescence decay on the blue side of the spectrum at this timescale, while a negative peak centered at ~720 nm indicates an increase in fluorescence on the red side. This conservative spectral shape has been observed frequently in

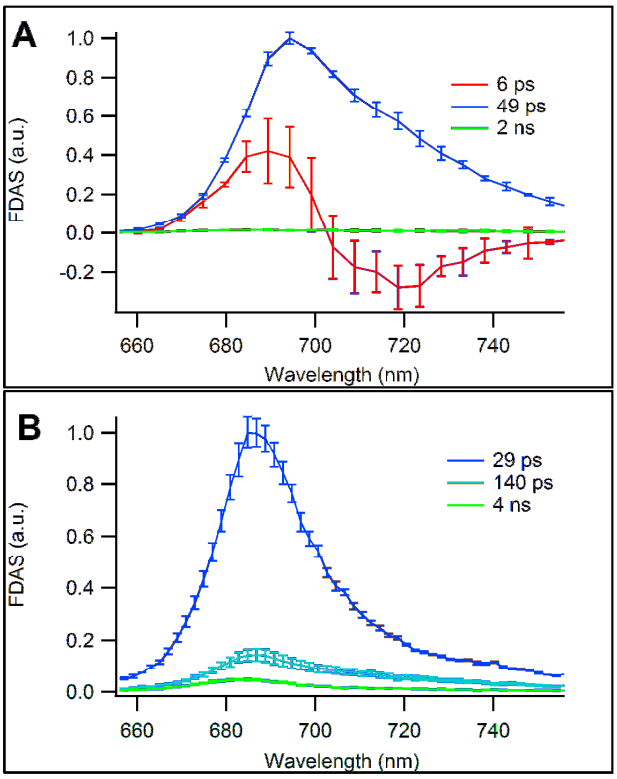

FIGURE 3-5 Representative fluorescence decay-associated spectra (FDAS) for PSI-LHCI from *Galdieria* (A) and the green alga *Chlamydomonas reinhardtii* (B) at room temperature. These spectra are averages from data collected at 800 ps, 1.5-ns, and 2-ns timescales; individual FDAS are available in the online supporting information accompanying this article. In *Galdieria* (A), the conservative 6-ps phase arises from energy equilibration; the photochemical trapping takes place in the 49-ps decay phase. In *Chlamydmonas* (B), the photochemical trapping is faster (29 ps), but is accompanied by a slow 140-ps phase that is absent in *Galdieria* samples.

spectroscopic studies of PSI and is characteristic of energy transfer from the blue pool of chlorophyll to the red-shifted chlorophylls i.e. the excitation energy transfer between pools of chlorophyll with different transition energies (21-24). The longest timescale (2 ns) showed both a longer lifetime (13 ps, rather than 6) and a less conservative spectral shape than the shorter timescales; the data collected at shorter timescales is more accurate due to better temporal resolution.

The second component shows a peak at ~695 nm and a long red tail extending out to at least 770 nm. The lifetimes obtained for this component are timescale-independent and are in the 47-50 ps range – longer than those typically seen for PSI cores, but shorter than the slow components associated with the trapping of LHCI-originated excitons in eukaryotic PSI-LHCI.

Finally, a third component was required for an accurate fit, but represents only about 2% of the overall decay amplitude. Despite the low amplitude of this component, it consistently fit to lifetimes in the 400-850 ps range, rather than the 3-7 ns range typical for uncoupled chlorophyll components. It is possible that this component arises from weakly coupled chlorophyll. It is highly unlikely, however, that this is the same type of LHCI component observed in studies of PSI-LHCI from other eukaryotes – its extremely low amplitude suggests that it probably does not represent a population of chlorophyll that receives significant initial excitation.

When the sample is cooled to 77K, the situation becomes significantly more complex. The difficulty of energy transfer out of the red-shifted states at low temperature leads to multi-exponential decay behavior that is more kinetically and spectrally heterogeneous than that seen at room temperature. Five exponential components were required to give an adequate fit to the streak camera data, but the lifetimes obtained were not extremely consistent between timescales (Fig. 3-6). This suggests that PSI from *Galdieria* contains several pools of red-shifted chlorophyll with potentially complex kinetic relationships. Because of the fairly broad range of timescales involved in fluorescence decay, there is no obvious

reason to consider the lifetimes obtained at one timescale to be universally more reliable than the others – it is probable that the shortest components will be most accurate at the shortest measurement timescale, while the longest components can be measured most accurately at the longer timescales. Despite this difficulty, comparison of the different FDAS allows us to reach consistent conclusions. The fastest component measured ranges from 7.7 to 10.1 ps, and shows a clear energy transfer character, similar to the ~6 ps component observed at room temperature. Like its room-temperature counterpart, it has a roughly conservative shape with a positive peak at ~695 nm and a much broader negative peak centered around 720 nm.

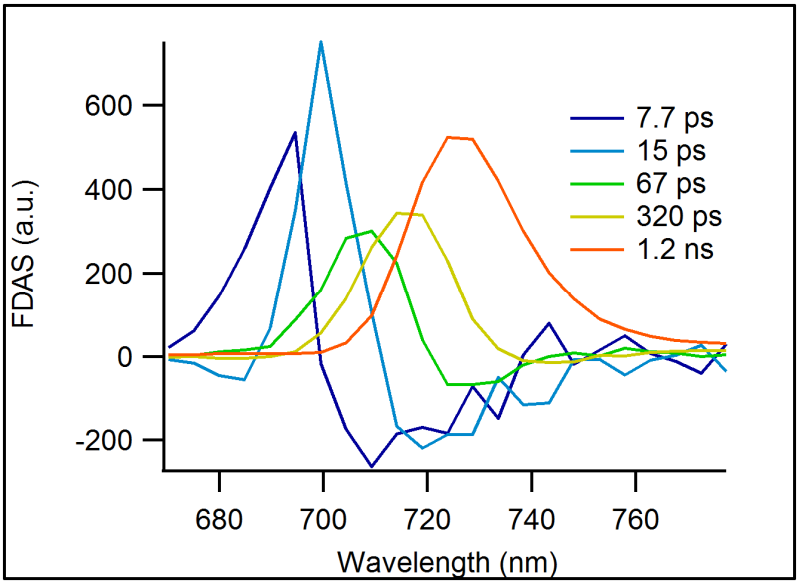

FIGURE 3-6 Representative FDAS for *Galdieria* PSI-LHCI at 77K. The first three phases represent energy equilibration between the bulk and red-shifted antenna states and within the red-shifted population; the two slowest states represent fluorescence from thermally trapped red-shifted chlorophyll sites

The second and third components also show some energy transfer character, although their lifetimes show broader variation (15-40 ps for the second, 67-160 ps for the third). As a rule, shorter lifetimes are obtained in the experiments conducted at shorter timescales, indicative of complex multi-exponential processes. These components are more consistent in their spectral shapes – the second component indicates energy transfer from a pool centered around 700-705 nm to one centered around 720-730 nm, while the third shows transfer from 710-715 nm to 730-740 nm. Of these three initial components, each successive component is shifted further to the red and shows a less conservative spectral shape, indicating a greater participation of red-shifted chlorophyll sites and an increase in trapping (possibly non-photochemical) relative to transfer with each successive component. Taken together, these indicate that the first few hundred picoseconds of fluorescence spectral evolution at 77K involve a shift from blue to red states, accompanied by increasing levels of trapping by P700 (i.e., quenching by $P700^{+}$) at longer timescales.

The fourth and fifth components also show variation in the lifetimes obtained (320-660 ps and 1.2-3.5 ns, respectively), with the longer measurement timescales yielding longer lifetimes. The 320-660 ps component shows a peak at ~720 nm and comparatively little amplitude to the red of 740 nm, while the nanosecond component peaks at ~730 nm and extends further into the red. Both components show exclusively positive amplitude, suggesting that no further energy transfer is taking place on these timescales – these components represent decay processes, either by slow transfer to P700 or effectively uncoupled

fluorescence. It is probable that these two components represent excitation decay in two distinct pools of red-shifted chlorophylls; one pool is centered at ~720 nm and is populated on a 15-40 ps timescale, while the other is centered at ~730 nm and is populated on a 67-160 ps timescale. As before, the more red-shifted spectral features are associated with longer lifetimes, consistent with a situation in which sites with lower transition energies are more kinetically disadvantaged at low temperatures. Comparison with the steady-state 77K spectrum (Fig. 3-1) shows that the small spectral features between about 680 and 700 nm correspond to positive lobes of the rapidly-decaying phases, while the major peak centered at about 720 nm arises from the slow-decaying components.

Fluorescence delay kinetics measured by TCSPC was used to confirm the results from ultrafast fluorescence spectroscopy. TCSPC recorded from 650 nm to 780 nm with a 10 nm interval. Four exponential components are necessary to fit the decay curves over the entire wavelength region (8 $\pm$ 1 ps, 60 $\pm$ 10 ps, 140 $\pm$ 10 ps, and 3.5 $\pm$ 1 ns) (Fig. 3-7). The TCSPC results further confirmed the kinetics for energy equilibration and the overall trapping processes obtained from the streak camera experiments. The first two decay components, showing lifetimes of 8 ps and 60 ps, dominate the entire wavelength region measured. Their spectral and temporal profiles are very similar to those obtained from streak camera measurements. The 8 ps component shows positive amplitude at the shorter wavelengths below 710 nm and negative amplitudes at the longer wavelengths, and the 60 ps component represents the overall decay of the fluorescence due to PSI core trapping. The two long-lived components peaking around 680 nm

contribute only a few percent of the total fluorescence signal and probably originate from some loosely coupled (140 ps) and uncoupled (3.5 ns) antenna complexes.

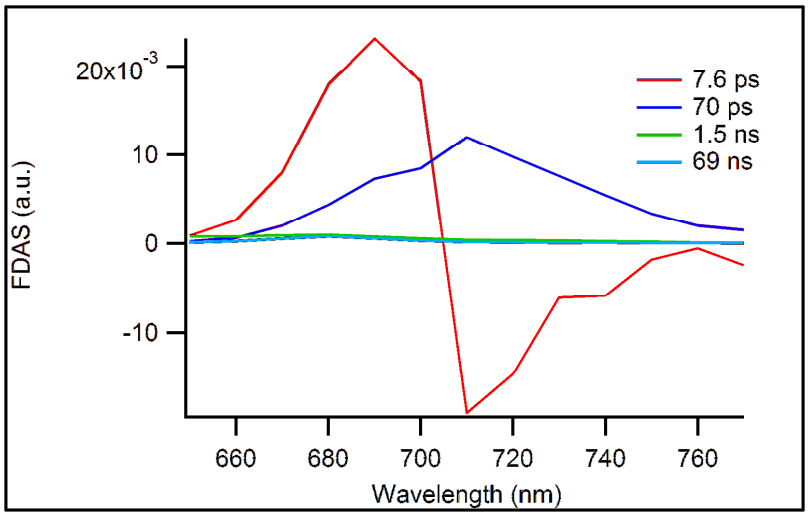

FIGURE 3-7 Fluorescence decay-associated spectra obtained by time-correlated single photon counting (TCSPC) for *Galdieria* PSI-LHCI. The two dominant components arise from downhill energy transfer (7.6 ps) and trapping by P700 (70 ps).

These two decay components likely originated from the same source as the 400-850 ps component in the room-temperature streak camera results but are better resolved in the TCSPC measurement because a higher signal-to-noise ratio can be achieved.

DISCUSSION

The analysis by single particle electron microscopy shows that the PSI complex of *Galdieria sulphuraria* is a monomeric, oval-shaped particle. Because several types of PSI complexes have been studied by high-resolution X-ray diffraction or

by lower-resolution electron microscopy, comparison may provide us hints about structural homologies and differences. PSI from a related red algal species, *Cyanidium caldarium*, has been found (36) to be somewhat heterogeneous but the largest particle had overall dimensions with a maximum size of 19×16 nm, slightly smaller than our dominant projection (19.6×18.5 nm). In the study with *Cyanidium*, cell cultures grown under high-light conditions (200 μmol photon m^{-2} s^{-1}), yielded small and medium sized PSI complexes whereas algae grown at low-light conditions (20 μmol photon m^{-2} s^{-1}), resulted in medium and bigger PSI complexes. In this study, *Galdieria* was grown only under low light conditions (25 μmol photon m^{-2} s^{-1}) and some PSI projection maps have dimensions that are similar (Fig. 3-4, C and D) or even bigger (Fig. 3-4, A and B) than the largest *Cyanidium* PSI structure. The projections shown in Fig. 3-4E and F, however, have dimensions that differ from the medium-sized (found both at high and low light conditions) and small-sized (found only at low light conditions) PSI particles from *Cyanidium*. Our *Galdieria* cell cultures are strongly inhibited at high light intensities and our work focused on low light adapted cells as this represents the ecologically relevant growth conditions for this organism.

A 2D map of PSI from the green alga *Chlamydomonas reinhardtii*, shown in Fig. 3-4B, permits a more detailed structural comparison (73). *Chlamydomonas* PSI measures 21.3×18.2 nm and comprises a monomeric core flanked by about 9 light-harvesting complexes (74). Comparison shows that both maps have similar features in the core (asterisks, Fig. 3-8, A and B), and a similar total surface area. The overall shape, however, is significantly different, with the *Galdieria* PSI-

LHCI complex being rounder and showing no visible gap between the PSI core and LHC belt. A comparison can also be made with the high-resolution X-ray structure of plant PSI (75).

Figure 3-8C shows an approximate fit of the map (green overlay). The plant structure fits in the right side of the 2D map of *Galdieria*. The fitting of the X-ray structure into our 2D map was done using the positions of similar densities in the *Chlamydomonas* and *Galdieria* 2D maps (indicated by dotted block arc shape and three astericks in Fig. 3-8, A and B) as fixed points. Details of the fitting are described in (34). The stromal ridge composed of PsaE, PsaC and PsaD is clearly visible in Fig. 3- 4, A, B and C (dotted block arc shape) and was matched with the X-ray structure position of these subunits. This indicates that *Galdieria* PSI binds at least four closely attached light-harvesting complexes. Although an exact estimation of the number is difficult, a possible estimation would lead to 7-9 LHCI/PSI. We propose that the additional LHC's form a second layer around the PSI core similar to (36), but alternate arrangements are also possible. It is clear, however, that most of the about 7-9 light-harvesting proteins, must be at one side of the core complex, similar to *C. caldarium* (36).

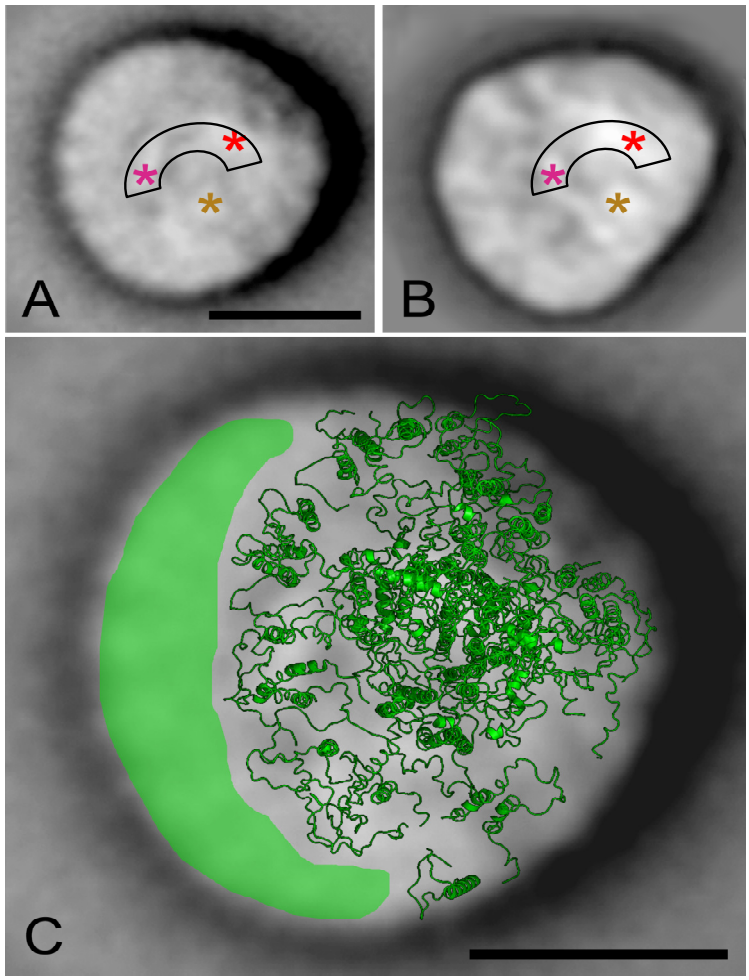

FIGURE 3-8 Comparison of *Galdieria* and *Chlamydomonas* PSI-LHCI projection maps and a global fitting of the high-resolution plant PSI structure (5). (A) *Galdieria* PSI-LHCI (B) *Chlamydomonas reinhardtii* PSI-LHCI. The asterisks and block arc mark the positions of similar densities in both maps, corresponding to core membrane extinsic subunits PsaE, PsaC and PsaD (34). (C) *Galdieria* PSI-LHCI map with the plant PSI-LHCI structure superimposed, as seen from the stromal side of the membrane. The areas marked green is suggested to be occupied by an additional number of 4-5 peripheral subunits. Scale bars equal 10 nm.

PSI particles can be broadly separated into two categories based on their fluorescence decay characteristics. Many form a single, strongly-coupled energy transfer system – this is the case in all known PSI core complexes, and their major

decay lifetimes range from about 18 ps in the green alga *C. reinhardtii* to more than 40 ps in the cyanobacterium *S. platensis* (76). Trapping lifetimes in these complexes are determined largely by chlorophyll sites whose transition energies have been lowered due to excitonic coupling; complexes with few of these "red chlorophylls" (such as *C. reinhardtii* and *Synechocystis*) show faster trapping, while those with a larger number (like *T. elongatus* and *S. platensis*) show slower trapping. Exciton transfer from these red-shifted pigments to P700 requires the system to "borrow" thermal energy from the environment; trapping from these red-shifted states shows strong temperature dependence and is often rate-limiting. In addition, the iron stress-induced PSI-IsiA complexes formed by many cyanobacteria form strongly-coupled light-harvesting systems with trapping lifetimes that can be limited by exciton migration (rather than thermally-assisted exciton escape from red sites), but are typically shorter than 50 ps (72, 77-79).

In green algae and plants, the PSI core is moderately coupled to extrinsic light-harvesting complexes such as the PSI-LHCI complexes (67, 80, 81). In addition to the fast trapping from excitons arising in the PSI core, the PSI-LHCI complexes samples of green algae and plants exhibit major fluorescence decay phases with lifetimes of 100 ps or more, which arise from excitations that begin in the extrinsic LHCI proteins and whose transfer to P700 is limited by a pigment gap at the PSI-LHCI interface.

Taken in isolation, the fluorescence decay data from *Galdieria* PSI are somewhat enigmatic – its room-temperature decay kinetics are dominated by a single trapping phase, similar to the tightly coupled cyanobacterial PSI-IsiA

complex and the PSI core complexes described above. This single trapping phase, however, is remarkably slow, and would suggest a large pool of red chlorophylls that substantially retards trapping at room temperature. At the same time, *Galdieria* is a eukaryote and is known to contain LHCI genes but the >100ps decay components typically associated with excitations beginning in LHCI appear to be missing (39). Another interpretation is suggested by the EM images; LHCI proteins are clearly visible in these images, but their association with PSI appears to be tighter than in green algae and higher plants (73, 82). This raises the possibility that exciton transfer in PSI-LHCI from *Galdieria* could be similar to the PSI-IsiA antenna system in cyanobacteria, where the addition of extrinsic antenna complexes dramatically increases the PSI absorption cross-section without introducing the substantial 100-200ps trapping components typically associated with excitons originating in LHCI (72, 77-79). The fairly slow trapping lifetime of *Galdieria* PSI is probably attributable in part to red-shifted chlorophyll sites (as in the case in *T. elongatus* and *S. platensis*). Our fluorescence emission spectra (Fig. 3-1) clearly indicate that *Galdieria* has a large red chlorophyll pool as found in *T.elongatus*. Another contribution to the slower trapping could come from the increase in the size of the antenna system and hence the lengthening of random exciton walks that terminate at P700 – a similar effect is probably responsible for the 38-ps trapping time observed in PSI-IsiA supercomplexes from *T. elongatus* (Chauhan et al., unpublished data).

These spectroscopic and structural features can be placed within an ecological context by contrasting *Galdieria* with other photosynthetic eukaryotes.

Many of these species live at fairly low cell densities and must cope with variable light conditions including photoinhibition. Higher plants and green algae, have evolved sophisticated cellular machinery for state transitions that regulate the association of LHCII with PSI and PSII based on ambient light conditions, as sensed by the redox state of the plastoquinone pool (83-85).

In contrast, *Galdieria* thrives in hot, acidic crevices, forming a dense cell layer in volcanic rocks and endolithic habitats (33). Besides being an extreme environment in terms of temperature and acidity, this habitat is also very stable and provides consistent low-light conditions. Laboratory cultures of *Galdieria* are strongly inhibited by high-light conditions (>40 μmol photon m^{-2} s^{-1}), while growth is fairly robust under low-light conditions (15-35 μmol photon m^{-2} s^{-1}) and extremely high cell densities (1.7 to 5 g of dry weight from 1L of cell culture) can be reached under photoautotrophic growth (Thangaraj et al., unpublished data). Similar high cell densities of *Galdieria sulphuraria* have been reported previously (57), while cell growth inhibition at high illumination has been observed for *Galdieria* and other Cyanidiales (86). In endolithic habitats, less than 1% of the surface photon flux is available for photosynthesis (33). These factors suggest that *Galdieria*'s photosynthetic systems may have been optimized over 1.3 billion years for low-light conditions. Consistent with this static, low-light environment, *Galdieria* lacks an LHCII gene, suggesting that it may have lost the ability to adapt to changing light conditions via state transitions. Further evidence for an antenna system adapted to static low-light conditions is provided by time-resolved spectroscopy and augmented by electron micrographs, which show a more

continuous electron density between PSI and LHCI than is seen in the more loosely-coupled complexes from green algae and higher plants. Thus, the PSI-LHCI complex in *Galdieria* forms a functionally tightly-coupled complex, in which trapping is faster and more efficient than in the PSI-LHCI complexes in green algae and higher plants.

This is consistent with a scenario in which *Galdieria* PSI diverged from an ancient photosynthetic eukaryote with loosely-attached antenna complexes which colonized static, low-light endolithic habitats and adapted to these conditions over billions of years. The selective pressure of growth under low-light conditions led to tighter functional coupling between lhcr proteins and the PSI core in *Galdieria* as increased photosynthetic efficiency was more critical for survival, possibly at the expense of regulatory flexibility via state transitions or other mechanisms.

This study has demonstrated that the oligomeric state of PSI in *Galdieria* is a monomer, with a belt of LHC proteins functionally tightly coupled to the PSI core. This is the first eukaryotic PSI-LHCI system for which a tight functional coupling has been reported. Our results indicate that, despite the broad evolutionary conservation of proteins involved in oxygenic photosynthesis, rather dramatic adaptations are possible under extreme conditions. Because of its ecological niche in a static, low-light environment, *Galdieria sulphuraria* appears to have reorganized the PSI-LHCI interface in a way that improves light-harvesting efficiency. Future studies will need to address whether the close coupling observed in this study is the result of a static, unregulatable arrangement of auxillary antenna proteins, or whether *Galdieria* possesses other means

(besides traditional state transitions) of adapting its light-harvesting machinery to variable light conditions. As more photosynthetic extremophiles are characterized in detail, we will surely learn more about the adaptive diversity that exists alongside the remarkable universality of oxygenic photosynthesis.

CHAPTER 4 CHARACTERIZATION OF SUBUNITS OF PHOTOSYSTEM II, A LARGE INTEGRAL MEMBRANE PROTEIN COMPLEX FROM GALDIERIA SULPHURARIA BY TOP-DOWN MASS SPECTROMETRY

INTRODUCTION

Mass spectrometry (MS) is an indispensable tool in proteomics research, because of its ability to analyze complex biological samples. Other techniques such as two-dimensional gel electrophoresis and protein microarrays have failed to provide an in-depth insight, as seen in mass spectrometry (87). Most of proteomic studies to-date has used "bottom up" mass spectrometry experiments. In this approach, the intact protein is cleaved into peptides using proteases (e.g., trypsin) and the unambiguous identification of proteins is carried out by an agreement between measured mass of four or five peptides with that of the calculated masses of the proteins in the database. A newer and emerging "top-down" MS approach involves gas-phase ionization of intact proteins and subsequent high-resolution mass measurement of intact protein ions. Following this, the intact proteins are further fragmented inside the mass spectrometer without prior digestion. This approach scans the entire sequence of the protein under examination, and provides a more complete characterization of protein isoforms and any post translational modifications than the bottom-up proteomics. This chapter focuses on the analysis of photosystem II (PSII) of *Galdieria* by top-down mass spectrometry. To the best of our knowledge, this is the first study to provide an extensive analysis on the identification of post translational modifications of photosystem II subunits in red

algae, in particular and in photosystem II, in general. The results of this study have been published in Thangaraj et al. (October 2010) in Proteomics journal.

Top-down proteomics uses high-resolution Fourier-transform ion cyclotron resonance mass spectrometry (FT-MS) for mass analysis of intact proteins and dissociation derived product ions for complete primary structure and post-translational modification (PTM) assignment. In recent years, top-down mass spectrometry has gained acceptance among researchers for their improved sequence coverage, sensitivity and accuracy in protein identification and modification. For wider applicability, top-down mass spectrometry should address the entire proteome including the membrane proteins that constitute 20 to 30% of the ORF's in fully sequenced genomes (87), with their important functions ranging from intracellular communication to small molecule transport. Integral membrane proteins have transmembrane regions that pose major challenges to mass spectrometry as they tend to be deficient in amino acids that carry charge and limited in solubility in aqueous solvents. Thus it can be argued that the most effective way to characterize these domains is to include them as part of the intact protein in a top-down experiment (88). To date, studies have shown that integral membrane proteins can be analyzed by ESI-MS with mass accuracies comparable to those achievable for soluble proteins, and top-down high resolution FT-MS has been demonstrated for both polyhelix bundle and transmembrane porin motifs (89-91).

In the past two decades, PSII complexes from cyanobacteria, green algae and higher plants have been extensively studied by mass spectrometry (89, 92).

Recently, high-resolution FT-ICR was applied to a number of different integral membrane proteins including polyhelix bundles and a porin (91). In this study we have systematically applied FT-MS to study the composition of PSII from the eukaryotic red alga *Galdieria*. A total of sixteen peripheral and small integral subunits were analyzed by high resolution FT-MS using both CAD and ECD, allowing assignment of precursor and product ions to mass accuracy typically less than 5 ppm. While the *Galdieria* PSII integral core complex is very similar to that of other eukaryotes, the peripheral OEC composition is more similar to cyanobacteria. The detection of five peripheral subunits including Psb27 and Psb28 in the red algal preparation may suggest heterogenous populations of PSII complexes.

MATERIALS AND METHODS

Cell culture and PSII isolation

Galdieria sulphuraria were grown at 42° C in 11 L capacity flasks containing a 10X medium at pH 2.0, with a constant supply of air, CO_2 and light irradiances of 25 μmol photon m^{-2} s^{-1} (Li-cor, model LI-189). For details on *Galdieria* cell culture, cell breakage, PSII isolation, please refer to chapter 2 (Fig. 4-1).

The original specimen referred to as *Galdieria sulphuraria* strain 074 was originally collected at Mount Lawu, Java, Indonesia and was a gift from Dr.Christine Oesterhelt, Max-Planck-Institut für Molekulare Pflanzenphysiologie, Am Mühlenberg 1, 14476 Golm, Germany, and was thought to be a single strain. But a later study to test the capacity of *Galdieria*'s growth under heterotrophic conditions revealed that there were two strains in the sample (93). Under

heterotrophic conditions, strain 074W (W -white) lost most of its pigment whereas 074G (G- green) stayed green on all substrates. After this study they are referred as strain 074G and 074W.

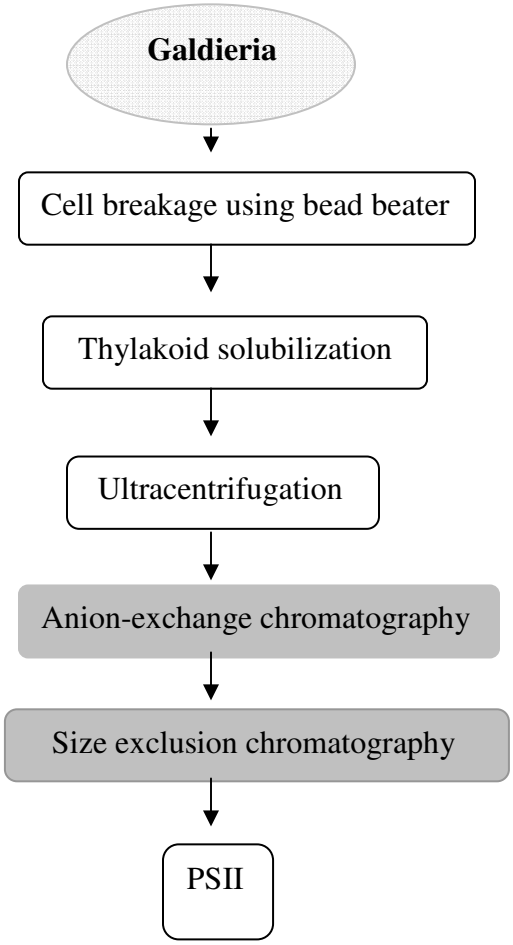

FIGURE 4-1 Flow chart summarizing the key steps in non-denaturing PSII membrane protein purification from *Galdieria sulphurararia*

Galdieria sulphuraria 074W was used to isolate PSII which is the same strain was used for the genomic sequence information. The small differences in the sequences that were revealed by our study may be due to a diversification of the

initial strain due to different growth conditions in the laboratories. The genome was sequenced from the laboratory strain that had been grown under photoheterotrophic conditions, whereas the PSII was isolated from the strain that had been maintained under photoautotrophic growth conditions since it was originally isolated.

Reverse phase column chromatography

Samples were precipitated using acetone. The suspension was split into two centrifuge tubes (125 μL each) and 1 mL 80% acetone in water (-20^{0}C stock) added to each tube, prior to vortex mixing (1 minute) and incubation at -20^{0}C for 1 hour. Precipitated protein was recovered by centrifugation (10,000 x g) and the supernatant removed. Pellets were dried briefly to allow evaporation of residual acetone (5 minutes, room temperature and pressure) and dissolved in 90% formic acid (total 100 μL) for immediate injection into an HPLC system prepared for reversed phase chromatography(63, 94). A column (5 μm, 300 Å PLRP/S, 2 x 150 mm; Varian) is previously equilibrated in 95% buffer A (0.1 % TFA in water), 5% B (0.05% TFA; 50% acetonitrile; 50% isopropanol) at 100 μL/minute at 40^{0}C for 30 minutes prior to sample injection. The column is eluted with a step gradient of increasing buffer B as previously described (63) and the eluent passed through a UV detector (280 nm) prior to a liquid flow splitter delivering 50 μL/minute to a low resolution mass spectrometer and 50 μL/minute to a fraction collector (1 minute/fraction). Fractions collected into microcentrifuge tubes were stored at –80^{0}C prior to off-line high-resolution nanospray analysis. LC-MS+ experiments were performed using a triple quadrupole instrument (AP III+, Applied

Biosystems) tuned and calibrated using a PEG mixture as previously described (89). Mass spectra were recorded by scanning from m/z 600 – 2300 with orifice voltage ramped with mass (60 – 120) using a 0.3 Da step size and a scan speed of 6 sec. Data were processed using BioMultiview 1.3.1 software (Applied Biosystems).

High resolution FT-MS mass spectrometry

HPLC fractions collected during LC-MS+ were subjected to direct infusion nanospray analysis. Samples were individually loaded into 2 μm i.d. externally-coated nanospray emitters (Proxeon, Cambridge, MA) and desorbed using spray voltage of between 1.7-1.9 kV (versus the inlet of the mass spectrometer) using the nanospray source supplied by the manufacturer. These conditions produced a flow rate of 20 – 50 nL/min. All samples were analyzed using a hybrid linear ion-trap/FT-ICR mass spectrometer (7 T, LTQ FT Ultra, Thermo Scientific, Bremen, Germany) operated with standard (up to m/z 2000) or extended mass range (up to m/z 4000). Ion transmission into the linear trap and further to the FT-ICR cell was automatically optimized for maximum ion signal. The ion count targets for the full scan FT-ICR and MS2 FT-ICR experiments were 2 x 10^6. The m/z resolving power of the FT-ICR mass analyzer was set at 100,000 (defined by m/Δm50% at m/z 400) unless otherwise stated. Individual charge states of the multiply protonated protein molecular ions were selected for isolation and collisional activation in the linear trap followed by the detection of resulting fragments in the FT-ICR cell (CAD). For the CAD studies, the precursor ions were activated using normalized collision energy settings in the range 10 - 15 at the default activation

q-value of 0.25. For ECD studies precursor ions were transmitted to the FT-ICR cell and electrons introduced with normalized energy in the range 5 -10, 10 ms duration and 50 ms delay. FTMS data was derived from an average of between 50 - 200 transient signals. The analysis of Psb27 was performed on a hybrid linear ion-trap Fourier-transform orbitrap mass analyzer (LTQ XL Orbitrap ETD; Thermo Scientific, Bremen, Germany) similarly to the LTQ-FT experiments. Thermal dissociation (CAD) was performed after the ion-trap in the C-trap (high-energy collisional dissociation; HCD). Electron transfer dissociation (ETD) was performed using fluoranthene anions produced in the instruments chemical ionization source according to manufacturer's instructions. Orbitrap product ion spectra were recalibrated using prominent *y*- and *z*- ions.

FTICR and FT-Orbitrap mass spectra were processed using ProSightPC software (ProSightPC 2.0, Thermo Scientific, Bremen, Germany) to produce monoisotopic mass lists (s/n = 1.1, fit 0%, remainder 0%, average table set to averagine) that were then assigned to protein sequences with various post-translational modifications. Protein identification was achieved by generating sequence tags (sequence tag compiler and sequence tag searching tool) and matching these tags to a *Galdieria* database. Product ion assignments for known proteins were made using the software operated in single protein mode with a 10 ppm mass accuracy threshold and with the Deltamass feature deactivated. ProSightPC reported mass accuracy of assigned monoisotopic mass values of precursor and product ions and the probability that some other database entry might match the same dataset (P score).

Galdieria PSII genomic annotation

For the identification and annotation of chloroplast-endcoded PSII subunits, a collection of all open reading frames (ORFs) identified on the two supercontigs stig_35 and stig_158 from the *Galdieria sulphuraria* Genome Project (http://genomics.msu.edu/galdieria) was prepared after closure of all gaps (K. Krause, A. Weber et al., publication in preparation). This ORF collection was searched for sequences with homology to the amino acid sequences of PSII subunits from *Thermosynechococcus elongatus* and *Arabidopsis thaliana* or other higher plants. The nuclear-encoded PSII subunit genes were identified by searching the translated *Galdieria* nucleotide databases for sequences orthologous to the remaining subunits. The presence of predicted target peptides were analysed using the TargetP 1.1 Server (http://www.cbs.dtu.dk/services/TargetP). All nucleotide sequences were conceptually translated and nucleotide as well as protein sequences were prepared for annotation in Genbank by using Sequin Version 9.50 (provided by Genbank). The accession numbers are: *psbA* - GU474525; *psbB* - GU474526; *psbC* - GU474527; *psbD*-GU474528; *psbE* - GU474529; *psbF* - GU474530; *psbH* - GU474531; *psbI* - GU474532; *psbJ* - GU474533; *psbK* - GU474534; *psbL* - GU474535; *psbM* - GU474520; *psbN* - GU474536; *psbO* - GU474521; *psbP* - GU474522; *psbQ* - GU971652; *psbQ*' – GU721104; *psbT* - GU474537; *psbU* - GU474523; *psbV* - GU474538; *psbW* - GU474539; *psbX* - GU474540; *psbY* - GU474541; *psbZ* - GU474542; psb27 - GU474524. Nuclear encoded subunits - PsbM, PsbO, PsbP, PsbQ, PsbQ', PsbU, Psb27. Chloroplast encoded subunits – PsbA, PsbB, PsbC, PsbD, PsbE, PsbF,

PsbH, PsbI, PsbJ, PsbK, PsbL, PsbN, PsbT, PsbV, Psb28 (PsbW), PsbX, PsbY and PsbZ.

Experimental design

Separate *Galdieria* PSII preparations have been analyzed by LC-MS+ four times (four biological replicates). Each top-down mass spectrometry experiment typically included CAD analyses of at least two different charge states and one ECD (ETD) experiment. Results from the experiment that yielded the most product ions are presented.

RESULTS

Chromatographic separation of PSII subunits

The primary reversed phase LC-MS+ separation yielded a retention map that was annotated with protein identities where they are known and intact masses where they remain unknown (Fig. 4-2). Mass accuracy on the low-resolution quadrupole instrument was typically 100 ppm and the spectra were used to guide targeted top-down high-resolution experiments to fully define primary structure and post-translational modifications of PSII subunits. The physical basis of the separation relies upon hydrophobicity and thus the first proteins to elute are the hydrophilic peripheral PSII subunits PsbO, PsbU, PsbV, Psb28 (PsbW) and Psb27 ('PsbZ-like'). These were followed by a set of proteins in the 16 kD class, identified as phycobiliproteins (ApcA, ApcB, ApcD, ApcF, CpcA, CpcB, CpcG) and a pair of 55 kD proteins identified as AtpA and AtpB of ATP synthase (data not shown). Association of phycobiliproteins with PSII is predictable while ATP synthase is probably a contaminant of the preparation. The remainder of the chromatogram

was dominated by elution of the small and large integral subunits of PSII spanning a substantial range of hydrophobicity, with the PsbE and PsbF subunits that bind cytochrome b_{559} eluting around 70 minutes and PsbZ not eluting until 133 minutes. Several of the small subunits (PsbF, PsbM, PsbT, PsbI, PsbH) had singly oxidized isoforms that eluted a little earlier than the unmodified population.

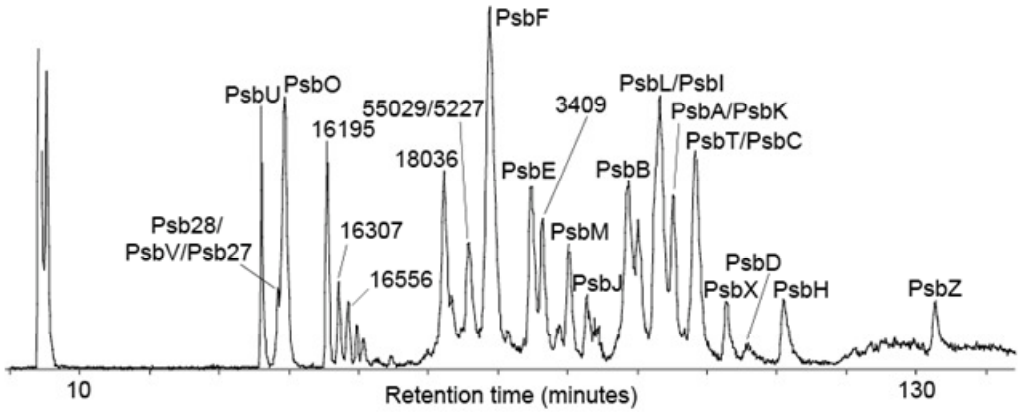

FIGURE 4-2 Reversed phase total ion chromatogram elution profile of PSII from the red alga, *Galdieria sulphuraria*. PSII proteins were precipitated with acetone and dissolved in formic acid for loading onto a reversed phase column as described in the experimental procedures. The column was eluted with a compound gradient of increasing organic concentration with eluent directed to a flow splitter for online electrospray-ionization MS and fraction collection. Total ion current was summed across the m/z range 600 – 2300 every 6 s scan (arbitrary units, linear scale). Peak heights are related to both ionization and elution efficiency of individual proteins. PSII proteins identified at different elution times are labeled. Mass of other proteins (intact mass tags) is given in Dalton (Da).

The intensity of different peaks in the total ion chromatogram shown in Fig. 4-2 is dependent on abundance and ionization efficiency and thus stoichiometry should not be inferred.

Table 4-1 lists intact mass tags (IMTs) that were assigned to PSII subunits based upon coincidence of measured average mass with calculated average mass based upon primary structure and limited post-translational modification. These assignments remain coincidental with little statistical confidence until a high-resolution top-down analysis is completed (Table 4-2).

TABLE 4-1 Average masses of PSII subunits from low resolution LC-MS+

PSII protein subunit	Genbank Accession #	# TMH[a]	Elution Time (min.)	Calculated average mass (Da)	Experimentally determined average mass (Da)	Proposed post-translational modification
Peripheral (extrinsic) subunits						
PsbO[b](33 KDa)	GU474521	0	39.4	28816.4	28821	1 – 21 removed, one disulfide bond
PsbU[b]	GU474523	0	36.1	10585.9	10587	1- 81 removed
PsbV (Cyt c 550)	GU474538	0	38.4	15704.2	15704	1-30 removed 168-177 removed + heme
Psb27[b] ('PsbZ-like')	GU474539	0	38.4	na[c]	12820	na
Psb28 (PsbW)	GU474524	0	38.9	13246.0	13247	-Met1
Smaller integral membrane subunits						
PsbE	GU474529	1	74.8	9392.5	9393	-Met1
PsbF	GU474530	1	68.8	4971.8	5015	-Met1 + acetylation
PsbH	GU474531	1	111.1	7483.9	7485	- Met1
PsbI	GU474532	1	93.2	4476.3	4505	Formyl-Met1
PsbJ	GU474533	1	82.8	3917.6	3960	-Met1+acetylation
PsbK	GU474534	1	95.1	4255.2	4256	1-8 removed
PsbL	GU474535	1	93.2	4247.9	4290	-Met1 + acetylation
PsbM[b]	GU474520	1	80.2	4599.3	4600	1-38 removed
PsbT	GU474537	1	97.8	4217.4	4245	Formyl-Met1
PsbX	GU474540	1	102.7	4534.5	4563	Formyl-Met1
PsbZ	GU474542	2	132.9	6826.4	6855	Formyl-Met1
Larger integral membrane subunits						
PsbA (D1)	GU474525	5	95.5	38160.7	38184	-Met1+ acetylation, 345-360 removed
PsbB (CP 47)	GU474526	5	88.7	56558.8	56551	-Met1+acetylation
PsbC (CP 43)	GU474527	6	97.8	50588.3	50927	1-14 removed
PsbD (D2)	GU474528	6	106.0	39344.1	39346	Met1+acetylation

[a.] Transmembrane helices, [b.] Nuclear encoded subunits, [c] Not available
Abbreviations: -Met1 – Methionine missing at position # 1; +Formyl-met1 – Formyl methionine at position # 1 in the N-terminus

Out of around 40 detected IMT's, 20 PSII subunits were assigned with different PTMs. The 3409 Da IMT eluting at 78 minutes is potentially a PSII subunit but has so far remained unidentified.

Larger integral membrane subunits

The four large subunits (PsbA, PsbB, PsbC and PsbD), which account for twenty-two of the total thirty four transmembrane alpha helices in PSII, eluted between 88 and 106 minutes along with other smaller subunits (Table 4-1). The large subunits PsbA, PsbB, PsbC and PsbD measured 38184, 56551, 50927 and 39350 Da respectively, largely consistent with their gene sequences and known N- and C- terminal post-translational modifications (Table 4-1). The experimentally determined average mass of 38184 Da for PsbA was consistent with the removal of initiating methionine at the N-terminus with acetylation of Thr 2, and removal of 15 amino acids at the C-terminus (Table 4-1) in conservation with other species. The difference of 23 Da with the calculated average mass (38160.7 Da) could be due to DNA sequence differences between strains. In PsbD, the difference between the calculated (39344.1 Da) and experimental (39346 Da) average masses is within experimental measurement error (Table 4-1). For subunit PsbB, the experimentally derived mass (56551 Da) is in good agreement with the calculated mass (56558.8 Da) taking into account the loss of initial methionine and N-terminal acetylation (Table 4-1). In PsbC, if 14 amino acids are removed to form a processed PsbC with a free N-terminus in conservation with higher plants, the calculated mass (50588.3) is lower than measured (50888 Da) by 300 Da, indicating either divergent N-terminal processing or some other DNA sequence discrepancy. Despite minor inconsistencies the intact mass tags of the larger integral subunits can be assigned with confidence. Since the main focus

of this study was to identify and characterize the smaller integral (< 10 kDa) and the peripheral subunits constituting PSII in *Galdieria* we did not perform further experiments on the large subunits.

Peripheral subunits

Of the three (PsbO, PsbU, PsbV) OEC subunits identified in *Galdieria*, PsbO and PsbU are encoded by the nucleus and carry an N- terminal signal peptide. PsbO has a signal peptide consisting of its first 21 amino acids so the mature form has 242 amino acids. The experimentally determined monoisotopic mass of 28796.7520 Da could be reconciled (Δ = 2.6387 ppm) with the calculated monoisotopic mass of 28796.67415 Da with inclusion of the formation of a disulfide bond (-2.01565 Da) between Cys23 and Cys47 (Figs. 4-2 and 4-3A). Assignment of product ions from a CAD experiment of the disulfide linked mature protein yielded 11 *y*- and 9 *b*- ion matches within a 10 ppm tolerance and a consequent P score of 1.41E-26 (Fig. 4-3A, Table 4-2). In the case of PsbU, the first 81 amino acids of the signal peptide are cleaved at the N terminus, to a form a mature protein of 93 amino acids, with a calculated monoisotopic mass of 10579.4347 Da (Table 4-2). Top-down CAD analysis of the N-terminal truncated protein confirmed the primary structure of PsbU with a experimentally determined monoisotopic mass of 10579.4648 Da, within 5 ppm of the calculated monoisotopic mass (Δ = 2.8361 ppm), and a CAD experiment yielded 32 *b*- and 23 *y*- product ions for a P score of 5.26E-75 (Fig. 4-3B, Table 4-2). The third extrinsic subunit PsbV was assigned to an intact mass tag of 15704 Da with proposed modifications including removal of 30 amino acid residues from the N-

terminus, removal of 10 residues from the C-terminus and attachment of a covalently bound heme group (615.16947 Da) (Fig. 4-2, Table 4-1). Analysis of the high- resolution CAD dataset for PsbV gave a mass difference of -2.0602 Da (-131.2860 ppm) with 11 *b*- and 15 *y*- ions matched. Further optimization of match between measured and calculated mass was reached by changing Thr 80 to Val (mature protein numbering) significantly increasing coverage with 19 *b*- and 24 *y*- product ions matched and a P score of 3.32E-45 (Δ = 5.1595 ppm) (Fig. 4-3C, Table 4-2).

Besides the 3 subunits of the OEC, 2 other peripheral subunits were identified, Psb27 and Psb28. In the primary LC-MS+ analysis, a hydrophilic protein eluted at 39 minutes with an intact mass tag of 13247 Da and was assigned as Psb28 with removal of Met1 (Fig. 4-2, Table 4-1). This protein is similar to the PsbW identified in *Synechocystis* sp. and will be referred to as Psb28 hereafter (see discussion). Psb28 was assigned to a monoisotopic mass peak of 13237.7755 Da (Table 4-2) using top-down mass spectrometry, confirming the identity and processing with 4 *b*- and 17 *y*- product ions and the precursor matched below 5 ppm (Δ = 4.6250 ppm) for a P score of 9.55E-28 (Table 4-2). The identity of Psb28 was also confirmed by ECD (Fig. 4-4) with 57

TABLE 4-2 Monoisotopic masses of PSII subunits from high resolution Fourier-transform mass spectrometry (FT-MS)

PSII protein subunit	Calculated Monoisotopic mass (Da)	Experimental Monoisotopic mass (Da)	Mass difference Delta (ppm)	P-score	Confirmed post-translational modification
Peripheral (extrinsic) subunits					
PsbO	28798.6898	28796.7520	2.6387	1.41E-26	1 – 21 removed, one disulfide bond
PsbU	10579.4347	10579.4648	2.8361	5.26E-75	1 – 81 removed
PsbV (Cyt. c_{550})	15692.8033	15692.7162	5.1594	3.32E-45	1 - 30 removed, heme (+615.16947) Thr80 to Val (- 1.972) 1-10 removed from C-terminus as in *C. caldarium*
Psb27 (PsbZ-like)	12811.4000	12811.3742	0.2939	8.93E-42 1.9E-100[a]	unknown N-terminus 1375.65 Da on Ala19
Psb28 (PsbW)	13237.6972	13237.7755	4.6250	9.55E-28 1.0E-152[a]	-Met1
Smaller integral membrane subunits					
PsbE (α-cyt. b_{559})	9386.7896	9386.8317	4.4238	2.81E-16	-Met1
PsbF (β-cyt. b_{559})	5010.6243	5010.6386	3.8488	6.95E-88	-Met1 + acetylation
PsbH	7479.1312	7479.1417	1.2749	1.53E-49	- Met1
PsbI	4501.4234	4501.4367	2.8954	6.85E-66	formylMet1
PsbJ	3957.1113	3957.1322	5.2626	3.25E-61	-Met1 + acetylation
PsbK	4252.5198	4252.5336	3.2322	2.64E-59	1 – 8 removed
PsbL	4287.2771	4287.2888	2.6928	2.15E-45	-Met1 + acetylation
PsbM	4596.4123	4596.4282	3.4407	2.21E-68	1-38 removed
PsbT	4242.3140	4242.3284	3.2844	2.23E-44	formylMet1
PsbX	4559.5632	4559.5807	3.7467	3.11E-45	formylMet1
PsbZ	6849.9577	6849.9597	0.0925	7.55E-42	formylMet1

[a.] From ECD/ETD experiments.

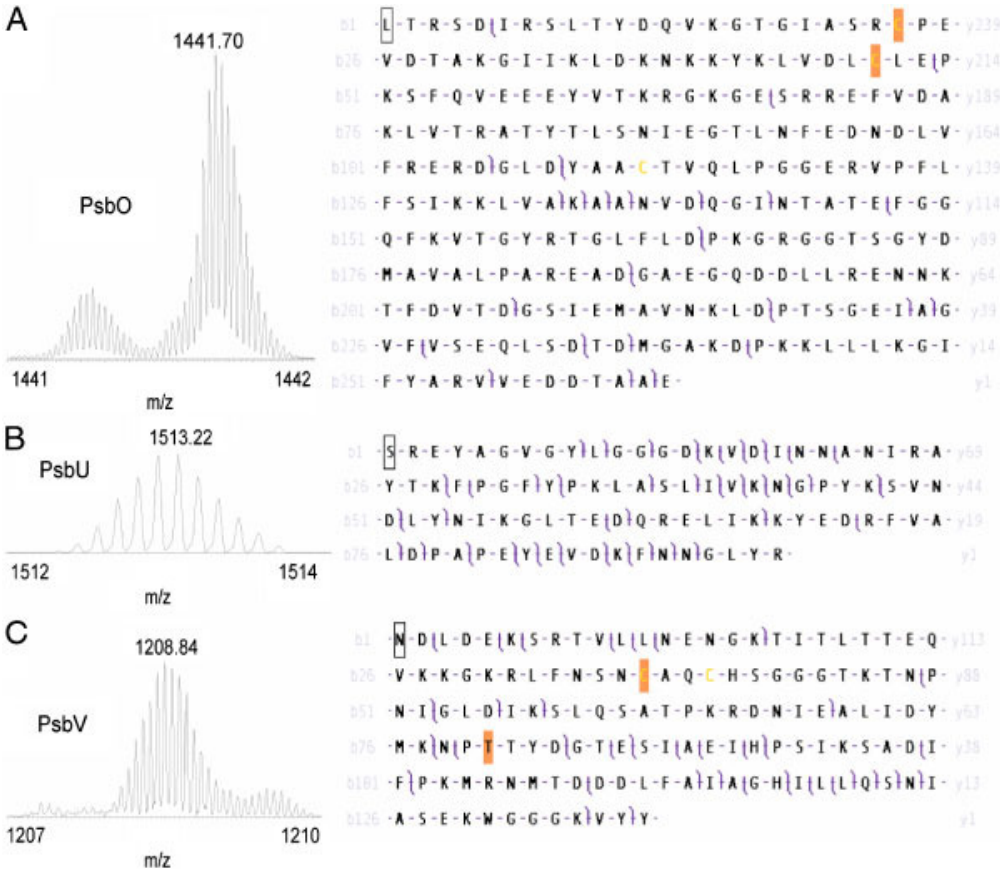

FIGURE 4-3 Top-down mass spectrometry of oxygen evolving complex subunits. Selected fractions were analyzed by static nanospray on a 7 Tesla LTQ-FT Ultra. Collisionally activated dissociation experiments on isolated precursor ions yielded complex tandem mass spectra that were matched to primary protein sequences using ProSightPC. The ion isolation used for each subunit is shown on the left while the *b*- and *y*- product ion assignments observed at 10 ppm tolerance are shown superimposed on the sequence to the right.

A. For subunit PsbO, an N-terminal signal sequence of 21 amino acids has been removed from the precursor sequence and highlighted Cys residues have been oxidized (-1.00782509 Da each) to account for disulfide bond formation. In the mature protein, 20% of product ions were matched to 19 *b*- and 10 *y*- ions giving a P score of 1.41E-26.

B. In PsbU, an 81 amino-acid signal peptide was removed from the precursor sequence. 25% of product ions were matched to 32 *b*- and 22 *y*- ions giving a P score of 5.26E-75.

C. In PsbV, 30 residues were removed from the N-terminus and 10 from the C-terminus of the precursor sequence to nominally match the measured intact mass tag. Change of Thr80 to Val optimized match of observed high-resolution precursor and product ion masses with 19 *b*- and 23 *y*- ions for a P score of 3.32E-45.

c- and 39 *z*- product ions, and agreement of calculated and measured monoisotopic masses for the precursor ion within 5 ppm (Δ = 4.6250 ppm) for a P score of 1.02E-152 (Fig. 4-4, Table 4-2). An intact mass tag of 12820 Da was assigned to Psb27 (psbz-like) using top-down mass spectrometry after attempts to assign it with low-resolution data were unsuccessful. In Fig. 4-5, we show the assignments for dissociation experiments performed on an LTQ-Orbitrap (HCD and ETD). Both experiments yield *b*- and *y*-, and *c*- and *z*- ions that support complete agreement with the C-terminal sequence over most of the polypeptide chain. However, the measured data strongly suggests that the sequence reported for Psb27 has some errors towards its N-terminus and we have therefore represented this region as an unknown modification on the Ala residue shown in Fig. 4-5 of mass 1375.65 Da to optimize *b*- and *c*- ion matches. Using this strategy we matched the experimental monoisotopic mass of 12811.3742 Da to that calculated at <1 ppm, and matched 12 *b*- and 23 *y*- ions in the CAD (HCD) experiment and 36 *c*- and 44 *z*- ions in the ETD experiment. The measured P scores for each experiment (respectively) confirm the accuracy of the identification (Fig. 4-5). The nature of the N-terminus is under further study.

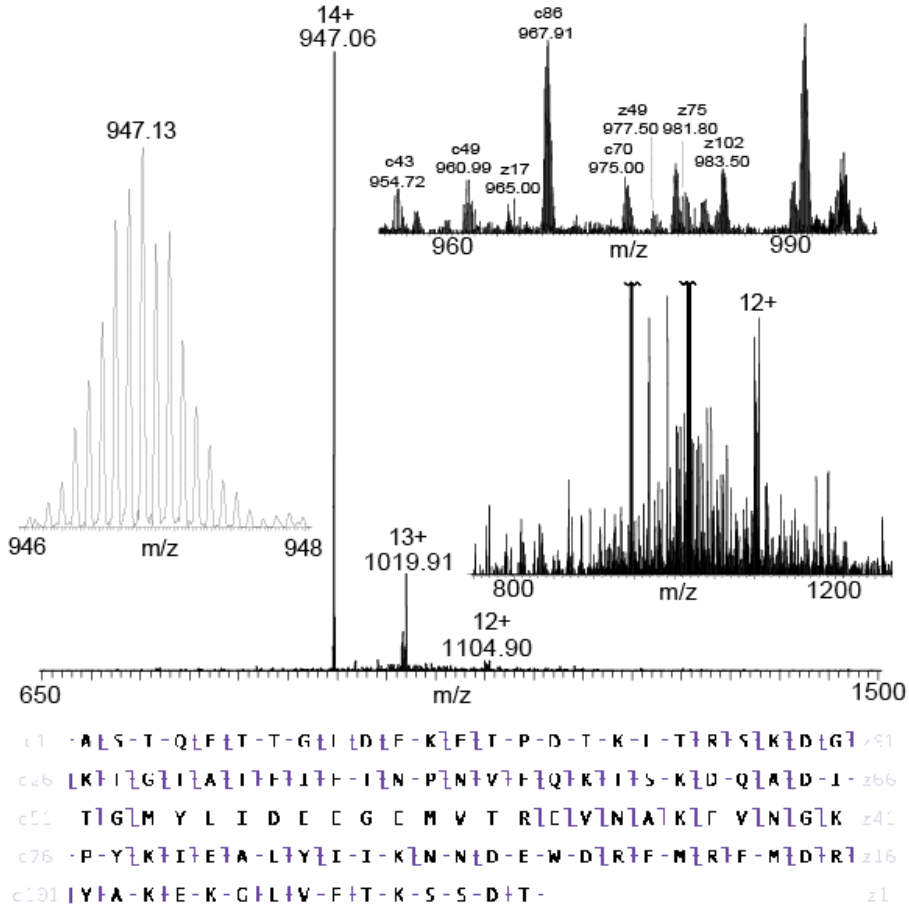

FIGURE 4-4 Top-down mass spectrometry of subunit Psb28 (PsbW). A protein of average mass 13247 Da detected by LC-MS+, was analyzed by top-down FT-MS with ECD. The 14-charge m/z 947 precursor ion was isolated as shown inset left. The product spectrum is shown from m/z 650 – 1500, expanded between in the range 800 – 1200 and expanded again in the range m/z 960 - 990. As shown in the full range spectrum, the ion current is dominated by charge reduction to 13+ and to a lesser extent 12+ species. Careful inspection of lower abundance ions nevertheless reveals a very rich product ion spectrum across the m/z 800 – 1200 range, and at higher detail between m/z 960 and 990. After removal of the initiating Met residue, 61% of the product ions were matched to 57 *c*- and 39 *z*- ions for a final P score of 1.02E-152. Selected *c*- and *z*- ions are labeled. In a separate CAD experiment on a m/z 1020 precursor ion 23% of product ions were matched giving a P score of 9.55E-28 (not shown).

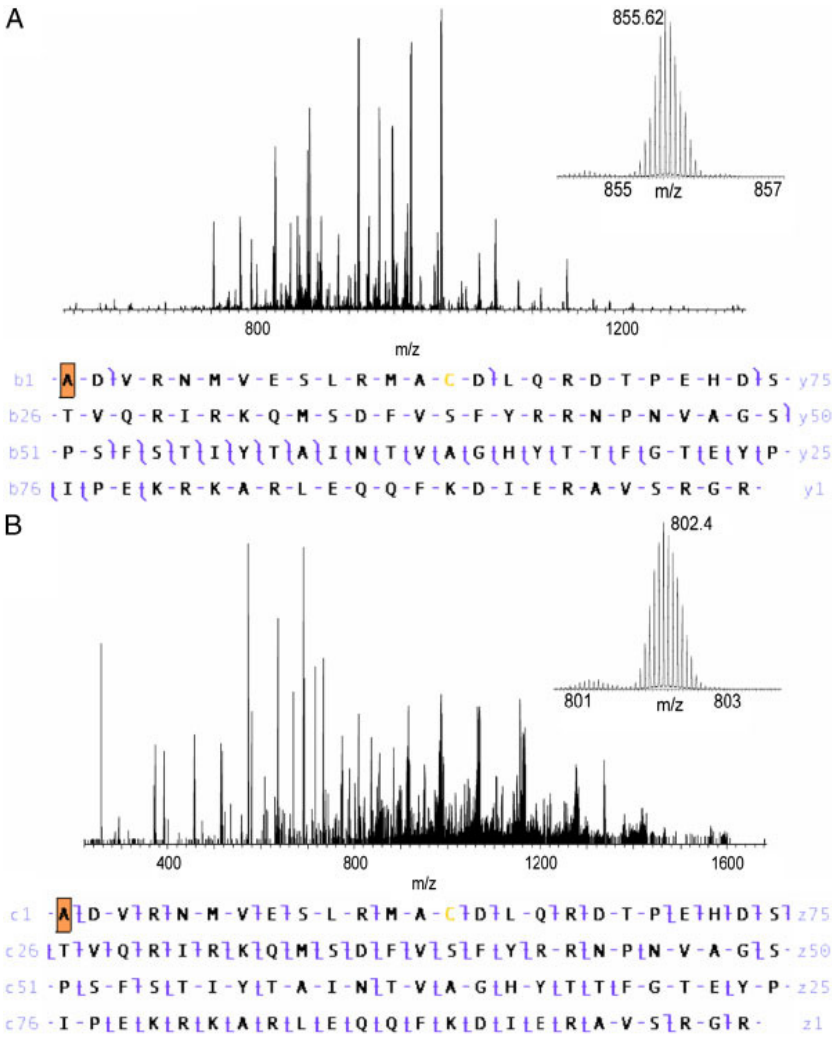

FIGURE 4-5 Top-down MS of subunit of Psb27 (PsbZ-like). A 12820Da IMT was confidently identified as Psb27 using top-down MS on an orbitrap mass analyzer with HCD (CAD) and ETD (ECD). (A) A 15-charge precursor of m/z 855 (ion isolation inset top right) was isolated and fragmented using HCD generating the compelx product ion mass spectrum shown (m/z 500-1400). The data were matched to the Psb27 sequence with the first Ala residue carrying with modification mass of 1375.65 Da to represent the as yet uncharacterized N-terminus of the protein. Briefly, 26% of product ions were matched to 12 b- and 23 y- ions for a P-score of 8.83E-42. (B). A 16-charge precursor of m/z 802 (ion isolation inset top right) was isolated and fragmented using ETD generating the complex product ion mass spectrum shown (m/z 300-1600). The data were matched to the Psb27 sequence with the first Ala residue carrying a modification of 1375.65 Da to represent the as yet characterized N-terminus of the protein. In total, 28% of product ions were matched to 36 c- and 44 z-ions for a P-score of 1.9E-100.

Considerable effort was put into finding PsbQ, PsbQ' and PsbP proteins, genes for which can be identified in the *Galdieria* genome. Attempts to match intact mass tags and top-down MS experiments in the 40 – 60 minute retention range to these sequences were unsuccessful so one minute fractions across the range 37 – 76 minutes were digested with trypsin and analyzed by nano-liquid chromatography with tandem mass spectrometry. While these experiments successfully identified many peptides from PsbO, PsbU, PsbV, Psb27, Psb28, ApcA, ApcB, ApcD, ApcF, CpcA, CpcB, AtpA, AtpB as well as some of the integral subunits there were no peptides detected for PsbQ, PsbQ' or PsbP (data not shown).

Smaller integral membrane subunits

In HPLC column run, subunits PsbE and PsbF of cyt b559 eluted at 74 and 68 minutes respectively. PsbE has 83 amino acids with a calculated average mass of 9392.5 Da in agreement with the protein eluting at 74 minutes (Fig. 4-2, Table 4-1). This protein amounts to 9393 Da, has lost its initiating methionine, with no other modifications. A top down CAD experiment confirmed the identity of PsbE without met1 and with a monoisotopic mass of 9386.8317 Da. Also the CAD dataset analysis provided 10b- and 8y- product ions as well as the precursor matched within 5 ppm (Δm = 4.4238 ppm) giving a P-score of 2.81E-6 (Fig. 4-6A, Table 4-2).

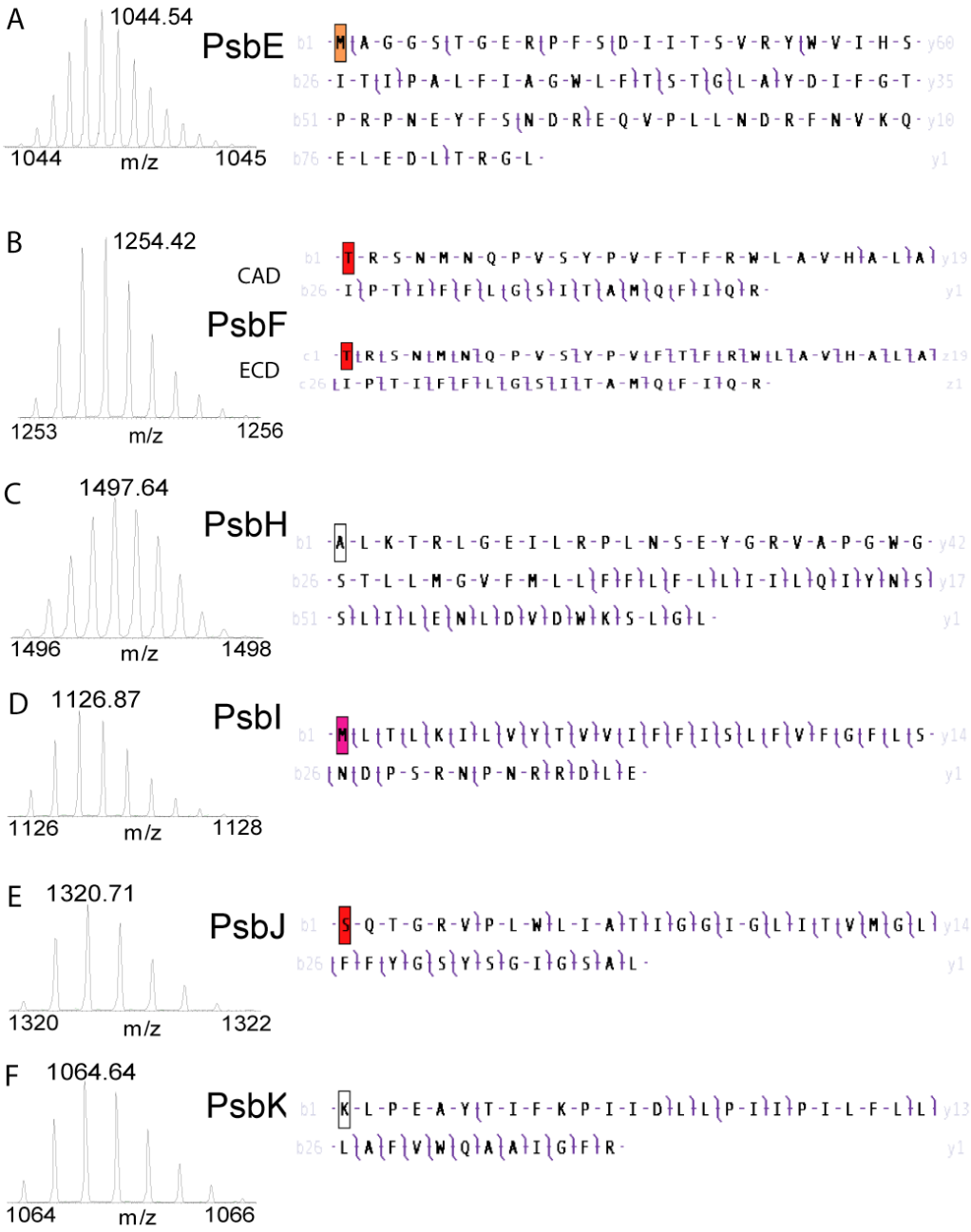
A
1044.54
PsbE
1044
m/z
1045
B
1254.42
CAD
PsbF
ECD
1253
m/z
1256
C
1497.64
PsbH
1496
m/z
1498
D
1126.87
PsbI
1126
m/z
1128
E
1320.71
PsbJ
1320
m/z
1322
F
1064.64
PsbK
1064
m/z
1066

Contd…

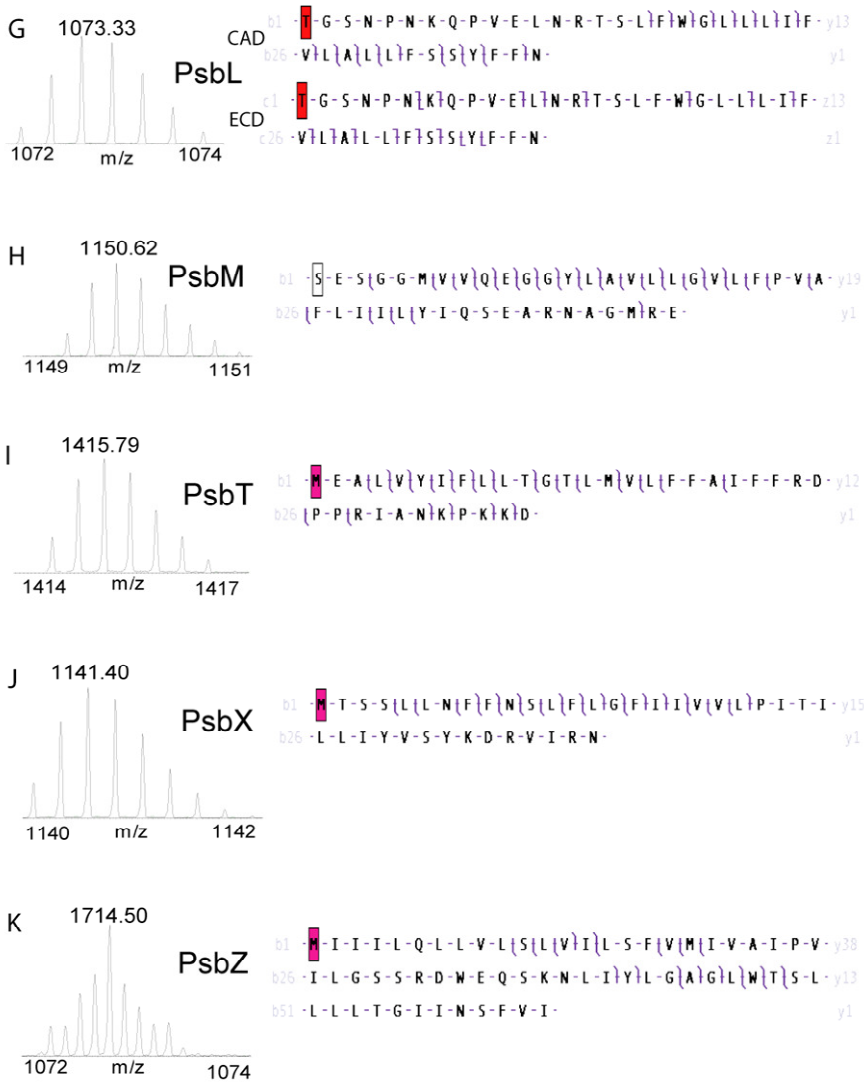

FIGURE 4-6 Top-down mass spectrometry of small integral membrane subunits A. PsbE, B. PsbF, C. PsbH, D. PsbI, E. PsbJ, F. PsbK G. PsbL H. PsbM I. PsbT J. PsbX and K. PsbZ. The ion isolation used for CAD/ECD for each subunit is shown on the left, while the product ion assignments (*b*- and *y*- ions for CAD; *c*- and *z*- ions for ECD) observed at 10 ppm tolerance are shown on the sequence to the right. A shaded box around a Met residue in position 1 indicates retention of the formyl group as translated. A shaded box around a different residue implies removal of one or more amino-acid residues from the N-terminus and N-acetylation. An open box around the first amino acid implies removal of one or more amino-acids with no further modification. Percentage of matched product ions for small subunits: PsbE – 6%; PsbF – 36/51%; PsbH – 59%; PsbI – 29%; PsbJ – 23%; PsbK – 29%; PsbL – 38%; PsbM – 40%; $PsbT_c$ – 33%; PsbX – 35% and PsbZ – 44%. P scores are given in Table 2.

In LC-MS+ experiment, subunit PsbF corresponds to a average mass peak of 5015 Da eluting at 68 minutes indicating a possibility of loss of met1 and acetylation at the N-terminus (Fig. 4-2, Table 4-1). An absolute mass search for the ECD data using Prosight PC 2.0 proposed different possible post translational modifications (PTM): 1. Loss of met1 at the N-terminus 2. Possibility of formylation or acetylation at met1 3. Loss of met1 and acetylation at N-terminus. The first result yielded zero matching 'c' fragment ions, whereas, the second result yielded zero matching 'c' fragment ion for formylation and one matching 'c' fragment ion for acetylation. However, the third result yielded 20c- and 25z-product ions bringing down the mass difference between calculated (5010.6243 Da) and measured (5010.6386 Da) monoisotopic masses less than 5 ppm (Δ = 3.8488 ppm) and P-score of 6.95E-88 (Fig. 4-6B, Table 4-2). Also the presence of overlapping c- and z- product ions confirms full sequence coverage and post translational modification in the mature polypeptide. As in ECD analysis, similar possible PTM's were obtained as in CAD data using Prosight PC 2.0. In CAD dataset, the confirmed PTM of acetylation of N-terminus after removal of met1 by ECD analysis contained 18b- and 10y- product ions with a mass difference of 3.8488 ppm and a P-score of 1.14E-51(Fig. 4-6B, Table 4-2). Other possible post translational modifications from CAD dataset yielded zero or one matching b-fragment ion. This CAD result along with ECD provided strong evidence that the identification and processing of PsbF is accurate in *Galdieria*.

In post-translationally modified form, PsbH is known to lose its met1 and has a free N-terminus. The experimentally determined monoisotopic mass of

7479.1417 Da for the HPLC peak eluting at 111 minutes is within 5 ppm of the calculated monoisotopic mass (7479.1312 Da) of mature PsbH (Δm = 1.2749 ppm) (Fig. 4-2; Table 4-2). Analysis of CAD dataset yielded 27b- and 4y- product ions and a P-score of 1.53E-59 (Fig. 4-6C, Table 4-2). Additionally, CAD dataset revealed that mature PsbH was fragmented more at the C-terminus than at the N-terminus.

The experimentally determined average mass peak of 4505 Da of subunit PsbI corresponds to the HPLC peak eluting at 94 minutes (Fig. 4-2, Table 4-1). This mass differs from the calculated average mass by 28.7 Da consistent with the addition of formyl group at the N-terminus in mature PsbI. Data analysis of top-down CAD experiment using Prosight PC 2.0 software, with no formylation at the N-terminus yielded 1b- and 25y- product ions. But after manual introduction of formyl group at N-terminus, protein sequence coverage increased significantly with 19b- and 26y- product ions, with an agreement between calculated and measured monoisotopic mass dropping below 5 ppm and a P-score of 6.85E-66 (Δm = 2.8954 ppm) (Fig. 4-6D, Table 4-2).

The HPLC peak eluting at 84 minutes with an average measured mass of 3960 Da corresponds to a post translationally modified form of PsbJ unit, lacking met1 and acetylated at the N-terminus (Fig. 4-2, Table 4-1). By using Prosight PC 2.0, analysis of the CAD dataset of the modified protein gave 23b- and 11 y-product ions as well as the precursor matched within 10 ppm giving a P-score of 3.25E-61(Δm = 5.2626 ppm) (Fig. 4-6E, Table 4-2).

In PsbK, cleavage of the first 9 residues was reported in literature. The experimentally determined average mass of 4256 Da for the HPLC peak eluting at 95 minutes differs from calculated mass by 0.8 Da, after removal of 8 amino-acids at the N-terminus (Fig. 4-2, Table 4-1). To confirm this cleavage, a precursor ion of 1064.64 Da was selected for CAD analysis and the product ion spectrum recorded. Short sequence tags were generated using "Compile sequence tag" feature in Prosight PC 2.0. Generated tags were used to search the entire created *Galdieria* photosynthetic proteins database. A sequence tag of 8 amino-acid residues matched with the untruncated PsbK nearby the C-terminus. Further analysis of CAD dataset of untruncated PsbK gave 1b- and 10y- product ions with a mass difference of -868.4960 Da between calculated and observed monoisotopic masses. Also the detection of the y37 product ion in untruncated PsbK protein along with the above mentioned data, confirmed a N-terminal cleavage. So, by removing the first 8 amino-acid residues, the measured mass was within 3.2322 ppm of that calculated monoisotopic mass. Furthermore, 18b- and 9y- product ions were matched giving a P-score of 2.64E-49 (Fig. 4-6F, Table 4-2).

For PsbL, the assigned mass peak (4290 Da) in the mass spectrum is attributed to a protein eluting at 93 minutes, lacking its initiating methionine and acetylated at the N-terminus (Fig. 4-2, Table 4-1). An obsolute mass search using Prosight PC 2.0 yielded 6y- product ions, until formylation were introduced in the N-terminus yielding 17b- and 6y- product ions, agreement between the calculated

(4287.2771 Da) and measured monoisotopic mass (4287.2888 Da) within 5 ppm with a P-score of 2.15E-45 (Fig. 4-6G, Table 4-2).

Subunit PsbM has an N-terminal signal peptide that is cleaved during its maturation. The first thirty eight amino acids are processed to give a mature protein consisting of 43 amino acids eluting at 80 minutes with a calculated monoisotopic mass of 4596.4100 Da (Fig. 4-2, Table 4-2). Top down CAD experiment confirmed the processed mature sequence of PsbM. The N terminal cleaved precursor matched with the top-down CAD 10 b- and 23 y- product ions within 5 ppm accuracy and an overall P-score of 2.21E-68 (Δ = 3.4407) (Fig. 4-6H, Table 4-2).

The average measured mass of 4245 Da for the HPLC peak eluting at 97 minutes differs from the calculated mass by 27.6 Da indicating formylation of the N-terminus in subunit PsbT (Fig. 4-2, Table 4-1). A top-down CAD experiment confirmed the identity and processed form of PsbT. CAD product ion list could only be matched to primary structure after manual modification of formylation at N-terminus yielding 11b- and 16y- product ions. After this modification, the experimental monoisotopic mass of 4242.3284 Da is in good agreement with calculated monoisotopic mass of 4242.3284 Da (Δ = 3.2813 ppm), with a P-score of 2.23E-44 (Fig. 4-6I, Table 4-2).

PsbX is known to be formylated at N-terminus in its mature form. The mature form of PsbX in the peak eluting at 102 minutes has an experimentally determined monoisotopic mass of 4559.5807 Da in agreement with the calculated monoisotopic mass of 4559.5632 (Fig. 4-2, Table 4-2). A top-down CAD

experiment confirmed the identity of PsbX with 11b- and 13y- product ions as well as the precursor matched within 5 ppm giving a P-score of 3.11E-45 (Δ = 3.7467 ppm) (Fig. 4-6J, Table 4-2).

As PsbX, PsbZ is also known to be formylated in N-terminus in its post-translationally modified form. The experimentally determined average mass of 6855 for the HPLC peak eluting at 133 minutes differs from calculated mass by 28.6 Da, consistent with the mass associated with a formyl group at the N-terminus (Fig. 4-2, Table 4-1). Initial analysis of the CAD dataset from top-down experiment using Prosight PC 2.0, with no modifications yielded 11 matching y-ions with a mass difference of 27.9955 Da, confirming the proposed modification in low resolution mass spectrometer. After manual modification of starting PTM as formylation, software analysis yielded 10b- and 11y- product ions, with the agreement between calculated and experimentally determined monoisotopic masses dropping below 1 ppm with a P-score of 7.55E-42 (Fig. 4-6K, Table 4-2).

DISCUSSION

Number of subunits/transmembrane helices

Top-down mass spectrometry has been used to characterize integral (63) and peripheral (90) thylakoid membrane proteins for several years now. Top-down high-resolution FT-MS was first applied to an integral thylakoid protein demonstrating the potential benefits of using ECD (90). Recently, the 8 subunits of the cytochrome b_6f complex from *Nostoc* were analyzed by top-down FT-MS for full characterization of post-translational modifications (63). Here we have used top-down FT-MS to characterize the smaller integral and the peripheral

subunits of PSII from *Galdieria*. A significant challenge was the lack of a highly annotated *Galdieria* proteome database and considerable effort was devoted to the search for PSII homologues. Despite the informatics work, the interpretation of the top-down data required manual adjustments of some sequences presumably due to sequence differences between the strain sequenced and that used for PSII preparations. Nevertheless we were able to define the identity of all the subunits at very high confidence. In total *Galdieria* PSII appears to have 4 large subunits, 11 smaller integral subunits and 3 peripheral OEC subunits for a total of 18 subunits. This total gives 2 less subunits and 2 less transmembrane helices than the cyanobacterial complex in agreement with the 34 transmembrane α-helices identified in spinach (95) and in contrast to the 36 transmembrane helices identified in PSII X-ray structure of *T. elongatus* (19), perhaps a little surprising given the similarity between the *Galdieria* OEC and that of the cyanobacteria. It remains possible that the small 3409 Da intact mass tag observed in the LC-MS+ experiment is a PSII subunit but we were unable to match top-down FT-MS data to any sequence in our *Galdieria* database. PsbN and ycf12 of the cyanobacterial complex were found in the *Galdieria* genome by homology but were not found in the protein analysis despite their inclusion in the database used for interpretation of the data. Final resolution of the issue will require a crystal structure of sufficient quality to count the number of transmembrane helices.

Post-translational Modifications

Top-down mass spectrometry allowed characterization of PTMs with molecular detail. Modification of small subunits shows a distinct pattern based on the

exposure of their N terminus to the stroma or lumen. Subunits PsbI, PsbK, PsbM, PsbT, PsbX and PsbZ have their N-terminii exposed to the lumen with PsbI, PsbT, PsbX and PsbZ retaining their initiating formyl-Met residue unmodified. PsbK and PsbM had transit peptides removed (Table 4-2). The other subunits PsbE, PsbF, PsbH, PsbJ and PsbL have their N-terminii exposed to the stroma and in all cases have their initiating Met residue removed. In the case of PsbF, PsbJ and PsbL their N-terminii are acetylated. The observed differences in modification for different subunits may be due to the availability of different processing enzymes in stroma and lumen (19) and accessibility of the N-termini to these enzymes (19).

Peripheral subunits

Galdieria genome has genes for all the identified oxygen evolving complex subunits involved in water-splitting reaction (PsbO, PsbU, PsbV, PsbP, PsbQ') in cyanobacteria, red algae, green algae and higher plants. Consistent with the nuclear and chloroplast genome analysis for other red alga, PsbO, PsbU and PsbQ' are found in the nuclear genome, while PsbV is encoded in chloroplast genome (22) It is quite surprising that *Galdieria* has only 3 oxygen evolving complex subunits, as atleast four oxygen evolving complex subunits are present in other members of cyanidiales (*Cyanidioschyzon merolae* – PsbO, PsbU, PsbP, PsbQ; *Cyanidium caldarium* – PsbO, PsbU, PsbV, PsbQ'). In cyanobacteria, hydrophilic oxygen evolving complex subunits (PsbO, PsbU and PsbV) are located in the chloroplast lumen. These subunits in combination with the protruding hydrophilic loops of D1, D2, CP43 and CP47 subunits bound the calcium and manganese ions

forming the water splitting complex. *Galdieria* has oxygen evolving complex subunits similar to cyanobacteria.

PsbO is the only extrinsic protein conserved during evolution from cyanobacteria to higher plants. As observed in cyanobacteria, red algae, green algae and higher plants, PsbO is nuclear encoded in *Galdieria* with a signal sequence of first 21 residues, which is also confirmed by SignalP (96). This is in contrast to the signal sequence of 26 residues identified by mass spectrometry in *T.elongatus* (cyanobacterium) and predicted signal sequence of 52, 76 and 84 residues for *Chlamydomonas reinhardtii* (green alga), *Cyanidium caldarium* (red alga) and *Spinacia oleracea* (higher plant) respectively (19, 97). Sequence alignment of *Galdieria* PsbO with these organisms reveals that N-terminal sequence in *Galdieria* is longer than cyanobacteria, similar with red algae and shorter than spinach (data not shown). Also, the identified disulfide bond between the cysteine residues in *Galdieria* is conserved, so there is a high possibility this disulfide bond is present in these organisms. Furthermore, *Galdieria* PsbO has a slightly higher amino acid identity with green algae (49%) and higher plants (47%) than with cyanobacteria (45%). This is in contrast to the sequence results of *Cyanidium caldarium*, a sister species of *Galdieria* where the PsbO gene is highly homologous to cyanobacteria.

PsbU has a mature protein of 93 amino acids, after the cleavage of first 81 residues of the transit peptide. C-terminal analysis of the transit peptide reveals the presence of consensus sequence A-X-A from position 79 to 81, a recognition site for thylakoid processing peptidase, an additional confirmation of our mass

spectrometry result (98). The signal peptide in *Galdieria* is longer in comparison with *T.elongatus* (30 residues) and *Cyanidium caldarium* (61 residues). Sequence comparison of *Galdieria*'s mature PsbU with *C. caldarium* and *T. elongatus* showed amino acid identities of 58% and 45% respectively (data not shown). In the mature PsbU protein, the second amino acid tyrosine from the C-terminus is conserved across all organisms, a likely residue for modulating the requirement of calcium and chloride ions for oxygen evolution(99). Apart from the transit peptide processing, no post translational modification was identified for this subunit and our results are in concurrence with the proteomic analysis of PSII in *T.elongatus* (19).

PsbV is present in cyanobacteria and red algae. In *Galdieria*, mature PsbV protein is obtained after the processing of short transit peptide (1-30 residues) which is in agreement with other red algae (*Cyanidium caldarium* and *Cyanidioschyzon merolae*) and cyanobacterium (*T.elongatus*) (19, 100). After the removal of transit peptide, the mature PsbV sequence did not match with the CAD data obtained from high resolution mass spectrometry. Previous proteomic studies have shown that modifications in orthologs (same gene in related species) are conserved and this can be used to predict the modification in related organisms. Also, *Galdieria* genome is recently annotated; there are chances of sequence errors which can be corrected by comparing orthologs. So a gene search for PsbV in *Cyanidium caldarium* and *Cyanidioschyzon merolae* was initiated. In UniProt database, PsbV has two sequence records for *Cyanidium caldarium* reported by Glockener et al. (Q9TLW2-1) (101)and Enami et al. (Q76FBO-1)(100). For our

convenience, they are named as CCPsbV1 and CCPsbV2 respectively. For Cyandioschyzon merolae (CMPsbV), only one PsbV sequence (Q85FS3) was registered. Comparison of *Galdieria*'s PsbV sequence with other red algal ones revealed a homology of 62%, 66% and 64% for CCPsbV1, CCPsbV2 and CMPsbV respectively. Further sequence analysis of CCPsbV1 and CMPsbV showed that *Galdieria* has ten extra residues at the C-terminus. Based on this we have trimmed the C-terminus by removing 10 amino acids and also optimized the data by changing one amino acid from Threonine to Valine which brought the mass difference (Δ) between the experimental and calculated monoisotopic mass below 10 ppm. High sequence homology of PsbV among cyanidiales, indicate that they might bind similarly with the intrinsic PSII proteins. Results from the cross linked binding studies of PsbV from *T. vulcanus* and *C. caldarium* with their PSII indicated that PsbV binding depends upon the structure of intrinsic proteins interacting with PsbV. Furthermore, results have shown that during the course of PSII evolution, PsbV binding sites has been changed between cyanobacteria and red algae(100). This change in binding site might have lead to the recruitment of PsbQ′ in red algae (*Cyanidium caldarium*) for the effective binding of PsbV to the intrinsic proteins(40). Cross – reconstitution studies of PsbU and PsbV from red algae indicated that these proteins might have a similar function those of PsbP (23 Da) and PsbQ (17 Da) in higher plants (41). Also, red algal oxygen evolving complex subunits (PsbO, PsbU, PsbV) did restore partial oxygen evolution in both cyanobacterial and higher plant PSII. This result

indicates that red algal PSII might act as a link between the photosystem II present in cyanobacteria and higher plants (41).

To our knowledge, no post-translational modification was reported or known for PsbW/PsbW-like/Psb28 protein in cyanobacteria, algae and higher plants(20). Designation of PsbW subunit in cyanobacteria, green algae and higher plants are inconsistent and quite confusing. Sequence analysis of the identified PsbW subunit in *Galdieria* genome is similar to the hydrophilic *Synechocystis sp* PsbW subunit with an amino acid identity of 54%, which has been recently named as Psb28; not with the hydrophobic PsbW protein of 6.l kDa identified in green algae and higher plants. Also, *Galdieria* Psb28 is chloroplast encoded as in cyanobacteria and other red algae, while in green algae and higher plants it is nuclear encoded. Based on these observations, Psb28 in red algae and cyanobacteria might have a different functions that of green algae and higher plants. Position of PsbW is strongly debated as whether it is part of PSII complex or a transiently associated subunit. Recent study in *Synechocystis* 6803 has shown that Psb28 is a PSII assembly factor associated with CP47 in PSII assembly intermediates and involved with the synthesis of chlorophyll binding proteins (102). Considering the sequence identity between *Synechocystis* 6803 and *Galdieria* for Psb28, we propose that Psb28 identified in *Galdieria* might perform a similar role as in *Synechocystis* 6803.

Sequence analysis of the *Galdieria* Psb27 using DOLOP server reveals the absence of lipobox sequence, found in cyanobacteria (103). This lipobox sequence is characteristic of bacterial lipoproteins, usually lacking in eukaryotes.

In cyanobacteria, Psb27 transiently associates with PSII during its biogenesis, facilitating the assembly of manganese, chloride and calcium ions and possibly hindering the premature binding of OEC subunits to the PSII core (104). Similar repair role has been confirmed for Psb27 in Arabidopsis. However, additional experiments are needed to confirm whether red algal Psb27 is a part of mature PSII or transiently associated subunit performing a repair role as found in cyanobacteria and higher plants (105).

Small integral membrane subunits

In *Galdieria*, the larger subunit of cytochrome b559 has a molecular mass of 9396.8317 Da and its PTM is similar to the findings in cyanobacteria (*T.elongatus* and *Synechocystis* 6803) and higher plants (*Hordeum vulgare* and *Nicotiana tabacum*) (19, 106, 107). The observed molecular mass is almost similar as in *T.elongatus* (9446 Da) and *H. vulgare* (9307 Da), but larger in *N. tabacum* (9250.7 Da). The smaller subunit of cytb559 has 43 amino acids with a molecular mass of 5010.6386 Da. Also the PsbF subunit is larger in comparison with *T.elongatus* (4.9 kDa), *N. tabacum* (4.3 kDa) and *H. vulgare* (4.4 kDa) (19, 106, 107). The post translational modification for this subunit is the same as observed in other organisms, a possibly indication for a similar role of these subunits in *Galdieria*. Regarding PsbE and PsbF function, they are essential for PSII assembly, possibly protecting PSII from photodamage as they might also be involved in secondary electron transport (20).

Literature survey revealed that los of met1 with a free N-terminus was reported for PsbH subunit in other organisms (19, 92, 106, 107). However,

phosphorylation at one or two sites at N-terminus has been identified in higher plants and they are influenced by light/dark cycles (108). A sequence comparison of PsbH between higher plant (*Spinacia oleracea*) and *Galdieria* have revealed that phosphorylation site is not conserved in *Galdieria*, similar to that in *T.elongatus*. Additionally no phosphorylation was detected at N-terminus of PsbH by high resolution mass spectrometry. Functional role of PsbH might differ between organisms. In C. *reinhardtii*, a PsbH deletion mutant contains no functional PSII, indicating an absolute necessity of this subunit for PSII activity (109). In contrast, a similar study in *Synechocystis* 6803, resulted in functional PSII but with a slow growth rate corresponding to the impairment in electron flow from Q_A to Q_B. In PSII X-ray structure in *T.elongatus*, PsbH is involved in binding of chlorophyll, carotenoids and lipids. On the whole, PsbH is essential for PSII activity both in eukaryotes and prokaryotes. Considering the amino acid identities (77% for *Synechocystis* 6803, 71 % for *T.elongatus*) and absence of conserved phosphorylation site, PsbH in *Galdieria* might play a similar role as observed in cyanobacteria (19).

For PsbI, the confirmed PTM of formyl methionine at N-terminus agree with the published data for cyanobacteria and higher plants (19, 92, 106). *Galdieria* PsbI sequence indicates a single transmembrane helix, with an amino acid identity of 68% for *Chlamydomonas sp. and T. elongatus*, 73% for *Synechocystis* 6803 and 77% for higher plants (*H.vulgare* and *N.tabacum*). PsbI mutants in *Synechocystis* 6803 and C. *reinhardtii* are sensitive to high light conditions and their oxygen evolving activity is lower (70 to 80 % lower for

Synechocystis; 10 to 20% for *Chlamydomonas*) than the wild type (20). Also, a PsbI mutant in *T. elongatus*, only synthesized PSII monomers indicating a role of PsbI in formation or stabilization of PSII dimmers (20).

PsbJ in *Galdieria* contains 38 amino acid residues and they are located in a gene cluster containing PsbE, PsbF and PsbL (19). As in *Galdieria*, loss of met1, followed by acetylation is the posttranslational modification as identified in cyanobacteria. Subunit PsbJ have been confirmed as a part of PSII core in *Synechocystis* 6803 and *T.elongatus*, but it is not detected in PSII preparation of *T.vulcanus* by N-terminal sequencing (19, 107, 110). This is probably due to the acetylation blocking of PsbJ at the N-terminus.

Subunit PsbK is identified in cyanobacteria, green alga and higher plants. But the N-terminal processing of PsbK is different between organisms (19, 106). In mature PsbK, first 9 residues are processed for *T.elongatus*, whereas in *N.tabacum* removal of first 24 residues was reported in literature. Both of these studies have reported no other modifications of N-terminus (a free n-terminus) and these results are in line with our study. Furthermore, the initial 6 amino acid residues (KLPEAY) at the N-terminus observed in *Galdieria* are conserved between *Galdieria* and cyanobacteria, green algae and higher plants. Functional studies of PsbK in *Synechocystis* 6803 and *Chlamydomonas* indicated a role of PsbK in plastoquinone binding and maintaining stability of PSII dimmers(20). The role of PsbK in electron transfer/plastoquinone diffusion is confirmed by the PSII X-ray structure of *T. elongatus* (19).

Chloroplast encoded PsbL is present both in cyanobacteria and higher plants. In *Galdieria*, PsbL has 37 amino acids and the acetylation identified for this subunit differs from the modifications reported in other organisms. In *T. elongatus* and *H. vulgare*, PsbL had no modification. Similarly, in *N. tabacum*, PsbL has no modification, but has lost its initial methionine (19, 92, 106). Difference in PTM in these eukaryotic and prokaryotic systems, might be due to the difference in their functional roles along with the differences in biogenesis mechanisms of PSII complex.

Subunit PsbM is plastid encoded in cyanobacteria, green algae and higher plants. In these organisms, the observed molecular mass for PsbM varies between 3803 and 4011 Da (*T.elongatus* - 4011 Da; *Synechocystis* 6803 – 3920Da; *N. tabacum* – 3808 Da; *P.sativum* – 3809 Da; *H. vulgare* – 3837 Da) with a post-translational modification of formyl methionine in their N-terminus (19, 92, 106). In *Chlamydomonas*, N-terminal sequencing showed a blocked N-terminus, but the PTM for this subunit has not been reported (111). Function of PsbM is not known in green algae and higher plants. A *ΔpsbM* mutant in *Synechocystis* 6803 showed normal oxygen evolving activity, but the mutant cells grow faster under low light conditions in comparison with wild type cells (20). In contrast to these findings, the experimental mass obtained for *Galdieria* PsbM has a molecular mass of 4596 Da, higher than the masses observed for other organisms. Additionally, PsbM in *Galdieria* is nuclear encoded, suggesting the transfer of this gene from plastid to nucleus and the signal peptide was acquired for its transfer from cytosol into plastids. Moreover, PsbM is not present in plastid and nuclear genome of *C.*

merolae and in plastid genome of *C. caldarium* (40, 101). To our knowledge, only *Guillardia theta*, a cryptophyte and *Phaeodactylum tricornutum*, a stramenophile algae are the only organisms that has nuclear encoded PsbM. Comparative sequence analysis of PsbM in *Galdieria*, *Guillardia* and *Phaeodactylum* reveal that signal peptide is not conserved, while the mature protein has an amino acid identity of 63% between these organisms. Both crytophytes and stramenophiles belong to chromista, and the plastids of these organisms are assumed to have originated from a red alga through secondary endosymbiosis (112). At this juncture, it is not clear whether PsbM has any evolutionary importance. But use of PsbM gene as a phylogenetic marker during the evolution of eukaryotes from primary, secondary and tertiary endosymbiosis would reveal some hidden truth for this subunit. In a different perspective, *Galdieria* is a primitive photosynthetic red alga, and it photosystems might be ancient than the current photosystems present in cyanobacteria, red algae, green algae and higher plants (9). In this case, different subunits of PSII in *Galdieria*'s genome might be reflect their ancient state and it is possible that this gene is originally a native of nucleus, but has acquired function in plastid during the reduction process of plastid genome contents and eventually transferred to plastid in other organisms during the course of evolution. By taking into account the absence of this subunit in other cyanidiales and their nucleus origin, PsbM in *Galdieria* might play an important role in *Galdieria* PSII. A mutagenesis study in *Galdieria* PSII would be helpful in knowing the function of this subunit.

$PsbT_c$ protein contains 36 amino acids with a single transmembrane span and a molecular mass of 4596.8282 Da. Observed formylation for $PsbT_c$ is in good agreement with the findings in *T.elongatus*, *P.sativum* and *N.tabacum* except for *H.vulgare*, acetylation is reported (19, 92, 106, 108). A disrupted gene study for this subunit in *T.elongatus* showed that PSII dimeric population dramatically reduced in mutant than in wild type indicating a role for $PsbT_c$ in PSII dimerization (20). In recent structural model of dimeric PSII complex, PsbT along with PsbL and PsbM are located at the PSII monomer interface (19). Identification of these subunits in *Galdieria* PSII might not be helpful in knowing its oligomeric state, as contradictory results have been reported based on the absence or presence of these subunits and their influence on formation of PSII dimers. Furthermore, a recent study has shown that intact architecture of PSII *invivo* in cyanobacteria and red algae is a monomer (58). It will be high interest to know the PSII oligomeric state in *Galdieria* as this organism performs photosynthesis under extreme conditions.

In cyanobacteria and green algae, PsbX is chloroplast encoded, while in higher plants it is encoded in nuclear genome (20). PsbX in *Galdieria* has 39 amino acids and sequence analyses for hydrophobicity indicate a single transmembrane α-helix with a post translational modification of formylation without any cleavage at N- or C-terminus. But mass spectrometric analysis of *T.elongatus*, shows a cleavage of first 10 amino acids due to the presence of extra lumen targeting presequence (113). This additional lumen targeting sequence is present only in a few cyanobacteria and higher plants. Sequence comparison of

PsbX from *Galdieria* with *T.elongatus* and *T.vulcanus* did reveal the absence of this signal sequence in *Galdieria* (data not shown). Results obtained in this study, confirmed this as there was no cleavage for PsbX. Modification of PsbX is not known in green algae and higher plants.

PsbZ is highly conserved across among photosynthetic organisms. Subunit PsbZ is chloroplast encoded and has 62 amino acids, a typical number observed in other organisms (19, 106, 108). Confirmed post translational modification of formylation in PsbZ is in good agreement with the results in *T.elongatus*, *P.sativum* and *N.tobacum*. *Galdieria* PsbZ has an amino acid identity of 51% and 40% with *T.elongatus* and *Synechocystis* 6803 respectively. In green algae and higher plants, PsbZ stabilizes the PSII-LHCII supercomplexes (20). *Galdieria* has phycobilisomes in place of LHCII supercomplexes, along with the sequence identity it has with cyanobacteria, PsbZ might be involved in photoprotection, a similar role noted in cyanobacteria.

CONCLUSION

Top-down high-resolution MS is clearly the technology of choice for absolute characterization of protein identity and modification. The reversed phase LC-MS+ platform presents an attractive primary separation that avoids problems associated with gels. Low resolution MS data from the primary LC-MS+ experiment is used to drive user directed data-dependent top-down MS experiments. Interpretation of top-down data relies upon accurate annotation of high-quality genomic data though it is now very easy to see where actual primary structure diverges from that predicted by translation of DNA sequence. The small integral and the

peripheral subunits of *Galdieria* PSII have been characterized with unprecedented detail, emphasizing the amenability of membrane proteins to analysis by top-down MS.

CHAPTER 5 STRUCTURAL AND FUNCTIONAL CHANGES OF PSI-LHCI SUPERCOMPLEXES OF *CHLAMYDOMONAS REINHARDTII* CELLS GROWN UNDER HIGH SALT CONDITIONS

INTRODUCTION

As mentioned in chapter 1, eukaryotic PSI uses its light harvesting complexes I and II (LHCI and LHCII) to increase its functional efficiency. Recent X-ray structural model of PSI-LHCI of *Pisum sativum* have shown that the protein-protein contacts between PSI and LHCI proteins are weaker in comparison with the contacts between the PSI core proteins inside the thylakoid membrane and these LHCI proteins are more accessible and amenable to regulatory enzymes (75). Several studies in different organisms (e.g. Tomato, Tobacco) have pointed out that the LHCI proteins are post-translationally modified in accordance with change in environmental conditions (114). From these studies, it is clear that the light harvesting regulations are clearly far from being understood and it varies between species. Also these functional studies are further compounded by the difficulty in isolating these large fragile membrane protein complexes. Further adding to the complexity, is that these membrane protein complexes are moving targets vulnerable to poorly understood process of environmental regulation.

The green alga, *Chlamydomonas reinhardtii* is widely used as a model for eukaryotic photosynthesis and we have used this organism to study the effects of high salt conditions on PSI-LHCI. Based on our literature survey, there have been

no studies on the effects of salt stress on PSI-LHCI and this chapter focuses on changes in protein profile of PSI-LHCI as well as the process of energy transfer and trapping. The results of this investigation are published in Subramanyam et al. (2010) in Planta journal (see, appendix C for co-authors permission). The present form of isolation protocol is largely the work of Dr. Rajagopal Subramanyam. The author along with Dr. Rajagopal Subramanyam have grown *Chlamydomonas* cells under salt conditions, isolated PSI-LHCI supercomplexes, performed SDS denaturing electrophoresis, in-gel trypsin digestion and immunoblot analysis experiments. All the MALDI-TOF and oxygen uptake experiments were performed by the author.

Salt stress

Salinity-stress effects on plant growth often involve impairment of photosynthesis. High amounts of sodium in the soil impair cell metabolism and photosynthesis by increasing osmotic pressure (115). The molecular mechanisms responsible for the salt-induced inactivation of the photosynthetic machinery have been studied extensively, with particular focus on photosystem II (PSII), *in vitro* and *in vivo* (116-118). When PSII membrane fragments are exposed to high concentrations of NaCl, the extrinsic proteins of the oxygen-evolving machinery of PSII dissociate from the membrane-intrinsic complex, resulting in impairment of oxygen evolution. In cyanobacterial cells, high concentrations of NaCl also inactivate Na^+/H^+ antiporters (116).

Exposure of the green alga *Dunaliella tertiolecta* to salinity stress results in a significant inhibition of photosynthesis, due to a decrease in PSII activity

(119). A decrease in PSII activity has also been associated with the transition to State 2. This was confirmed by Endo and coworkers, who also suggested a connection between the decrease in PSII quantum yield caused by salinity stress and that caused by state transitions in *Chlamydomonas reinhardtii* (120). In the red alga *Porphyra perforata*, Satoh and colleagues demonstrated that the salinity stress-induced decrease in PSII activity was due to a decrease in the excitation energy reaching PSII reaction centers, as well as damage to the oxidizing side of PSII (121). Salt stress also inhibits PSII activity in higher plants, including salt-tolerant plants such as mangroves (122-125). In some reports, the effects of salt stress on PSII were due to the dissociation of the 23 kDa polypeptide extrinsically bound to PSII (126). Salt stress has also been reported to reduce D_1 protein turnover in both cyanobacteria and plants (127, 128).

The mechanism of salt stress has also been well established in cyanobacteria (129-131). It leads to electron transport inhibition at both the donor and acceptor sides of PSII, damage to the phycobilisomes (membrane-extrinsic antenna of PSII) as reflected by a significant decrease in phycocyanin content, and a shift in the distribution of excitation energy from PSII to PSI as suggested by an increase in qN (129-131). In a study using the cyanobacterium *Spirulina*, the downregulation of PSII reaction center proteins was observed without any inhibition of electron transfer on the donor and acceptor sides of PSII, suggesting that the effects of salt stress on PSII may vary between species (129). A very recent paper reported that there were no significant changes in the levels of the CP47, CP43, cytochrome c550, and D1 proteins (132). The PsbO content in

isolated thylakoids, however, decreased. Recent reports show that the effects of salt stress on higher plants and cyanobacteria are due to the generation of reactive oxygen species, which affects both the reduced and oxidized sites of PSII (128, 133). Allakhverdiev and coworkers reported that, in addition to PSII, PSI is equally inactivated by osmotic stress – the present study is focused on further exploring the role of PSI damage in salt stress (127).

In eukaryotes, the light-harvesting capacity of PSI and PSII is augmented by the membrane-intrinsic light harvesting complexes LHCI and LHCII. The LHCI proteins are associated only with PSI and deliver excitation energy to the PSI core. To the best of our knowledge, there have been no studies on the effects of salt stress on PSI-LHCI supercomplexes. We have used *C. reinhardtii* as a model system to study the effects of high salt conditions on PSI-LHCI. The present study focuses on changes in the protein profile of PSI-LHCI as well as the processes of energy transfer and trapping.

MATERIALS AND METHODS

Chlamydomonas cell culture

C. reinhardtii cells were grown in a growth medium with its ingredients listed in Table 5-1. Cells were grown under both control (NaCl-free) and salt stress (100 mM NaCl) conditions with continuous illumination (30-40 μE m^{-2} S^{-1}) on a shaker at 115 rpm to a density where OD_{650nm} ~1.

TABLE 5-1 Composition of *Chlamydomonas* growth medium

Chlamydomonas growth medium (1 L)		CC10X (1 L)		Hutner's trace elements (1 L)	
CC10X	100 mL	Tris-HCl	25 g	EDTA, disodium salt	50 g
1M KH_2PO_4	1 mL	Glacial acetic acid	10 mL	$ZnSO_4 \cdot 7H_2O$	22 g
Yeast extract	1 g	NH_4NO_3	5 g	H_3BO_3	11.4 g
		$MgSO_4 \cdot 7H_2O$	1 g	$MnCl_2 \cdot 4H_2O$	5.06 g
		$CaCl_2 \cdot 2H_2O$	0.2 g	$CoCl_2 \cdot 6H_2O$	1.61 g
		KCl	1 g	$CuSO4 \cdot 5H_2O$	1.57 g
		Hutner's trace elements	10 mL	$(NH_4)_6Mo_7O_{24} \cdot 4H_2O$	1.10 g
				$FeSO_4 \cdot 7H_2O$	4.99 g

The cells were harvested at 6500 rpm for 10 min in a sorvall GS-03 rotor (Dupont, Wilimington, DE), then washed and resuspended in a buffer containing surcrose, 25 mM HEPES (pH 7.5, KOH), 10 mM $MgCl_2$, and 5 mM $CaCl_2$. Protease activity was inhibited by adding 1 mM each of amino caproic acid and benzamidine, and the cells were ruptured using a French press at 1080 psi.

Thylakoid isolation

The cell lysate obtained from the French press was spun at 5000-6000 rpm in a sorvall SS-34 rotor to harvest the thylakoid membranes, which were left in the pellet. The pellet was resuspended in a buffer containing 0.3 M sucrose, 5 mM HEPES (pH 7.5, KOH), and 10 mM EDTA. The thylakoids were then pelleted at 2000 x g for 10 min in an SS-34 rotor, and resuspended in a buffer containing 5 mM Tris-HCl (pH 7.5), 0.2 M sorbitol, 5 mM $CaCl_2$, and 10 mM $MgCl_2$.

Solubilization and purification of the PS-LHCI supercomplex

A mild detergent was used to solubilized the thylakoid membrane proteins and remove the PSI-LHCI complex from the membrane in the form of detergent-micelles. This was done by adding 0.9% β-DDM to pellet resuspension (with a Chl concentration of 0.8 to 1.0 mg/ml) and stirring it in ice for 20 min. The

solublized thylakoid suspension was centrifuged at 48400 x g using a Ti70 rotor (Beckman Coulter Inc., Fullerton, CA); the pellet contained fragments of unsolubilized membrane and was discarded, leaving the detergent-solubilized membrane proteins in the supernatant.

Linear sucrose density gradients were prepared by placing 9.5 mL of a solution containing 0.5 M sucrose, 5 mM Tricine (pH 8.0, NaOH), 0.03% β-DDM, and 0.5 M betaine into six 12 mL centrifuge tubes. The tubes were then frozen for 2 hours at -20^0 C and thawed for 3 hours at 4^0 C. This establishes a linear density gradient, in which the solution is most dense at the bottom of the centrifuge tube and most dilute at the top. The solution containing solubilized thylakoid proteins is carefully loaded on top of the density gradient solution, and the centrifuge tubes are loaded into an SW-41 (Beckman Coulter Inc., Fullerton, CA) swinging bucket rotor. The density gradients are spun in the ultracentrifuge for 17 hours at 180,000 x g. After sucrose density gradient centrifugation of solubilized thylakoid membranes, three bands were clearly resolved. For this study, the lowest band of PSI-LHCI supercomplexes (F3) were collected from the sucrose gradient and diluted with 3 volumes of 5 mM Tris-HCl, 0.05% β-DDM and 5 mM $CaCl_2$ at pH 8.0. The diluted samples were then concentrated using a Centricon 100 (Amicon, Houston, TX) at 4000 x g in an SS-34 rotor at 4^0 C. The reason for the dilution and subsequent reconcentration was to remove as much sucrose as possible.

Oxygen uptake and SOD activity measurements

PSI-mediated electron transfer from reduced dichloro phenol indophenol ($DCIPH_2$) to methyl viologen (MV) was measured by light-induced O_2 consumption using a Hansatech oxygen electrode at 22°C. White light illumination (250 W m^{-2}) was provided by a 150-W quartz-halogen projector lamp. The reaction mixture was composed of PSI-LHCI supercomplexes (15 mg Chl/ml), 20 mM Tricine-KOH (pH 8), 200 mM MV, 1 mM NaN_2, 100 mM $DCIPH_2$, 5 mM ascorbate, and 10 mM 3-(3,4 dichlorophenyl)-1,1-dimethylurea (DCMU). Samples were incubated in the dark for 5 min before measuring.

For Superoxide dismutase (SOD) activity measurements, thylakoid membranes were suspended in 10mM Tris-HCl (pH 7.5), 0.3 M sorbitol, 1.5m M $CaCl_2$, 10 mM $MgCl_2$, and activity was assayed according to Beauchamp and Fridovich (1971). The required cocktail for SOD activity estimation was prepared by mixing 27 ml of 50mM sodium phosphate buffer (pH 7.8), 1.5 ml of methionine (300 mg ml^{-1}), 1 ml of NBT (14.4 mg 10 ml^{-1}), 0.75 ml of Triton X 100 and 1.5 ml of EDTA. 10 µl of riboflavin (4.4 mg 100 ml-1) and 50 µg of protein were then added to this mixture. After the contents were mixed in a cuvette, they were illuminated for 12 min using a Comptalux bulb and the absorbance was measured at 560 nm.

SDS-denaturing gel electrophoresis and in-gel trypsin digestion

For the analysis of the protein composition of PSI-LHCI supercomplexes from *C. reinhardtii,* samples were size-fractionated by gradient SDS-PAGE (15-23%). Equal amounts of protein (100 µg) were loaded on each lane. The PSI-LHCI

supercomplexes were solubilized in 2% SDS and 0.1 M dithiothreitol, and the gel was stained with Coomassie brilliant blue R250. The desired bands were excised and diced into 1 mm^3 fragments, and then washed three times with 400 µl 50% acetonitrile/50 mM Tris-HCl, pH 8.0, for 15 min to remove the Coomassie blue dye. Gel fragments were then soaked in 100% acetonitrile for 5 min, acetonitrile was removed and the sample was dried in a SpeedVac for 20 min at room temperature. Dried gel slices were rehydrated in 40 µl of 50 mM Tris-HCl, pH 8.0, containing 400 ng of porcine trypsin (Princeton separations, sequencing grade). The samples were digested for 18 h at 37^{o}C, extracted with 50% acetonitrile/5% trifluoroacetic acid for 30 min and dried on a SpeedVac.

MALDI-TOF mass spectrometry and database searches

Tryptic peptides were desalted using C18 ZipTips (Millipore) and eluted with 10 µl of 50% acetonitrile/ 0.1% trifluoroacetic acid. 2 µl aliquots of the sample were mixed with 1.5 µl of matrix (a saturated solution of α-cyano-4-hydroxycinnamic acid in 50% acetonitrile/0.1% trifluoroacetic acid) and a droplet of the mixture (about 1.5 µl) was spotted on the sample plate and dried. Mass spectra were collected on an Applied Biosystems Voyager DE-STR mass spectrometer and analyzed with Data Explorer software. From the monoisotopic masses obtained, the amino acid sequences of matching tryptic fragments of *C. reinhardtii* PSI-LHCI proteins were obtained using the MS-Fit program of the online Protein Prospector software package (UCSF, San Francisco) and the ExPASy Proteomics Server, as previously reported (134).

Immunoblot analysis

PSI-LHCI polypeptides were separated by polyacrylamide gel electrophoresis (PAGE). Electrophoresis was performed on a 15% separating and 4% stacking gel of polyacrylamide. Equal quantities of protein were loaded on to each lane. An equal volume of 2x buffer was added to the aliquots. To identify and quantify the polypeptides contained in the PSI-LHCI supercomplex, immunoblotting was carried out essentially as described by (135). Immunoblotting was performed by electrophoretic transfer of proteins to PVDF membranes. The membrane was incubated with polyclonal antibodies raised in rabbits. We have used the specific primary antibodies against PsaB, PsaC, PsaE and PsaF. PsaB and PsaC were purchased from Agrisera, Sweden and PsaE and PsaF antibodies were a gift from Prof. Kevin Redding, Arizona State University, USA. Subsequently, secondary antibodies ligated to horseradish peroxidase were applied. Chemiluminescence reagents were used to develop the PVDF membrane. The images were recorded on a Bio-Rad CCD camera.

Circular dichroism measurements

Visible circular dichroism spectra were measured in a Jasco 710 spectropolarimeter. The optical path length of the cell was 1 cm, and the distance of the sample from the photomultiplier was 5 cm. The spectra were recorded in 1 nm steps with an integration time of 0.3 s and a band pass of 2 nm.

Ultrafast fluorescence spectroscopy

The time vs. wavelength fluorescence intensity surfaces were recorded on a system consisting of an ultrafast laser and a streak camera, as described

previously (Lidell et al. 2008). Briefly, 130 fs light pulses at 800 nm were generated by a mode-locked Ti:S laser (Mira 900, Coherent Laser) pumped by a frequency-doubled Nd:YVO_4 laser (44% from an 18 W Verdi, Coherent Laser). The repetition rate of the Ti:S laser was reduced to 4.75 MHz by a pulse picker (Model 9200, Coherent Laser). The excitation light (800 nm) was frequency doubled to 400 nm and focused onto a sample cuvette with a 5 mm path length. Fluorescence was collected at a right angle to the excitation beam and focused on the entrance slit of a Chromex 250IS spectrograph which was coupled to a Hamamatsu C5680 streak camera with a M5675 synchroscan sweep unit. The streak images were recorded on a Hamamatsu C4742 CCD camera. Measurements were performed on 800 ps, 1.4 ns, and 2 ns timescales, with 1024 pixels of time resolution. The FWHM of the overall time response of this system was ~6 ps at the 800 ps timescale, ~12 ps at the 1.4 ns timescale, and ~20 ps at the 2 ns timescale. The spectral resolution was 0.124 nm in the spectral range of 650-777 nm (1024 pixels). To avoid singlet-singlet annihilation, the pulse energy was reduced to 0.1 nJ using a neutral density filter. The probability of a single supercomplex absorbing multiple photons in a single laser pulse was estimated using Poisson statistics and it was found that less than 2% of emitted photons could have come from supercomplexes which had received multiple excitations (136). Global analysis was performed using locally-written software in MATLAB. The 1024 kinetic traces were binned, resulting in a spectral resolution of 1.24 nm. A Gaussian shaped instrument response function was used in the fitting.

RESULTS

Trial experiments were carried out to determine a suitable concentration of NaCl to use for salt-stress studies of *C. reinhardtii*. The cells were grown with NaCl concentrations ranging from 10 to 1000 mM. Cells could not be grown at concentrations greater than 150 mM; 100 mM concentration was used for stress conditions in this study. Both control and salt-stressed cells were grown to ~1 OD at 650 nm. A delay in growth was observed in medium with 100 mM NaCl (data not shown).

Sucrose gradient analysis

PSI-LHCI supercomplexes were isolated using sucrose density gradient centrifugation. The detergent extracts of the thylakoid membranes were loaded onto the gradient at equal Chl levels (0.8 mg/mL Chl). After the centrifugation, three distinct bands were observed in both the control and salt stress samples; the fractions corresponded to F1 (LHCII), F2 (PSI-LHCI and PSII) and F3 (PSI-LHCI supercomplexes), as shown in our previous report (134) (Fig. 5-1). For this study, PSI-LHCI supercomplexes (F3) were collected from the sucrose gradient. No significant difference in the bands was observed between the control and salt stress samples (Fig. 5-1).

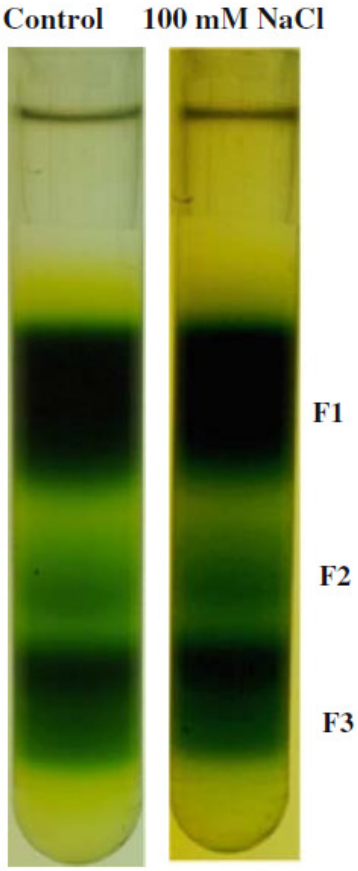

FIGURE 5-1 Separation of PSI-LHCI supercomplexes from solubilized thylakoid membranes by sucrose density centrifugation. See Materials and Methods for further details.

Oxygen uptake analysis and antioxidant enzyme analysis

The electron transfer activity of purified PSI-LHCI supercomplexes from *C. reinhardtii* cells grown at 50 and 100 mM NaCl was measured by assaying O_2 uptake, as described in materials and methods section. PSI activity was reduced by 18% and 39%, respectively (Fig. 5-2) compared to the control sample.

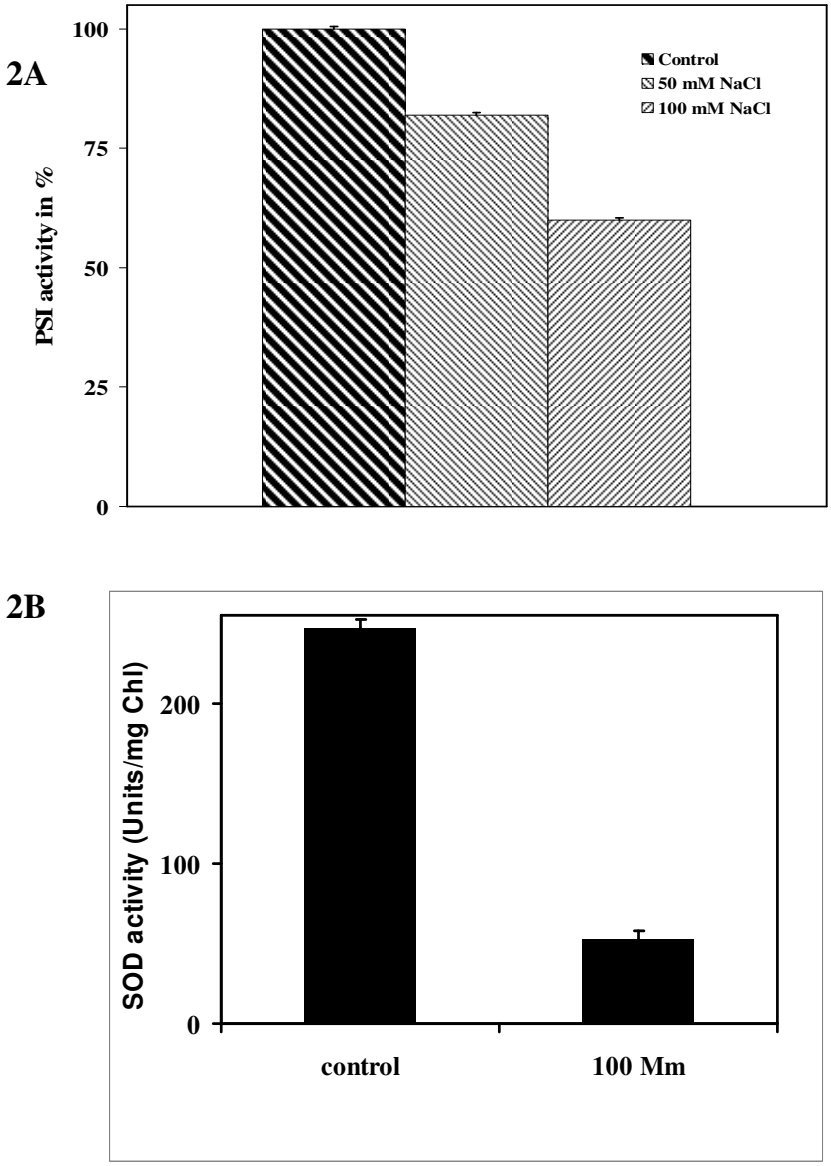

FIGURE 5-2. Oxygen uptake activity and SOD activity of PSI-LHCI supercomplexes isolated from cells grown at control (0 mM), 50 mM and 100 mM NaCl. The PSI activity is 350 µmol/mg^{-1} Chl h^{-1}. A) Oxygen uptake activity B) Total SOD activity.

This result indicates that the activity of the reducing side of PSI is reduced under salt stress. Total SOD activity was decreased by 78% in thylakoids isolated from

cells grown at 100 mM, relative to cells grown under control conditions (Fig. 5-2 B).

Visible CD data analysis

Visible CD spectroscopy is a sensitive monitor of excitonic pigment–pigment interactions and pigment–protein interactions. In the Q_y region, there are two negative peaks at 640 and 672 nm and one positive peak at 656 nm (Fig. 5-3).

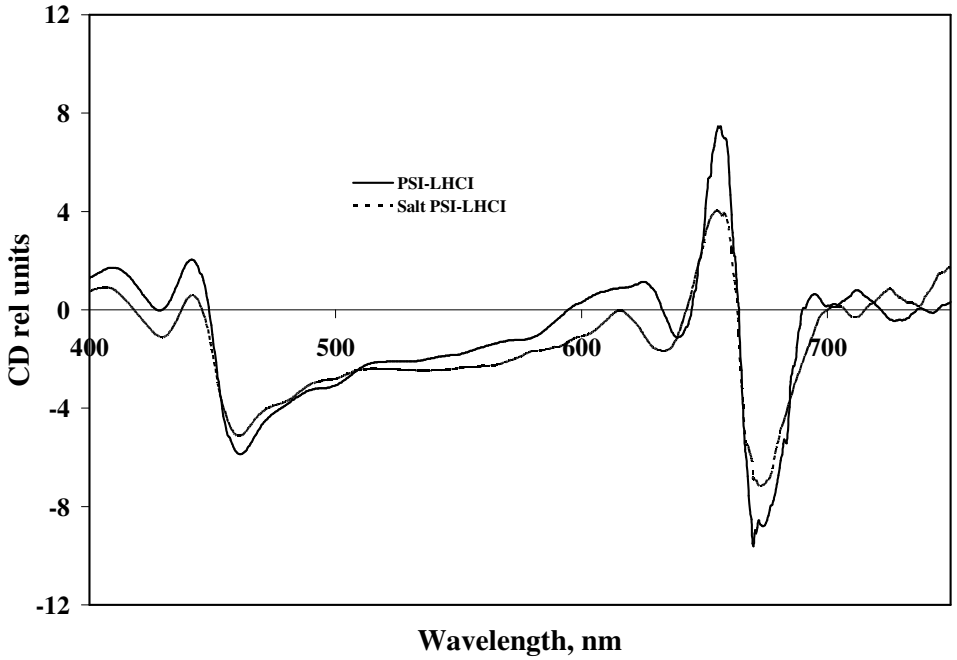

FIGURE 5-3 Visible CD spectra of isolated PSI–LHCI supercomplexes from control and salt-stressed *C. reinhardtii* cells. The Chl content of the samples was adjusted to 10 μg/mL. CD was measured in absorbance units. However, for easier comparison, the data are plotted in relative units. Experimental conditions are given in Materials and Methods.

The two major bands at 656 and 672 nm are due to Chl dimmers caused by excitonic interaction of Chla in PSI-LHCI supercomplexes, while the negative peak at 640 nm is characteristic of Chl *b* (134, 137). In the Soret region, the positive peak at 443 nm originates from Chl *a*, while the negative peak at 460 nm

is characteristic of Chl *b*. The visible CD spectrum of PSI-LHCI supercomplexes isolated from *C. reinhardtii* cells grown at high salt (100 mM) shows a decrease in the amplitude of the major peaks at 656 and 672 nm. The negative peak at 642 nm showed an increase in amplitude relative to the control, along with a blue shift of about 7 nm. The Soret band peaks at 443 and 460 nm also decreased in intensity. The differences in the peak intensity indicate significant differences in pigment interactions in PSI-LHCI complexes from salt stressed cells

Salt stress effect on the protein content of PSI-LHCI

The proteins were separated by SDS-gel electrophoresis and individual proteins identified by MALDI-TOF mass spectrometry and immunoblotting. Figs. 5-4 and

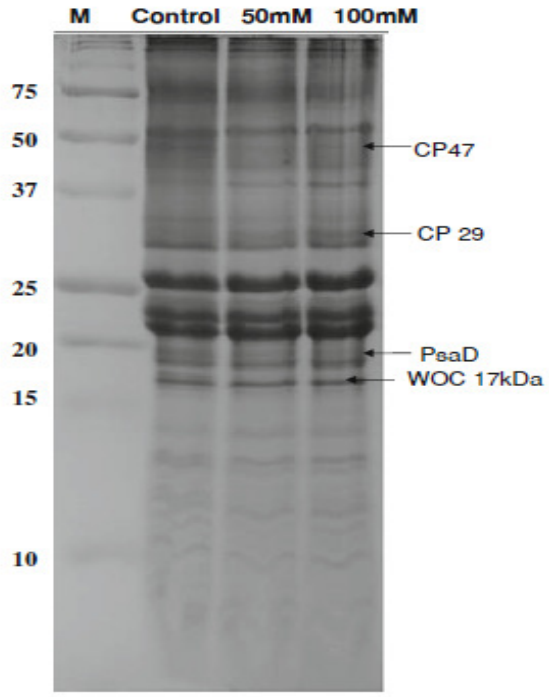

FIGURE 5-4 Comparison of the SDS–PAGE polypeptide profiles of thylakoids from *C. reinhardtii* cells grown under control and salt-stress conditions. A 15-23% gradient gel was used for SDS-PAGE. Equal amounts of protein (100 µg) were loaded onto each lane.

5-5 show that there is no change in content of the reaction center core proteins PsaA and PsaB. Thylakoids isolated from cells grown at different NaCl concentrations (0, 50 and 100 mM) show that several proteins, including components of PSII and PSI, were affected (Fig. 5-4). It appears that, under the experimental conditions used, both PSII and PSI are down regulated by salt stress. Surprisingly, levels of the Lhca proteins remain unchanged (Label LHCI bands in gel, Fig. 5-5A), suggesting that the important changes in antenna function may come from disruption of pigment binding to proteins or disruption of the

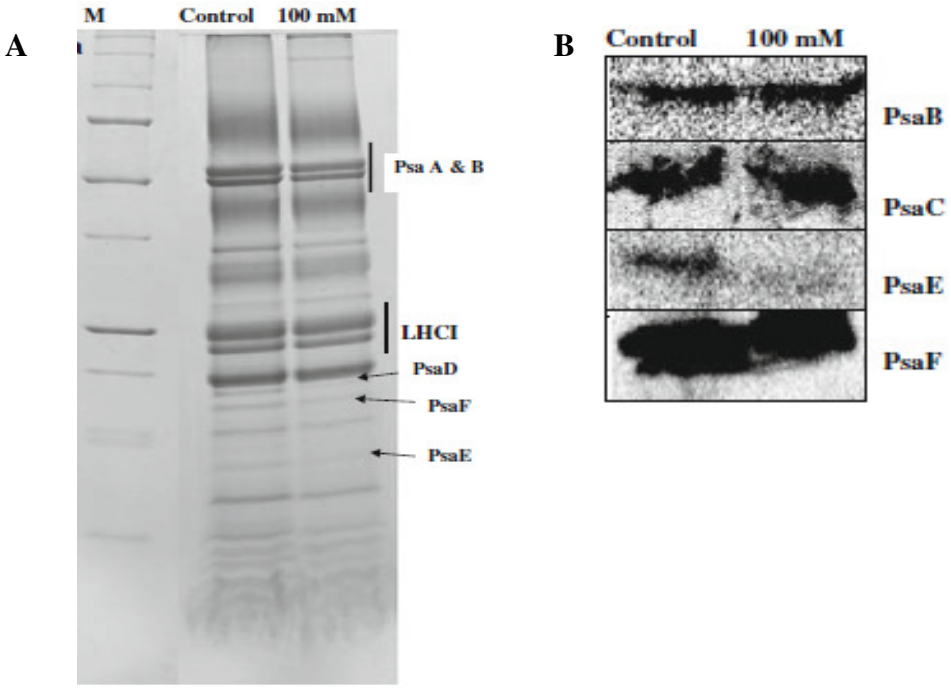

FIGURE 5-5 Comparison of the SDS-PAGE polypeptide profiles and immunoblotting of PSI-LHCI supercomplexes from *C. reinhardtii* cells grown under control and salt-stress conditions. A) 15-23% gradient gel was used for SDS-PAGE. Equal amounts of protein (100 µg) were loaded onto each lane. PsaD (a), PsaF (b) and PsaE (c) were identified by MALDI-TOF. B) Quantitative immunoblot analysis of PSI-LHCI supercomplexes from isolated from control (NaCl-free) and salt-stress (100 mM NaCl) cells. All experimental conditions are given in Materials and Methods.

PSI-LHCI interface, rather than from reduced Lhca protein synthesis. More importantly, levels of the PsaD, PsaF and PsaE proteins were reduced (Fig. 5-5A). The content of PsaD is decreased upon increasing concentration of NaCl; the PsaD band is clearly visible in the control thylakoids (Fig. 5-4). This band has been identified as PsaD by MALDI-TOF. The monoisotopic masses obtained from MALDI-TOF were analyzed using the Aldente peptide mass fingerprinting tool (http://www.expasy.org/tools/aldente/) and a match was found to PsaD from *C. reinhardtii* in thylakoids. Of all the PSI subunits, PsaE seems to be the most sensitive and is completely depleted by salt stress (Fig. 5-5B). The immunoblot data also confirm that levels of these subunits were reduced due to salt stress. In contrast to the other membrane-extrinsic subunits, levels of PsaC did not change.

Flouroscence decay kinetics

Fluorescence decay spectra were measured using an ultrafast streak camera setup for PSI-LHCI supercomplexes isolated under salt stress, and for control conditions. For each sample, kinetics were measured on 800 ps, 1.4 ns, and 2 ns timescales and fit to three decay components.

The component with the shortest lifetime was very consistent across samples and timescales, with a lifetime of ~33 ps. Based on comparison with previous studies of excitation trapping in PSI , this component of the fluorescence decay can be attributed to the trapping of excitons originating within the PSI core (76). The second component, which has previously been associated with the trapping of excitons originating in the peripheral LHCI complexes, is more heterogeneous (138). As is shown in Table 5-2, however, the variations between

samples measured at different time scales are more significant than the differences between the three samples. Although fitting the fluorescence decay with three exponentials provides a convenient description of the kinetics, it must be kept in mind that the real process being measured is far more complicated – the lifetimes found by global analysis merely provide characteristic time scales for various decay processes. Variation of the lifetime found by global analysis with measurement timescale can be attributed to heterogeneity within this decay phase.

TABLE 5-2 Trapping lifetimes obtained from ultrafast flouorescence spectroscopy

Sample	τ_1	τ_2
Control	32.1 ± 3.6 ps	172.26 ± 42.4
NaCl stress	31.6 ± 3.8 ps	156.5 ± 32.8
Timescale		
800 ps	29.8 ± 3.4 ps	136.1 ± 23.6
1.4 ns	33.4 ± 2.4 ps	161.1 ± 13.2
2 ns	34.9 ± 1.7 ps	196.5 ± 21.2

Only the lifetimes of the first two components are presented; the third was typically fixed at 4 ns during fitting and does not represent functional antenna pigments.

Far more insight into the nature of these decay phases can be obtained by examining the spectral shapes of the three decay components. The shape of the first (~33 ps) component is extremely consistent among the samples measured (Fig. 5-6A). Given that the PsaA and PsaB proteins, which bind the bulk of PSI's core antenna, appear based on immunoblotting results to be largely unaffected by

salt stress, this suggests strongly that only pigments bound to the PSI core contribute to this component. This is consistent with structural studies that show that the PSI core is a stable, tightly-integrated complex (14, 75). Similar conservation can be seen in the spectral shapes of the third component (3-4 ns); such lifetimes are typically attributed to detergent-solubilized Chl that is not coupled to PSI (Fig. 5-6C). It should be noted that the amplitude of the nanosecond component was much lower in the control sample than in the stress samples and the spectral shapes could only be compared after normalization. This indicates that the PSI-LHCI from salt stressed cells contains more uncoupled pigments.

The major difference in the decay-associated spectra of the control and salt-stress samples can be seen in the spectral shape of the 120-220 ps component (Fig. 5-6B). While the decay lifetimes are relatively unchanged by cell growth under salt stress conditions, this component shows a decrease in emission intensity on the red side of the peak in the salt-stressed samples. Red emission in *C. reinhardtii* PSI has previously been associated with strongly-coupled pigments bound by the LHCI proteins and so this loss of red emission can be attributed to a disruption of the LHCI antenna system (139-141).

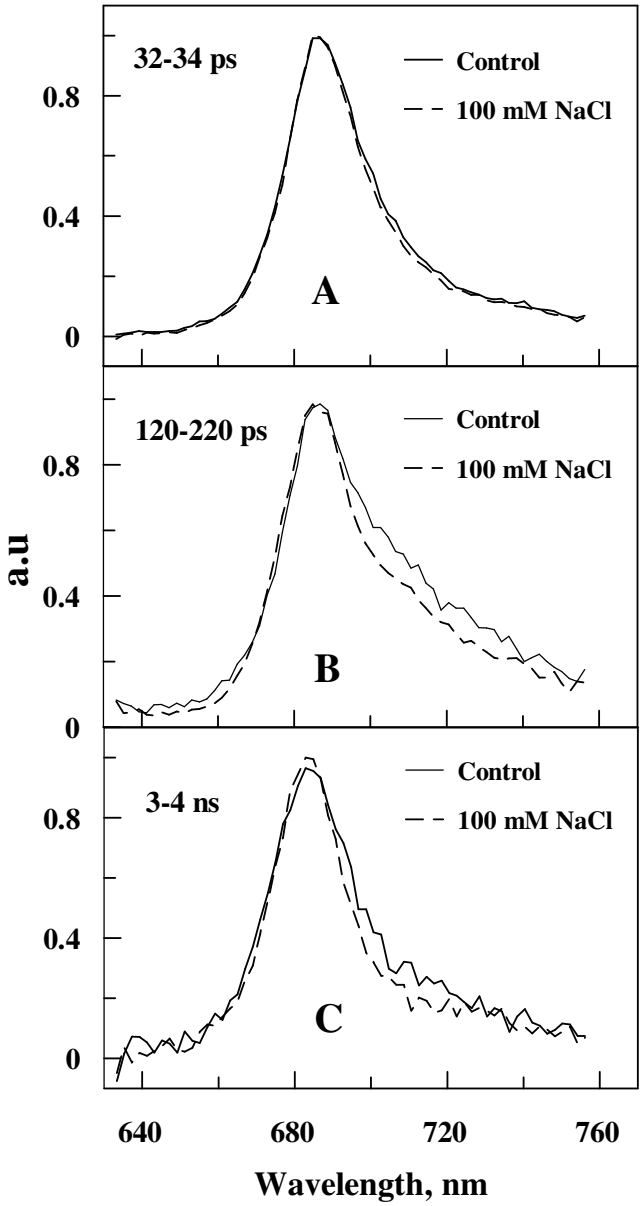

FIGURE 5-6 Representative fluorescence decay-associated spectra (FDAS) obtained from ultrafast fluorescence spectroscopy measurements from isolated PSI-LHCI supercomplexes obtained from *C. reinhardtii* grown under control (NaCl-free) and stress (100 mM NaCl) conditions. Fluorescence decay lifetimes are A) 35-38 ps B) 122-211 ps and C) 2-4 ns. Each curve shown is the average of the fitted curves from the three data sets collected for each sample.

DISCUSSION

The primary objective of this work was to evaluate the effects of salt stress on PSI-LHCI supercomplexes from *C. reinhardtii*, in an effort to understand the effects of stress on PSI function. Previous research has shown that many types of abiotic stress affect PSII, but the extent of damage for PSI is less well studied. Our results indicate, , that stress-related damage to PSI is also significant and may be an important part of the organism's overall stress response.

C. reinhardtii cells were grown at NaCl concentrations of 0 (control) and 100 mM, reaching an OD of ~1 at 650 nm. The control cells reached this growth within four days; growth in high-salt medium took five days to reach the same density. High salt conditions clearly impair cell growth; the goal of this study has been to establish the degree to which this growth impairment results from damage to PSI-LHCI. In particular, we have attempted to determine the structural integrity of PSI-LHCI under salt stress, as well as functional changes associated with structural rearrangements. The electron transfer activity was decreased (Fig. 5-2), but levels of the subunits PsaA and PsaB, which form the core of PSI and bind the majority of the cofactors of the electron transfer chain (ETC) (P700, A, A_O, phylloquinones (A_1) and the 4Fe4S clusters, F_X) (ETC) , were unchanged. This suggests that the impairment may lie in energy transfer from LHCI to PSI core, or in damage to the acceptor side of PSI (terminal FeS clusters F_A + F_B), rather than to the oxidizing side of the ETC.

In keeping with these results, the fluorescence decay component associated with trapping in the PSI core was virtually unchanged between the

control and salt stress samples (Fig. 5-6A). Differences were quite apparent in the second component (Fig. 5-6B), which decays on the 120-220 ps timescale. The curves look similar on the blue side of the emission peak, but the stressed samples show significantly less emission on the red side than the control sample. Red-shifted pigments in photosynthetic systems typically arise from strongly-coupled dimers of Chl molecules and may exert a significant influence on the exciton trapping dynamics. Previous spectroscopic studies of green algal PSI have indicated that the PSI core in *C. reinhardtii* does not contain any pigments with transition energies lower than that of P700 – longer-wavelength pigments are associated only with the peripheral LHCI complexes (139-141). The loss of red-shifted emission in the salt samples can therefore be attributed to the change in pigment-pigment interactions of LHCI complexes under stress conditions.

The visible CD data show an increase in amplitude at 676 and 656 nm, which can be attributed to a loss of tightly coupled Chl *a* in the LHCI antenna. The peak associated with Chl *b* shifts from 640 to 630 nm under salt stress conditions (Fig. 5-3), suggesting a change in pigment-pigment interactions and may arise, for example, from a change of the Chl *a* to Chl *b* distance.

The stromal acceptor side of the PSI reaction center is damaged by high salt conditions. Our results show (Figs. 5-4 and 5-5) a clear reduction in the membrane-extrinsic PsaD and PsaE subunits, as well as the transmembrane PsaF subunit of PSI. The reduction is most dramatic in the case of PsaE in both thylakoids and isolated PSI-LHCI supercomplexes. The crystal structure of *Thermosynechococcus* PSI shows that PsaE stabilizes the stromal hump and the

interaction between the PsaA/B heterodimer and PsaC (14, 142). The higher plant PSI structure retains the same organization as the cyanobacterial complex (75); we assume that green algal PSI also retains the same overall architecture. From our data, it is clear that the degradation of the PSI stromal ridge begins at PsaE and PsaD. The PsaE protein is located at the reducing side of photosystem I (PSI) and stabilizes the stromal hump that is involved in docking the soluble electron acceptors, particularly ferredoxin /flavodoxin (14, 142). While PsaC binds the terminal electron acceptors F_A and F_B and is essential for the function of PSI, PsaD and PsaE stabilize PsaC and the stromal hump that is involved in ferredoxin binding (143-145).

The damage to PSI subunits is associated with a decrease in SOD activity; this decrease probably results in higher levels of reactive oxygen species. Similar results have been observed in Cd stress in plants (146-148). The loss of PsaE at the reducing side of PSI may cause electron leakage to oxygen in the light (Mehler reaction), resulting in the formation of reactive oxygen species which could in turn damage the Fe-S clusters. These results agree with a very recent report of a deletion mutant of *psaE* in the cyanobacterium *Synechocystis sp.* strain PCC 6803, which shows increased photodamage due to formation of oxygen radicals (149). As a result, the ferredoxin docking site near the stromal Fe-S clusters is destabilized, crippling electron transfer through PSI.

Mutagenesis studies have indicated that the subunits on the reducing side of PSI assemble in a well-defined order: PsaC first, followed by PsaD and PsaE (150, 151). Under salt-stress conditions, the dramatic decrease in levels of PsaD

(Fig. 5-4) is results in the near-elimination of PsaE (Fig. 5-5B); this correlation supports a scheme in which the presence of PsaD is a prerequisite for PsaE binding (152). Immunoblotting results also indicate that the levels of PsaC are virtually unchanged under salt stress (Fig. 5-5B); this is consistent with an assembly pathway in which PsaC binds first and is removed last when the complex is disassembled. This likely does not mean, however, that the function of PsaC is unimpacted by salt stress (153); PsaD has been proposed to play a role in the structural stabilization of the otherwise labile PsaC (143, 154, 155), and the magnetic properties of the terminal FeS clusters F_A and F_B, which bind to PsaC, are affected by the presence of PsaD (156, 157). In summary, these results indicate that the acceptor side of PSI is strongly affected by salt stress and the electron transfer capabilities of F_A and F_B could be severely impacted, even if levels of PsaC are unchanged. Furthermore, it is known that the LHCI proteins attach to PSI near PsaF so the loss of PsaF under salt stress could explain the loss of LHCI-associated red emission observed in the fluorescence decay-associated spectra (26, 75) (Fig. 5-6). All of these results appear to be triggered by the accumulation of ROS damage in the absence of effective protection from SOD; this supports the idea that accumulation of SOD in response to salt, drought and cold stress plays a crucial role in helping the cell to survive under environmental stress conditions.

The SOD is influencing the changes in PSI organization. However, the PSII was also damaged and thus *C.reinhardtii* cell growth was impaired due to change in both PSI and PSII.

CHAPTER 6 CONCLUSIONS

In this dissertation new knowledge was acquired about the photosystem I/light harvesting complexes (PSI-LHCI) and photosystem II (PSII) from the thermo-acidophilic red alga, *Galdieria sulphuraria* and the effect of salt stress on the PSI-LHCI complex of the green alga, *Chlamydomonas reinhardtii*. The work presented here shed new light into the evolution of PSI-LHCI and PSII. Results of this thesis on top-down mass spectrometry usage for characterization of large integral membrane proteins are of exteme interest to the general scientific community.

An introduction on photosynthesis and current knowledge of photosynthetic membrane protein complexes was described in chapter 1. In chapter 2, isolation and purification of PSI-LHCI supercomplex and PSII from *Galdieria sulphuraria* were described. Both isolated photosystems are of high purity and photochemically active and are used for experiments conducted in chapter 3 and 4.

In chapter 3, our study described for the first time a functionally tightly coupled PSI-LHCI complex in an eukaryote (*Galdieria sulphuraria*) using electron microscopy and ultra-fast fluorescence spectroscopy. Electron micrographs of *Galdieria* PSI-LHCI revealed a tightly coupled complex that may contain a second layer of light harvesting complexes (LHC's) on one side of the monomer. In contrast to higher plants PSI-LHCI complex which contains 4 light harvesting proteins, *Galdieria* PSI-LHCI supercomplex contains 8 to 10 light harvesting proteins per monomer. The most exciting results are from the ultra-fast

fluorescence spectroscopy which shows for the first time that the large PSI-LHCI complex in *Galdieria* is tightly functionally coupled where excitation energy transfer between LHCI to the PSI reaction center occurs in a timescale of 47 ps. In comparison, the PSI-LHCI complex of green algae and plants excitation energy transfer between LHCI and PSI reaction center occurs in a timescale of 120 ps or longer which is remarkable as these complexes have only four light harvesting proteins. Biochemical characterization of the isolated *Galdieria* PSI-LHCI complex is highly stable and remains intact during the purification process. This is futher confirmed by the ultrafast fluorescence spectroscopy results which shows that by less than 2% of long live chlorophyll fluorescence component is coming from the uncoupled free chlorophylls. This tight coupling between the PSI and LHCI proteins is essential for efficient light harvesting for *Galdieria*, as they thrive in acidic crevices in volcanic rocks and endolithic habitats which has consistent low light conditions.

LHC proteins are proposed to have evolved following a series of duplication and fusion events of Hlips (high light-induced proteins) present in an ancient photosynthetic organism, an ancestor of today's cyanobacteria, algae and higher plants. Phylogenetic studies have shown that LHC proteins of rhodophyta (red alga) diverged early from an ancestral LHC protein in an ancient photosynthetic eukaryote and developed independently as chlorophyll-a binding LHC proteins. Further, it is been proposed that a first fully functional light harvesting protein will be more likely associated with PSI than with PSII (158). With *Galdieria* assumed to represent an ancient PSI, we can assume the LHC

proteins associated with its PSI core most likely represents an ancestral LHC protein evolved from an ancestral prokaryote, older than the current LHC proteins present in other red algae, green algae and higher plants. Furthermore, the five LHC proteins identified in *Galdieria* have a 56 % sequence identity with each other, forming a homogenous family, indicating that they had evolved from a common ancestor (39). Considering *Galdieria*'s habitat, there are only a few pockets of acidic sites distributed in the Earth. Additionally, *Galdieria* is restricted to migration, as they are susceptible to dessication, mesophilic conditions and neutral pH. So *Galdieria* must be geographically isolated in their acidic habitats, which in turn reduces chance of horizontal gene transfer from other organisms. So our hypothesis is, *Galdieria* PSI diverged from an ancient photosynthetic eukaryote with loosely attached antenna complexes, but owing to their habitat and movement restriction they have adapted in their low light habitat for hundred million years. Over time, tighter coupling between lhcr proteins with PSI core in *Galdieria* might have occurred later due to survival pressure under light deprived conditions. Adaptation to this unique environment niche over years might explain the reason for the uniqueness of 30 % of the *Galdieria* genome in comparison with other Cyanidiales. Like *Galdieria*, cyanobacteria habitats are often characterized by light deprived conditions. But *Galdieria* and cyanobacteria might have taken different routes in evolution process for efficient light harvesting: cyanobacteria had changed its PSI oligomeric state from monomer to trimer, while *Galdieria* PSI with its primary loosely attached light harvesting complexes has optimized its LHCr proteins to a tighter coupling with its PSI core.

Our hypothesis is strengthen by the results of a phylogenetic study, stating that *Galdieria* and its sister species (cyanidiales) has a long evolutionary history and they represent one of the ancient forms of red algae, diverged about 1.3 billions years ago from other red algae forming distinct lineage. It will be of high interest for future studies to address whether the close coupling observed in our study is the result of a static, unregulatable arrangement of auxillary antenna proteins, or whether *Galdieria* possesses other means (besides traditional state transitions) of adapting its light-harvesting machinery to variable light conditions. Also, a phylogenetic analysis study of *Galdieria* lhcr proteins will beneficial to clarify our fore-mentioned hypothesis.

In chapter 4, high-resolution top-down MS was used to characterize eleven integral and five peripheral subunits of a large integral membrane protein, photosystem II (750 kDa) of the eukaryotic red alga, *Galdieria sulphuraria*. *Galdieria* PSII was used as a model protein to show the amenability of integral membrane proteins to top-down MS. *Galdieria* PSII has been characterized with unprecedented detail with identification of post translational modification of all the peripheral and small membrane subunits. This study is a technology advancement paving the way for the usage of top-down mass spectrometry for characterization of other large integral membrane proteins.

The primary separation used LC MS with concomitant fraction collection (LC-MS+), yielding around 40 intact mass tags at 100 ppm mass accuracy on a low-resolution ESI mass spectrometer, whose retention time and mass were used to guide subsequent high-resolution top-down nano-electrospray FT ion-cyclotron

resonance MS experiments (FT-MS). Both collisionally activated and electron capture dissociation were used to confirm the presence of eleven small subunits to mass accuracy within 5 ppm; PsbE, PsbF, PsbH, PsbI, PsbJ, PsbK, PsbL, PsbM, PsbT, PsbX and PsbZ. All subunits showed covalent modifications that fall into three classes including retention of initiating formyl-methionine, removal of methionine at the N-terminus with or without acetylation, and removal of a longer N-terminal peptide. Peripheral subunits identified by top-down analysis included oxygen-evolving complex subunits PsbO, PsbU, PsbV, as well as two new subunits, Psb28 (PsbW) and Psb27 (‘‘PsbZ-like’’) not present in cyanobacteria. Top-down high-resolution MS provides the necessary precision, typically less than 5 ppm, for identification and characterization of polypeptide composition of this important membrane protein complex. By using top-down mass spectrometry, it is easy to see where the actual primary structure diverges from that predicted by translation of DNA sequence. Top-down high-resolution MS is clearly the technology of choice for absolute characterization of protein identity and modification.

In chapter 5, we have used *Chlamydomonas reinhardtii* as a model system to study the effects of high salt conditions on PSI-LHCI supercomplexes. This is the first study that shows a rearrangement of PSI-LHCI supercomplexes under salt stress and identified functional changes that occur in PSI-LHCI supercomplex under high salt conditions. Our results indicate that the acceptor side of PSI consisting of PsaC, PsaD and PsaE is affected by salt stress. This result might also have a high general impact because nearly 20 to 25 % of the world arable land is

affected by soil salinity. These results may be used for example in the future to develop agricultural crop plants which can grow under higher salt conditions for higher crop yield.

REFERENCES

1. Fromme, P., editor. 2005. Photosynthetic protein complexes : A Structural Approach. Wiley-Blackwell, Weinheim.

2. Blankenship, R. E. 2002. Molecular Mechanisms of Photosynthesis. Blackwell Science, Oxford.

3. Holland, H. D. 1997. Geochemistry - Evidence for life on Earth more than 3850 million years ago. Science 275:38-39.

4. Olson, J. M. 2006. Photosynthesis in the Archean Era. Photosynthesis Research 88:109-117.

5. Canfield, D. E., K. S. Habicht, and B. Thamdrup. 2000. The Archean sulfur cycle and the early history of atmospheric oxygen. Science 288:658-661.

6. Jahnke, L. L., R. E. Summons, J. M. Hope, and D. J. des Marais. 1999. Carbon isotopic fractionation in lipids from methanotrophic bacteria II: The effects of physiology and environmental parameters on the biosynthesis and isotopic signatures of biomarkers. Geochimica Et Cosmochimica Acta 63:79-93.

7. Marais, D. J. D., H. Strauss, R. E. Summons, and J. M. Hayes. 1992. Carbon isotope evidence for the stepwise oxidation of the proterozoic environment Nature 359:605-609.

8. Nelson, N., and A. Ben-Shem. 2004. The complex architecture of oxygenic photosynthesis. Nature Reviews Molecular Cell Biology 5:971-982.

9. Vanselow, C., A. P. M. Weber, K. Krause, and P. Fromme. 2009. Genetic analysis of the Photosystem I subunits from the red alga, Galdieria sulphuraria. Biochimica Et Biophysica Acta-Bioenergetics 1787:46-59.

10. Loll, B., J. Kern, W. Saenger, A. Zouni, and J. Biesiadka. 2005. Towards complete cofactor arrangement in the 3.0 angstrom resolution structure of photosystem II. Nature 438:1040-1044.

11. Kurisu, G., H. M. Zhang, J. L. Smith, and W. A. Cramer. 2003. Structure of the cytochrome b(6)f complex of oxygenic photosynthesis: Tuning the cavity. Science 302:1009-1014.

12. Inoue, T., M. Gotowda, H. Sugawara, T. Kohzuma, F. Yoshizaki, Y. Sugimura, and Y. Kai. 1999. Structure comparison between oxidized and reduced plastocyanin from a fern, Dryopteris crassirhizoma. Biochemistry 38:13853-13861.

13. Sawaya, M. R., D. W. Krogmann, A. Serag, K. K. Ho, T. O. Yeates, and C. A. Kerfeld. 2001. Structures of cytochrome c-549 and cytochrome c(6) from the cyanobacterium Arthrospira maxima. Biochemistry 40:9215-9225.

14. Jordan, P., P. Fromme, H. T. Witt, O. Klukas, W. Saenger, and N. Krauss. 2001. Three-dimensional structure of cyanobacterial photosystem I at 2.5 angstrom resolution. Nature 411:909-917.

15. Morales, R., M. H. Chron, G. Hudry-Clergeon, Y. Petillot, S. Norager, M. Medina, and M. Frey. 1999. Refined X-ray structures of the oxidized, at 1.3 angstrom, and reduced, at 1.17 angstrom, [2Fe-2S] ferredoxin from the cyanobacterium Anabaena PCC7119 show redox-linked conformational changes. Biochemistry 38:15764-15773.

16. Serre, L., F. Vellieux, M. Medina, C. GomezMoreno, J. C. FontecillaCamps, and M. Frey. 1996. Crystal structures of a ferredoxin:NADP(+) reductase and of a complex with NADP(+). Biochemical Society Transactions 24:S10-S10.

17. Serre, L., F. M. D. Vellieux, M. Medina, C. GomezMoreno, J. C. FontecillaCamps, and M. Frey. 1996. X-ray structure of the Ferredoxin:NADP(+) reductase from the cyanobacterium Anabaena PCC 7119 at 1.8 angstrom resolution, and crystallographic studies of NADP(+) binding at 2.25 angstrom resolution. Journal of Molecular Biology 263:20-39.

18. Abrahams, J. P., A. G. W. Leslie, R. Lutter, and J. E. Walker. 1994. Structure at 2.8-angstrom of F1-ATPase from bovine-heart-mitochondria Nature 370:621-628.

19. Guskov, A., J. Kern, A. Gabdulkhakov, M. Broser, A. Zouni, and W. Saenger. 2009. Cyanobacterial photosystem II at 2.9-angstrom resolution and the role of quinones, lipids, channels and chloride. Nature Structural & Molecular Biology 16:334-342.

20. Shi, L. X., and W. P. Schroder. 2004. The low molecular mass subunits of the photosynthetic supracomplex, photosystem II. Biochimica Et Biophysica Acta-Bioenergetics 1608:75-96.

21. Grotjohann, I., C. Jolley, and P. Fromme. 2004. Evolution of photosynthesis and oxygen evolution: Implications from the structural comparison of Photosystems I and II. Physical Chemistry Chemical Physics 6:4743-4753.

22. Enami, I., T. Suzuki, O. Tada, Y. Nakada, K. Nakamura, A. Tohri, H. Ohta, I. Inoue, and J. R. Shen. 2005. Distribution of the extrinsic proteins as a potential marker for the evolution of photosynthetic oxygen-evolving photosystem II. Febs Journal 272:5020-5030.

23. Kammel, M., J. Kern, W. Lubitz, and R. Bittl. 2003. Photosystem II single crystals studied by transient EPR: the light-induced triplet state. Biochimica Et Biophysica Acta-Bioenergetics 1605:47-54.

24. Campbell, M. K. 2006. Biochemistry. Thomas Brooke/Cole, Belmont, CA.

25. Fromme, P., P. Jordan, and N. Krauss. 2001. Structure of photosystem I. Biochimica Et Biophysica Acta-Bioenergetics 1507:5-31.

26. Ben-Shem, A., F. Frolow, and N. Nelson. 2003. Crystal structure of plant photosystem I. Nature 426:630-635.

27. Amunts, A., O. Drory, and N. Nelson. 2007. The structure of a plant photosystem I supercomplex at 3.4 angstrom resolution. Nature 447:58-63.

28. Amunts, A., and N. Nelson. 2009. Plant Photosystem I Design in the Light of Evolution. Structure 17:637-650.

29. Kouril, R., A. Zygadlo, A. A. Arteni, C. D. de Wit, J. P. Dekker, P. E. Jensen, H. V. Scheller, and E. J. Boekema. 2005. Structural characterization of a complex of photosystem I and light-harvesting complex II of Arabidopsis thaliana. Biochemistry 44:10935-10940.

30. Takahashi, H., M. Iwai, Y. Takahashi, and J. Minagawa. 2006. Identification of the mobile light-harvesting complex II polypeptides for state transitions in Chlamydomonas reinhardtii. Proceedings of the National Academy of Sciences of the United States of America 103:477-482.

31. Ciniglia, C., H. S. Yoon, A. Pollio, G. Pinto, and D. Bhattacharya. 2004. Hidden biodiversity of the extremophilic Cyanidiales red algae. Molecular Ecology 13:1827-1838.

32. Weber, A. P. M., C. Oesterhelt, W. Gross, A. Brautigam, L. A. Imboden, I. Krassovskaya, N. Linka, J. Truchina, J. Schneidereit, H. Voll, L. M. Voll, M. Zimmermann, A. Jamai, W. R. Riekhof, B. Yu, R. M. Garavito, and C. Benning. 2004. EST-analysis of the thermo-acidophilic red microalga Galdieria sulphuraria reveals potential for lipid A biosynthesis and unveils the pathway of carbon export from rhodoplasts. Plant Molecular Biology 55:17-32.

33. Yoon, H. S., C. Ciniglia, M. Wu, J. M. Comeron, G. Pinto, A. Pollio, and D. Bhattacharya. 2006. Establishment of endolithic populations of extremophilic Cyanidiales (Rhodophyta). Bmc Evolutionary Biology 6:12.

34. Oesterhelt, C., S. Vogelbein, R. P. Shrestha, M. Stanke, and A. P. M. Weber. 2008. The genome of the thermoacidophilic red microalga Galdieria sulphuraria encodes a small family of secreted class III peroxidases that might be involved in cell wall modification. Planta 227:353-362.

35. Linka, M., A. Jamai, and A. P. M. Weber. 2008. Functional Characterization of the Plastidic Phosphate Translocator Gene Family from the Thermo-Acidophilic Red Alga Galdieria sulphuraria Reveals Specific Adaptations of Primary Carbon Partitioning in Green Plants and Red Algae. Plant Physiology 148:1487-1496.

36. Gardian, Z., L. Bumba, A. Schrofel, M. Herbstova, J. Nebesarova, and F. Vacha. 2007. Organisation of Photosystern I and Photosystem II in red alga Cyanidium caldarium: Encounter of cyanobacterial and higher plant concepts. Biochimica Et Biophysica Acta-Bioenergetics 1767:725-731.

37. Adachi, H., I. Enami, T. Henmi, N. Kamiya, and J. Shen. 2007. Purification and crystallization of photosystem II complex from a red alga Cyanidium caldarium. Photosynthesis Research 91:PS440.

38. Adachi, H., Y. Umena, I. Enami, T. Henmi, N. Kamiya, and J. R. Shen. 2009. Towards structural elucidation of eukaryotic photosystem II: Purification, crystallization and preliminary X-ray diffraction analysis of photosystem II from a red alga. Biochimica Et Biophysica Acta-Bioenergetics 1787:121-128.

39. Marquardt, J., B. Lutz, S. Wans, E. Rhiel, and W. E. Krumbein. 2001. The gene family coding for the light-harvesting polypeptides of Photosystem I of the red alga Galdieria sulphuraria. Photosynthesis Research 68:121-130.

40. Enami, I., S. Kikuchi, T. Fukuda, H. Ohta, and J. R. Shen. 1998. Binding and functional properties of four extrinsic proteins of photosystem II from

a red alga, Cyanidium caldarium, as studied by release - Reconstitution experiments. Biochemistry 37:2787-2793.

41. Enami, I., S. Yoshihara, A. Tohri, A. Okumura, H. Ohta, and J. R. Shen. 2000. Cross-reconstitution of various extrinsic proteins and photosystem II complexes from cyanobacteria, red algae and higher plants. Plant and Cell Physiology 41:1354-1364.

42. Dekker, J. P., E. J. Boekema, H. T. Witt, and M. Rogner. 1988. Refined purification and further characterization of oxygen-evolving and Tris-treated photosystem II particles from the thermophilic cyanobacterium *Synechococcus sp.* Biochimica Et Biophysica Acta 936:307-318.

43. Kern, J., B. Loll, C. Luneberg, D. DiFiore, J. Biesiadka, K. D. Irrgang, and A. Zouni. 2005. Purification, characterisation and crystallisation of photosystem II from Thermosynechococcus elongatus cultivated in a new type of photobioreactor. Biochimica Et Biophysica Acta-Bioenergetics 1706:147-157.

44. Li, Y. X., Z. Q. Gao, D. M. Li, G. C. Wang, and F. Wang. 2010. Isolation and characterization of the oxygen-evolving photosystem II complex from the economical red alga Bangia fusco-purpurea. Russian Journal of Plant Physiology 57:609-614.

45. Nagao, R., T. Tomo, E. Noguchi, S. Nakajima, T. Suzuki, A. Okumura, Y. Kashino, M. Mimuro, M. Ikeuchi, and I. Enami. 2010. Purification characterization of a stable oxygen-evolving Photosystem II complex from a marine centric diatom, *Chaetoceros gracilis* Biochimica Et Biophysica Acta-Bioenergetics 1797:576-576.

46. Porra, R. J., W. A. Thompson, and P. E. Kriedemann. 1989. Determination of accurate extinction coefficients and simultaneous-equations for assaying chlorophyll-a and chlorophyll-b extracted with 4 different solvents - verification of the concentration of chlorphyll standards by atomic-absorption spectroscopy Biochimica et Biophysica Acta 975:384-394.

47. Schagger, H. 2006. Tricine-SDS-PAGE. Nature Protocols 1:16-22.

48. Lees, J. G., and B. A. Wallace. 2002. Synchrotron radiation circular dichroism and conventional circular dichroism spectroscopy: A comparison. Spectroscopy-an International Journal 16:121-125.

49. Wallace, B. A., and R. W. Janes. 2003. Circular dichroism and synchrotron radiation circular dichroism spectroscopy: tools for drug

discovery (vol 31, pg 631, 2003). Biochemical Society Transactions 31:1531-1531.

50. Miles, A. J., F. Wien, J. G. Lees, A. Rodger, R. W. Janes, and B. A. Wallace. 2003. Calibration and standardisation of synchrotron radiation circular dichroism and conventional circular dichroism spectrophotometers. Spectroscopy-an International Journal 17:653-661.

51. Lees, J. G., B. R. Smith, F. Wien, A. J. Miles, and B. A. Wallace. 2004. CDtool - an integrated software package for circular dichroism spectroscopic data processing, analysis, and archiving. Analytical Biochemistry 332:285-289.

52. Whitmore, L., and B. A. Wallace. 2004. DICHROWEB, an online server for protein secondary structure analyses from circular dichroism spectroscopic data. Nucleic Acids Research 32:W668-W673.

53. Vanstokkum, I. H. M., H. J. W. Spoelder, M. Bloemendal, R. Vangrondelle, and F. C. A. Groen. 1990. Estimation of protein secondary structure and error analysis from circular-dichroism spectra. Analytical Biochemistry 191:110-118.

54. Sreerama, N., S. Y. Venyaminov, and R. W. Woody. 1999. Estimation of the number of alpha-helical and beta-strand segments in proteins using circular dichroism spectroscopy. Protein Science 8:370-380.

55. Sreerama, N., and R. W. Woody. 2000. Estimation of protein secondary structure from circular dichroism spectra: Comparison of CONTIN, SELCON, and CDSSTR methods with an expanded reference set. Analytical Biochemistry 287:252-260.

56. Lees, J. G., A. J. Miles, F. Wien, and B. A. Wallace. 2006. A reference database for circular dichroism spectroscopy covering fold and secondary structure space. Bioinformatics 22:1955-1962.

57. Gross, W., and C. Schnarrenberger. 1995. Heterotrophic growth of 2 strains of the acido-thermophilic red alga Galdieria sulphuraria Plant and Cell Physiology 36:633-638.

58. Takahashi, T., N. Inoue-Kashino, S. Ozawa, Y. Takahashi, Y. Kashino, and K. Satoh. 2009. Photosystem II Complex in Vivo Is a Monomer. Journal of Biological Chemistry 284:15598-15606.

59. Fromme, P., and H. T. Witt. 1998. Improved isolation and crystallization of Photosystem I for structural analysis. Biochimica Et Biophysica Acta-Bioenergetics 1365:175-184.

60. Hiyama, T., and B. Ke. 1972. Difference spectra and extinction coefficients of P700 Biochimica et Biophysica Acta 267:160-&.

61. Witt, H., E. Schlodder, C. Teutloff, J. Niklas, E. Bordignon, D. Carbonera, S. Kohler, A. Labahn, and W. Lubitz. 2002. Hydrogen bonding to P700: Site-directed mutagenesis of threonine A739 of photosystem I in Chlamydomonas reinhardtii. Biochemistry 41:8557-8569.

62. Kitmitto, A., A. Holzenburg, and R. C. Ford. 1997. Two-dimensional crystals of photosystem I in higher plant grana margins. Journal of Biological Chemistry 272:19497-19501.

63. Whitelegge, J. P., H. M. Zhang, R. Aguilera, R. M. Taylor, and W. A. Cramer. 2002. Full subunit coverage liquid chromatography electrospray ionization mass spectrometry (LCMS+) of an oligomeric membrane protein - Cytochrome b6f complex from spinach and the cyanobacterium Mastigocladus laminosus. Mol. Cell. Proteomics 1:816-827.

64. Nally, J. E., J. P. Whitelegge, S. Bassilian, D. R. Blanco, and M. A. Lovett. 2007. Characterization of the outer membrane Proteome of Leptospira interrogans expressed during acute lethal infection. Infection and Immunity 75:766-773.

65. Oostergetel, G. T., W. Keegstra, and A. Brisson. 1998. Automation of specimen selection and data acquisition for protein electron crystallography. Ultramicroscopy 74:47-59.

66. Arteni, A. A., G. Ajlani, and E. J. Boekema. 2009. Structural organisation of phycobilisomes from Synechocystis sp strain PCC6803 and their interaction with the membrane. Biochimica et Biophysica Acta 1787.

67. Subramanyam, R., C. Jolley, B. Thangaraj, S. Nellaepalli, A. N. Webber, and P. Fromme. 2010. Structural and functional changes of PSI-LHCI supercomplexes of Chlamydomonas reinhardtii cells grown under high salt conditions. Planta 231:913-922.

68. Jolley, C. 2007. Structure and dynamics in photosystem I. In Department of Physics. Arizona State University, Tempe, Arizona.

69. Liddell, P. A., M. Gervaldo, J. W. Bridgewater, A. E. Keirstead, S. Lin, T. A. Moore, A. L. Moore, and D. Gust. 2008. Porphyrin-based hole conducting electropolymer. Chemistry of Materials 20:135-142.

70. Nakamura, A., M. Akai, E. Yoshida, T. Taki, and T. Watanabe. 2003. Reversed-phase HPLC determination of chlorophyll a ' and phylloquinone in Photosystem I of oxygenic photosynthetic organisms - Universal existence of one chlorophyll a ' molecule in Photosystem I. European Journal of Biochemistry 270:2446-2458.

71. Yoshida, E., A. Nakamura, and T. Watanabe. 2003. Reversed-phase HPLC determination of chlorophyll a ' and naphthoquinones in photosystem I of red algae: Existence of two menaquinone-4 molecules in photosystem I of Cyanidium caldarium. Analytical Sciences 19:1001-1005.

72. Boekema, E. J., A. Hifney, A. E. Yakushevska, M. Piotrowski, W. Keegstra, S. Berry, K. P. Michel, E. K. Pistorius, and J. Kruip. 2001. A giant chlorophyll-protein complex induced by iron defciency in cyanobacteria. Nature 412:745-748.

73. Germano, M., A. E. Yakushevska, W. Keegstra, H. J. van Gorkom, J. P. Dekker, and E. J. Boekema. 2002. Supramolecular organization of photosystem I and light- harvesting complex I in Chlamydomonas reinhardtii. Febs Letters 525:121-125.

74. Dekker, J. P., and E. J. Boekema. 2005. Supramolecular organization of thylakoid membrane proteins in green plants. Biochimica Et Biophysica Acta-Bioenergetics 1706:12-39.

75. Amunts, A., N. Nelson, and O. Drory. 2007. The structure of plant photosystem I at 3.4 angstrom resolution. Photosynthesis Research 91:PS249.

76. Gobets, B., and R. van Grondelle. 2001. Energy transfer and trapping in photosystem I. Biochimica Et Biophysica Acta-Bioenergetics 1507:80-99.

77. Bibby, T. S., J. Nield, and J. Barber. 2001. Iron deficiency induces the formation of an antenna ring around trimeric photosystem I in cyanobacteria. Nature 412:743-745.

78. Andrizhiyevskaya, E. G., D. Frolov, R. van Grondelle, and J. P. Dekker. 2004. Energy transfer and trapping in the Photosystem I complex of Synechococcus PCC 7942 and in its supercomplex with IsiA. Biochimica Et Biophysica Acta-Bioenergetics 1656:104-113.

79. Melkozernov, A. N., T. S. Bibby, S. Lin, J. Barber, and R. E. Blankenship. 2003. Time-resolved absorption and emission show that the CP43 ' antenna ring of iron-stressed Synechocystis sp PCC6803 is efficiently coupled to the photosystem I reaction center core. Biochemistry 42:3893-3903.

80. Melkozernov, A. N., J. Kargul, S. Lin, J. Barber, and R. E. Blankenship. 2005. Spectral and kinetic analysis of the energy coupling in the PSI-LHC I supercomplex from the green alga Chlamydomonas reinhardtii at 77 K. Photosynthesis Research 86:203-215.

81. Ihalainen, J. A., I. H. M. van Stokkum, K. Gibasiewicz, M. Germano, R. van Grondelle, and J. P. Dekker. 2005. Kinetics of excitation trapping in intact Photosystem I of Chlamydomonas reinhardtii and Arabidopsis thaliana. Biochimica Et Biophysica Acta-Bioenergetics 1706:267-275.

82. Boekema, E. J., P. E. Jensen, E. Schlodder, J. F. L. van Breemen, H. van Roon, H. V. Scheller, and J. P. Dekker. 2001. Green plant photosystem I binds light-harvesting complex I on one side of the complex. Biochemistry 40:1029-1036.

83. Allen, J. F. 2003. State transitions - a question of balance. Science 299:1530-1532.

84. Rochaix, J. D. 2002. Chlamydomonas, a model system for studying the assembly and dynamics of photosynthetic complexes. Febs Letters 529:34-38.

85. Wollman, F. A. 2001. State transitions reveal the dynamics and flexibility of the photosynthetic apparatus. Embo Journal 20:3623-3630.

86. Oesterhelt, C., E. Schmalzlin, J. M. Schmitt, and H. Lokstein. 2007. Regulation of photosynthesis in the unicellular acidophilic red alga Galdieria sulphuraria. Plant Journal 51:500-511.

87. Nam, H. J., J. Jeon, and S. Kim. 2009. Bioinformatic approaches for the structure and function of membrane proteins. Bmb Reports 42:697-704.

88. Whitelegge, J., F. Halgand, P. Souda, and V. Zabrouskov. 2006. Top-down mass spectrometry of integral membrane proteins. Expert Rev. Proteomics 3:585-596.

89. Whitelegge, J. P., C. B. Gundersen, and K. F. Faull. 1998. Electrospray-ionization mass spectrometry of intact intrinsic membrane proteins. Protein Science 7:1423-1430.

90. Zabrouskov, V., and J. P. Whitelegge. 2007. Increased coverage in the transmembrane domain with activated-ion electron capture dissociation for top-down Fourier-transform mass spectrometry of integral membrane proteins. Journal of Proteome Research 6:2205-2210.

91. Whitelegge, J. 2009. Confident Assignment of Post-Translational Modifications Using Top-Down Mass Spectrometry. Mol. Cell. Proteomics:S15-S15.

92. Ploscher, M., B. Granvogl, M. Zoryan, V. Reisinger, and L. A. Eichacker. 2009. Mass spectrometric characterization of membrane integral low molecular weight proteins from photosystem II in barley etioplasts. Proteomics 9:625-635.

93. Gross, W. 2000. Ecophysiology of algae living in highly acidic environments. Hydrobiologia 433:31-37.

94. Whitelegge, J. 2004. HPLC and Mass Spectrometry of Intrinsic Membrane Proteins. In HPLC of Peptides and Proteins:Methods and Protocols. M.-I. Aguilar, editor. Humana Press, New Jersey. 323-340.

95. Yakushevska, A. E., P. E. Jensen, W. Keegstra, H. van Roon, H. V. Scheller, E. J. Boekema, and J. P. Dekker. 2001. Supermolecular organization of photosystem II and its associated light-harvesting antenna in Arabidopsis thaliana. Eur. J. Biochem. 268:6020-6028.

96. Bendtsen, J. D., H. Nielsen, G. von Heijne, and S. Brunak. 2004. Improved prediction of signal peptides: SignalP 3.0. Journal of Molecular Biology 340:783-795.

97. Tohri, A., T. Suzuki, S. Okuyama, K. Kamino, A. Motoki, M. Hirano, H. Ohta, J. R. Shen, Y. Yamamoto, and I. Enami. 2002. Comparison of the structure of the extrinsic 33 kDa protein from different organisms. Plant and Cell Physiology 43:429-439.

98. Ohta, H., A. Okumura, S. Okuyama, A. Akiyama, M. Iwai, S. Yoshihara, J. R. Shen, M. Kamo, and I. Enami. 1999. Cloning, expression of the psbU gene, and functional studies of the recombinant 12-kDa protein of photosystem II from a red alga Cyanidium caldarium. Biochemical and Biophysical Research Communications 260:245-250.

99. Okumura, A., H. Ohta, Y. Inoue, and I. Enami. 2001. Identification of functional domains of the extrinsic 12 kDa protein in red algal PSII by limited proteolysis and directed mutagenesis. Plant and Cell Physiology 42:1331-1337.

100. Enami, I., M. Iwai, A. Akiyama, T. Suzuki, A. Okumura, T. Katoh, O. Tada, H. Ohta, and J. R. Shen. 2003. Comparison of binding and functional properties of two extrinsic components, Cyt c550 and a 12 kDa protein, in cyanobacterial PSII with those in red algal PSII. Plant and Cell Physiology 44:820-827.

101. Glockner, G., A. Rosenthal, and K. Valentin. 2000. The structure and gene repertoire of an ancient red algal plastid genome. Journal of Molecular Evolution 51:382-390.

102. Dobakova, M., R. Sobotka, M. Tichy, and J. Komenda. 2009. Psb28 Protein Is Involved in the Biogenesis of the Photosystem II Inner Antenna CP47 (PsbB) in the Cyanobacterium Synechocystis sp PCC 6803. Plant Physiology 149:1076-1086.

103. Babu, M. M., and K. Sankaran. 2002. DOLOP-database of bacterial lipoproteins. Bioinformatics 18:641-643.

104. Roose, J. L., and H. B. Pakrasi. 2008. The Psb27 protein facilitates manganese cluster assembly in photosystem II. Journal of Biological Chemistry 283:4044-4050.

105. Chen, H., D. Y. Zhang, J. K. Guo, H. Wu, M. F. Jin, Q. T. Lu, C. M. Lu, and L. X. Zhang. 2006. A Psb27 homologue in Arabidopsis thaliana is required for efficient repair of photodamaged photosystem II. Plant Mol.Biol. 61:567-575.

106. Granvogl, B., M. Zoryan, M. Plocher, and L. A. Eichacker. 2008. Localization of 13 one-helix integral membrane proteins in photosystem II subcomplexes. Analytical Biochemistry 383:279-288.

107. Kashino, Y., W. M. Lauber, J. A. Carroll, Q. J. Wang, J. Whitmarsh, K. Satoh, and H. B. Pakrasi. 2002. Proteomic analysis of a highly active photosystem II preparation from the cyanobacterium Synechocystis sp PCC 6803 reveals the presence of novel polypeptides. Biochemistry 41:8004-8012.

108. Gomez, S. M., J. N. Nishio, K. F. Faull, and J. P. Whitelegge. 2002. The chloroplast grana proteome defined by intact mass measurements from liquid chromatography mass spectrometry. Mol. Cell. Proteomics 1:46-59.

109. O'Connor, H. E., S. V. Ruffle, A. J. Cain, Z. Deak, I. Vass, J. H. A. Nugent, and S. Purton. 1998. The 9-kDa phosphoprotein of photosystem II. Generation and characterisation of Chlamydomonas mutants lacking

PSII-H and a site-directed mutant lacking the phosphorylation site. Biochim. Biophys. Acta-Bioenerg. 1364:63-72.

110. Kashino, Y., H. Koike, M. Yoshio, H. Egashira, M. Ikeuchi, H. B. Pakrasi, and K. Satoh. 2002. Low-molecular-mass polypeptide components of a photosystem II preparation from the thermophilic cyanobacterium Thermosynechococcus vulcanus. Plant and Cell Physiology 43:1366-1373.

111. Devitry, C., B. A. Diner, and J. L. Popot. 1991. Photosystem-II particles from Chlamydomonas-reinhardtii - purification, molecular-weight, small subunit composition, and protein-phosphorylation. Journal of Biological Chemistry 266:16614-16621.

112. Yoon, H. S., J. D. Hackett, and D. Bhattacharya. 2006. A genomic and phylogenetic perspective on endosymbiosis and algal origin. Journal of Applied Phycology 18:475-481.

113. Katoh, H., and M. Ikeuchi. 2001. Targeted disruption of psbX and biochemical characterization of photosystem II complex in the thermophilic cyanobacterium Synechococcus elongatus. Plant and Cell Physiology 42:179-188.

114. Storf, S., E. J. Stauber, M. Hippler, and V. H. R. Schmid. 2004. Proteomic analysis of the photosystem I light-harvesting antenna in tomato (Lycopersicon esculentum). Biochemistry 43:9214-9224.

115. Brini, F., M. Hanin, I. Mezghani, G. A. Berkowitz, and K. Masmoudi. 2007. Overexpression of wheat Na+/H+ antiporter TNHX1 and H+-pyrophosphatase TVP1 improve salt- and drought-stress tolerance in Arabidopsis thaliana plants. Journal of Experimental Botany 58:301-308.

116. Allakhverdiev, S. I., Y. Nishiyama, I. Suzuki, Y. Tasaka, and N. Murata. 1999. Genetic engineering of the unsaturation of fatty acids in membrane lipids alters the tolerance of Synechocystis to salt stress. Proceedings of the National Academy of Sciences of the United States of America 96:5862-5867.

117. Dernetriou, G., C. Neonaki, E. Navakoudis, and K. Kotzabasis. 2007. Salt stress impact on the molecular structure and function of the photosynthetic apparatus - The protective role of polyamines. Biochimica Et Biophysica Acta-Bioenergetics 1767:272-280.

118. Miyao, M., and N. Murata. 1983. Partial disintegration and reconstitution of the photosynthetic oxygen evolution system - binding of 24 kDa and 18 kDa polypeptides Biochimica Et Biophysica Acta 725:87-93.

119. Gilmour, D. J., M. F. Hipkins, A. N. Webber, N. R. Baker, and A. D. Boney. 1985. The effect of ionic stress on photosynthesis in Dunaliella teriolecta - chlorophyll fluorescence kinetics and spectral characteristics Planta 163:250-256.

120. Endo, T., U. Schreiber, and K. Asada. 1995. Suppression of quantum yield of photosystem II by hyperosmotic stress in *Chlamydomonas reinhardtii* Plant and Cell Physiology 36:1253-1258.

121. Satoh, K., C. M. Smith, and D. C. Fork. 1983. Effect of salinity on primary processes of photosynthesis in the red alga *Porphyra perforta* Plant Physiology 73:643-647.

122. Everard, J. D., R. Gucci, S. C. Kann, J. A. Flore, and W. H. Loescher. 1994. Gas-exchange and carbon partitioning in the leaves of celery (*Apium graveolens*) at various levels of root zone salinity Plant Physiology 106:281-292.

123. Misra, A. N., S. M. Sahu, M. Misra, N. K. Ramaswamy, and T. S. Desai. 1999. Sodium chloride salt stress induced changes in thylakoid pigment-protein complexes, photosystem II activity and thermoluminescence glow peaks. Zeitschrift Fur Naturforschung C-a Journal of Biosciences 54:640-644.

124. Parida, A. K., A. B. Das, and B. Mittra. 2003. Effects of NaCl stress on the structure, pigment complex composition, and photosynthetic activity of mangrove Bruguiera parviflora chloroplasts. Photosynthetica 41:191-200.

125. Tiwari, B. S., A. Bose, and B. Ghosh. 1997. Photosynthesis in rice under a salt stress. Photosynthetica 34:303-306.

126. Murata, N., P. S. Mohanty, H. Hayashi, and G. C. Papageorgiou. 1992. Glycinebetaine stabilizes the association of extrinsic proteins with the photosynthetic oxygen evolving complex Febs Letters 296:187-189.

127. Allakhverdiev, S. I., and N. Murata. 2008. Salt stress inhibits photosystems II and I in cyanobacteria. Photosynthesis Research 98:529-539.

128. Al-Taweel, K., T. Iwaki, Y. Yabuta, S. Shigeoka, N. Murata, and A. Wadano. 2007. A bacterial transgene for catalase protects translation of D1 protein during exposure of salt-stressed tobacco leaves to strong light. Plant Physiology 145:258-265.

129. Lu, C. M., and A. Vonshak. 1999. Characterization of PSII photochemistry in salt-adapted cells of cyanobacterium Spirulina platensis. New Phytologist 141:231-239.

130. Sudhir, P. R., D. Pogoryelov, L. Kovacs, G. Garab, and S. D. S. Murthy. 2005. The effects of salt stress on photosynthetic electron transport and thylakoid membrane proteins in the cyanobacterium Spirulina platensis. Journal of Biochemistry and Molecular Biology 38:481-485.

131. Verma, K., and P. Mohanty. 2000. Changes of the photosynthetic apparatus in Spirulina cyanobacterium by sodium stress. Zeitschrift Fur Naturforschung C-a Journal of Biosciences 55:16-22.

132. Gong, H. M., Y. L. Tang, J. Wang, X. G. Wen, L. X. Zhang, and C. M. Lu. 2008. Characterization of photosystem II in salt-stressed cyanobacterial Spirulina platensis cells. Biochimica Et Biophysica Acta-Bioenergetics 1777:488-495.

133. Takahashi, S., and N. Murata. 2008. How do environmental stresses accelerate photoinhibition? Trends in Plant Science 13:178-182.

134. Subramanyam, R., C. Jolley, D. C. Brune, P. Fromme, and A. N. Webber. 2006. Characterization of a novel photosystem I-LHCI supercomplex isolated from Chlamydomonas reinhardtii under anaerobic (State II) conditions. Febs Letters 580:233-238.

135. Towbin, H., T. Staehelin, and J. Gordon. 1979. Electrophoretic transfer of proteins from polyacrylamide gels to nitrocellulose sheets - procedure and some applications Proceedings of the National Academy of Sciences of the United States of America 76:4350-4354.

136. Cho, H. M., L. J. Mancino, and R. E. Blankenship. 1984. Light saturation curves and quantum yields in reaction centers from photosynthetic bacteria Biophysical Journal 45:455-461.

137. Bassi, R., and D. Simpson. 1987. Chlorophyll-protein complexes of barley photosystem I European Journal of Biochemistry 163:221-230.

138. Ihalainen, J. A., F. Klimmek, U. Ganeteg, I. H. M. van Stokkum, R. van Grondelle, S. Jansson, and J. P. Dekker. 2005. Excitation energy trapping in photosystem I complexes depleted in Lhca1 and Lhca4. Febs Letters 579:4787-4791.

139. Gibasiewicz, K., V. M. Ramesh, S. Lin, N. W. Woodbury, and A. N. Webber. 2002. Excitation dynamics in eukaryotic pS I from

Chlamydomonas reinhardtii CC 2696 at 10 K. Direct detection of the reaction center exciton states. Journal of Physical Chemistry B 106:6322-6330.

140. Gibasiewicz, K., V. M. Ramesh, A. N. Melkozernov, S. Lin, N. W. Woodbury, R. E. Blankenship, and A. N. Webber. 2001. Excitation dynamics in the core antenna of PSI from Chlamydomonas reinhardtii CC 2696 at room temperature. Journal of Physical Chemistry B 105:11498-11506.

141. Gibasiewicz, K., A. Szrajner, J. A. Ihalainen, M. Germano, J. P. Dekker, and R. van Grondelle. 2005. Characterization of low-energy chlorophylls in the PSI-LHCI supercomplex from Chlamydomonas reinhardtii. A site-selective fluorescence study. Journal of Physical Chemistry B 109:21180-21186.

142. Jensen, P. E., R. Bassi, E. J. Boekema, J. P. Dekker, S. Jansson, D. Leister, C. Robinson, and H. V. Scheller. 2007. Structure, function and regulation of plant photosystem I. Biochimica Et Biophysica Acta-Bioenergetics 1767:335-352.

143. Chitnis, P. R., Q. Xu, V. P. Chitnis, and R. Nechushtai. 1995. Function and organization of photosystem I - polypeptides Photosynthesis Research 45:181-181.

144. Ohoka, H., Y. Takahashi, K. Kuriyama, K. Saeki, and H. Matsubara. 1988. The protein responsible for center A/B in spinach photosystem I - isolation with iron-sulfur cluster(s) and complete sequence analysis Journal of Biochemistry 103:962-968.

145. Setif, P., N. Fischer, B. Lagoutte, H. Bottin, and J. D. Rochaix. 2002. The ferredoxin docking site of photosystem I. Biochimica Et Biophysica Acta-Bioenergetics 1555:204-209.

146. Chaoui, A., S. Mazhoudi, M. H. Ghorbal, and E. ElFerjani. 1997. Cadmium and zinc induction of lipid peroxidation and effects on antioxidant enzyme activities in bean (Phaseolus vulgaris L). Plant Science 127:139-147.

147. Sandalio, L. M., H. C. Dalurzo, M. Gomez, M. C. Romero-Puertas, and L. A. del Rio. 2001. Cadmium-induced changes in the growth and oxidative metabolism of pea plants. Journal of Experimental Botany 52:2115-2126.

148. Somashekaraiah, B. V., K. Padmaja, and A. R. K. Prasad. 1992. Phytotoxicity of cadmium ions on germinating seedlings of mung bean

(Phaseolus vulgaris) - involvement of lipid peroxides in chlorophyll degradation Physiologia Plantarum 85:85-89.

149. Jeanjean, R., A. Latifi, H. C. P. Matthijs, and M. Havaux. 2008. The PsaE subunit of photosystem I prevents light-induced formation of reduced oxygen species in the cyanobacterium Synechocystis sp PCC 6803. Biochimica Et Biophysica Acta-Bioenergetics 1777:308-316.

150. Yu, J. P., L. B. Smart, Y. S. Jung, J. Golbeck, and L. McIntosh. 1995. Absence of PsaC subunit allows assembly of photosystem-I core but prevents the binding of PsaD and PsaE in *Synechocystis sp PCC6803* Plant Molecular Biology 29:331-342.

151. Zhao, J., W. B. Snyder, U. Muhlenhoff, E. Rhiel, P. V. Warren, J. H. Golbeck, and D. A. Bryant. 1993. Cloning and characterization of the PsaE gene of the cyanobacterium Synechococcus sp PCC 7002 - characterization of a PsaE mutant and overproduction of the protein in *Escherichia coli* Molecular Microbiology 9:183-194.

152. Luneberg, J., P. Fromme, P. Jekow, and E. Schlodder. 1994. Spectroscopic characterization of PSI-core complexes from thermophilic *Synechococcus sp* - identical reoxidation kinetics of A(1) before and after removal of the iron sulfur clusters F-A and F-B Febs Letters 338:197-202.

153. Jolley, C. C., S. A. Wells, B. M. Hespenheide, M. F. Thorpe, and P. Fromme. 2006. Docking of photosystem I subunit C using a constrained geometric simulation. Journal of the American Chemical Society 128:8803-8812.

154. Chitnis, V. P., Y. S. Jung, L. Albee, J. H. Golbeck, and P. R. Chitnis. 1996. Mutational analysis of photosystem I polypeptides - Role of PsaD and the Lysyl 106 residue in the reductase activity of photosystem I. Journal of Biological Chemistry 271:11772-11780.

155. Li, N., J. D. Zhao, P. V. Warren, J. T. Warden, D. A. Bryant, and J. H. Golbeck. 1991. PsaD is required for the stable binding of PsaC to the photosystem I core protein of *Synechococcus sp PCC-6301* Biochemistry 30:7863-7872.

156. Golbeck, J. H. 1999. A comparative analysis of the spin state distribution of in vitro and in vivo mutants of PsaC - A biochemical argument for the sequence of electron transfer in Photosystem I as F-X -> F-A -> F-B -> ferredoxin/flavodoxin. Photosynthesis Research 61:107-144.

157. Vassiliev, I. R., M. L. Antonkine, and J. H. Golbeck. 2001. Iron-sulfur clusters in type I reaction centers. Biochimica Et Biophysica Acta-Bioenergetics 1507:139-160.

158. Durnford, D. G., J. A. Deane, S. Tan, G. I. McFadden, E. Gantt, and B. R. Green. 1999. A phylogenetic assessment of the eukaryotic light-harvesting antenna proteins, with implications for plastid evolution. Journal of Molecular Evolution 48:59-68.

APPENDIX A

STOCK GROWTH MEDIA SOLUTIONS FOR GALDIERIA SULPHURARIA

Appendix A. Stock media solutions for *Galdieria sulphuraria*

Trace elements solution (1 litre)
2.86 g H_3Bo_3
1.82 g $MnCl_2.4H_2O$
220 mg $ZnSO_4.7H_2O$
130 mg $(NH_4)_6\ Mo_7O_{27}.4H_2O$
80 mg $CuSO_4.5H_2O$
40 mg $NaVo_3.4H_2O$
40 mg $CoCl_2.6H_2O$

Fe-EDTA solution (100 ml)
690 mg FeSO4
930 mg EDTA
Heat it to dissolve it.

10X Growth Medium (1 litre)
1.5 mg $(NH_4)_2SO_4$
300 mg $MgSO_4.7H_2O$
300 mg KH_2PO_4
20 mg $CaCl_2.2H_2O$
1.5 ml Fe-EDTA solution
2 ml trace element solution

Adjust the pH of the medium to 2 with sulfuric acid.

APPENDIX B
MS/MS FRAGMENTATION OF LIGHT HARVESTING COMPLEXES (LHCr) OF GALDIERIA SULPHURARIA

MS/MS fragmentation of **Lhcr1** peptide (**VPPVLAHDVYVK**) by Mascot software

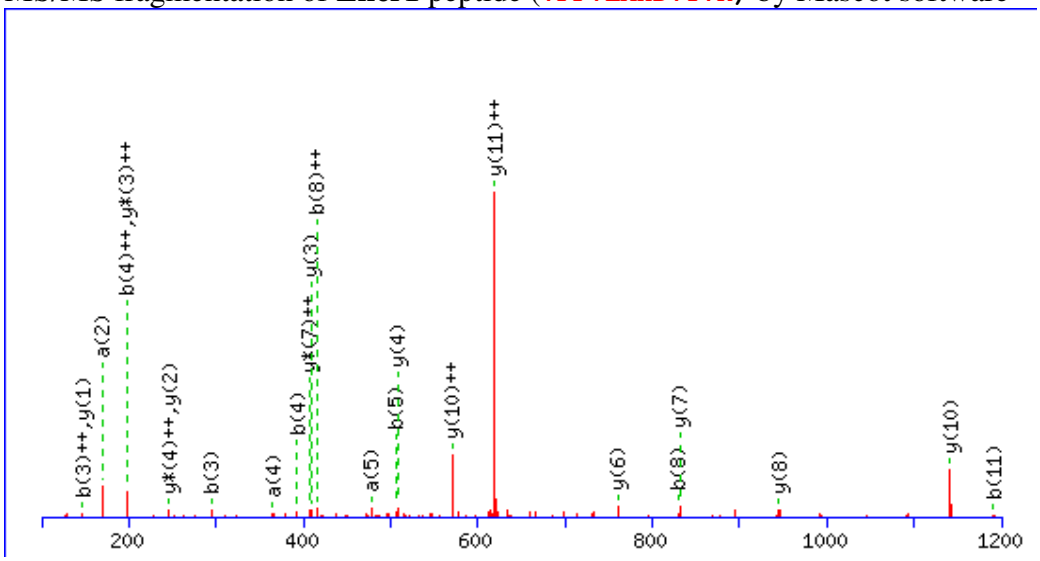

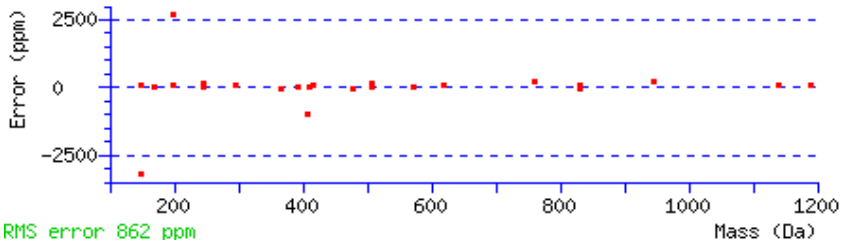

Monoisotopic mass of neutral peptide Mr(calc): 1335.7551
Ions Score: 56 Expect: 0.043
Matches (Bold Red): 25/88 fragment ions using 40 most intense peaks

#	a	a^{++}	b	b^{++}	Seq.	y	y^{++}	y*	y*$^{++}$	#
1	72.0808	36.5440	100.0757	50.5415	V					12
2	**169.1335**	85.0704	**197.1285**	99.0679	P	1237.6939	**619.3506**	1220.6674	610.8373	11
3	266.1863	133.5968	**294.1812**	**147.5942**	P	**1140.6412**	**570.8242**	1123.6146	562.3109	10
4	**365.2547**	183.1310	**393.2496**	**197.1285**	V	1043.5884	522.2978	1026.5619	513.7846	9
5	**478.3388**	239.6730	**506.3337**	253.6705	L	**944.5200**	472.7636	927.4934	464.2504	8
6	549.3759	275.1916	577.3708	289.1890	A	**831.4359**	416.2216	814.4094	**407.7083**	7
7	686.4348	343.7210	714.4297	357.7185	H	**760.3988**	380.7030	743.3723	372.1898	6
8	801.4618	401.2345	**829.4567**	**415.2320**	D	623.3399	312.1736	606.3134	303.6603	5
9	900.5302	450.7687	928.5251	464.7662	V	**508.3130**	254.6601	491.2864	**246.1468**	4
10	1063.5935	532.3004	1091.5884	546.2978	Y	**409.2445**	205.1259	392.2180	**196.6126**	3
11	1162.6619	581.8346	**1190.6568**	595.8320	V	**246.1812**	123.5942	229.1547	115.0810	2
12					K	**147.1128**	74.0600	130.0863	65.5468	1

MS/MS fragmentation of **LHCr2** peptide (**EPGYFGFDPLGLGK**) by Mascot software

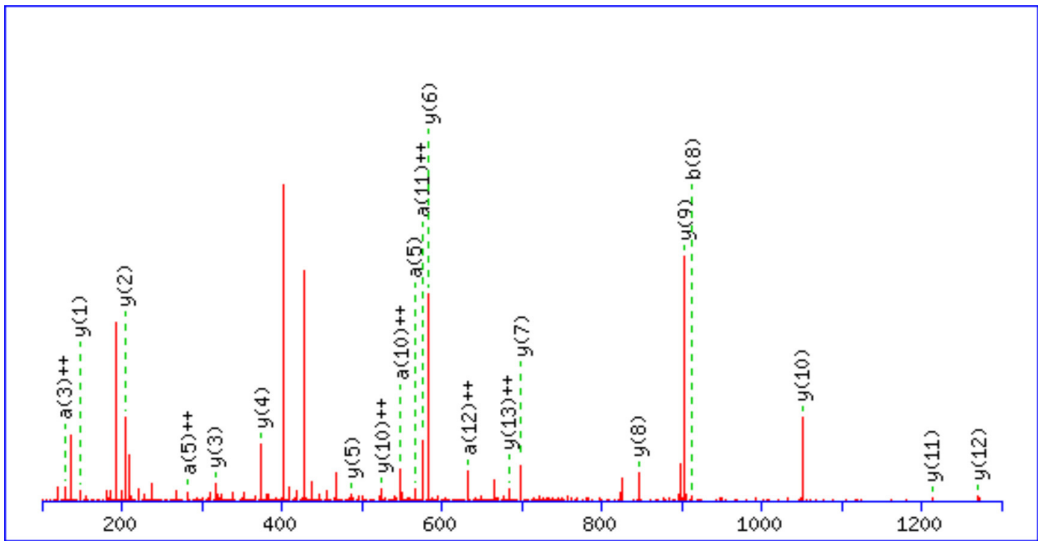

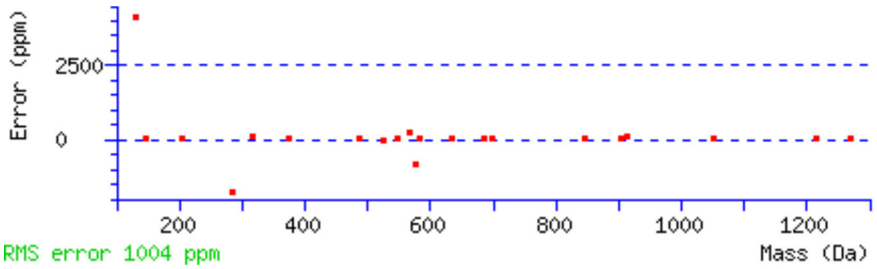

Monoisotopic mass of neutral peptide Mr(calc): 1495.7347
Fixed modifications: Carbamidomethyl (C)
Ions Score: 62 **Expect:** 0.01
Matches (Bold Red): 21/104 fragment ions using 68 most intense peaks

#	a	a^{++}	b	b^{++}	Seq.	y	y^{++}	y^*	y^{*++}	#
1	102.0550	51.5311	130.0499	65.5286	E					14
2	199.1077	100.0575	227.1026	114.0550	P	1367.6994	**684.3533**	1350.6729	675.8401	13
3	256.1292	**128.5682**	284.1241	142.5657	G	**1270.6467**	635.8270	1253.6201	627.3137	12
4	419.1925	210.0999	447.1874	224.0974	Y	**1213.6252**	607.3162	1196.5986	598.8030	11
5	**566.2609**	**283.6341**	594.2558	297.6316	F	**1050.5619**	**525.7846**	1033.5353	517.2713	10
6	623.2824	312.1448	651.2773	326.1423	G	**903.4934**	452.2504	886.4669	443.7371	9
7	770.3508	385.6790	798.3457	399.6765	F	**846.4720**	423.7396	829.4454	415.2264	8
8	885.3777	443.1925	**913.3727**	457.1900	D	**699.4036**	350.2054	682.3770	341.6921	7
9	982.4305	491.7189	1010.4254	505.7164	P	**584.3766**	292.6919	567.3501	284.1787	6
10	1095.5146	**548.2609**	1123.5095	562.2584	L	**487.3239**	244.1656	470.2973	235.6523	5
11	1152.5360	**576.7717**	1180.5310	590.7691	G	**374.2398**	187.6235	357.2132	179.1103	4
12	1265.6201	**633.3137**	1293.6150	647.3111	L	**317.2183**	159.1128	300.1918	150.5995	3
13	1322.6416	661.8244	1350.6365	675.8219	G	**204.1343**	102.5708	187.1077	94.0575	2
14					K	**147.1128**	74.0600	130.0863	65.5468	1

MS/MS fragmentation of **LHCr3** peptide (**EPGYFGFDPLGLAK**) by Mascot software

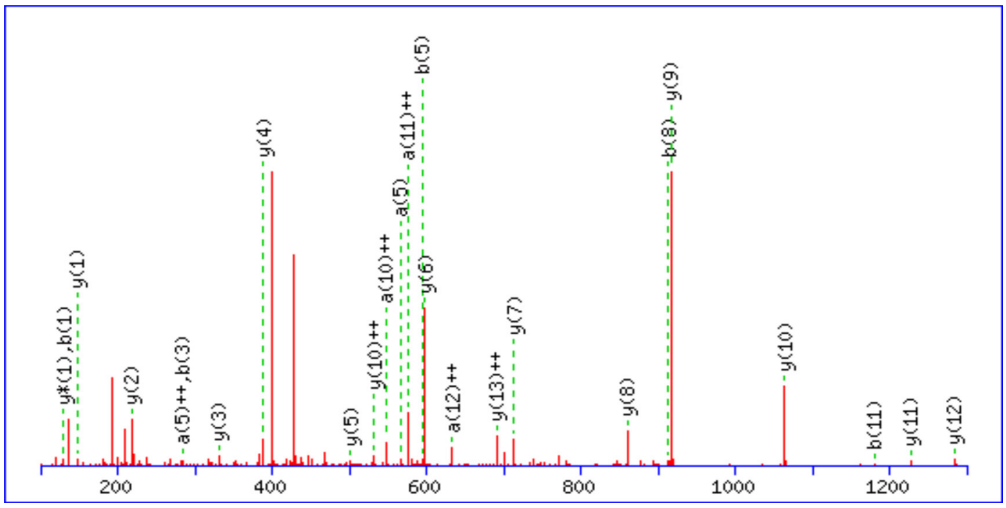

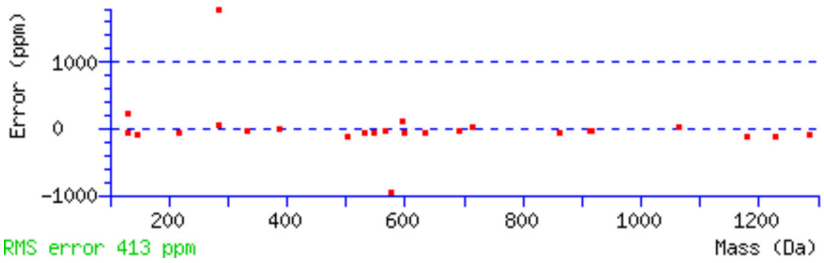

Monoisotopic mass of neutral peptide Mr(calc): 1509.7504
Fixed modifications: Carbamidomethyl (C)
Ions Score: 84 **Expect:** 6.2e-05
Matches (Bold Red): 25/104 fragment ions using 50 most intense peaks

#	a	a^{++}	b	b^{++}	Seq.	y	y^{++}	y^*	y^{*++}	#
1	102.0550	51.5311	**130.0499**	65.5286	E					14
2	199.1077	100.0575	227.1026	114.0550	P	1381.7151	**691.3612**	1364.6885	682.8479	13
3	256.1292	128.5682	**284.1241**	142.5657	G	**1284.6623**	642.8348	1267.6358	634.3215	12
4	419.1925	210.0999	447.1874	224.0974	Y	**1227.6408**	614.3241	1210.6143	605.8108	11
5	**566.2609**	**283.6341**	**594.2558**	297.6316	F	**1064.5775**	**532.7924**	1047.5510	524.2791	10
6	623.2824	312.1448	651.2773	326.1423	G	**917.5091**	459.2582	900.4825	450.7449	9
7	770.3508	385.6790	798.3457	399.6765	F	**860.4876**	430.7475	843.4611	422.2342	8
8	885.3777	443.1925	**913.3727**	457.1900	D	**713.4192**	357.2132	696.3927	348.7000	7
9	982.4305	491.7189	1010.4254	505.7164	P	**598.3923**	299.6998	581.3657	291.1865	6
10	1095.5146	**548.2609**	1123.5095	562.2584	L	**501.3395**	251.1734	484.3130	242.6601	5
11	1152.5360	**576.7717**	**1180.5310**	590.7691	G	**388.2554**	194.6314	371.2289	186.1181	4
12	1265.6201	**633.3137**	1293.6150	647.3111	L	**331.2340**	166.1206	314.2074	157.6074	3
13	1336.6572	668.8322	1364.6521	682.8297	A	**218.1499**	109.5786	201.1234	101.0653	2
14					K	**147.1128**	74.0600	**130.0863**	65.5468	1

MS/MS fragmentation of **LHCr5** peptide (**LDESMPGYAGFDPLGFSDKFDVK**) by Mascot software

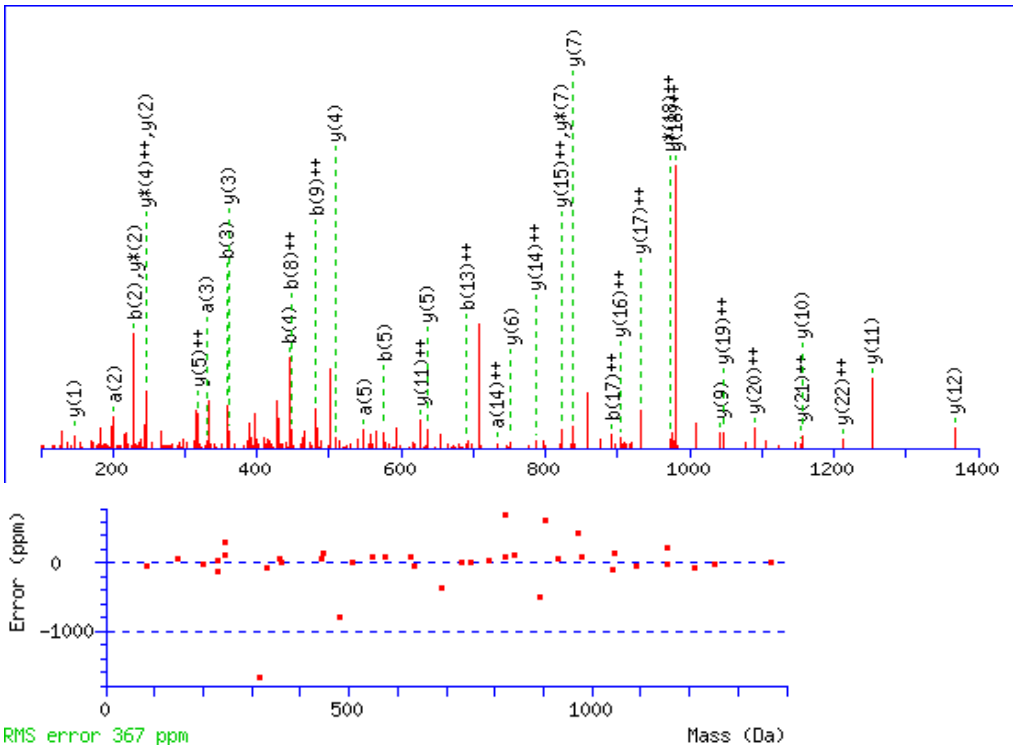

Monoisotopic mass of neutral peptide Mr(calc): 2534.1676
Ions Score: 71 **Expect:** 0.0012
Matches (Bold Red): 39/192 fragment ions using 98 most intense peaks

#	a	a^{++}	a*	a*$^{++}$	b	b^{++}	b*	b*$^{++}$	Seq.	y	y^{++}	y*	y*$^{++}$	#
1	**86.0964**	43.5519			114.0913	57.5493			L					23
2	**201.1234**	101.0653			**229.1183**	115.0628			D	2422.0908	**1211.5490**	2405.0642	1203.0357	22
3	**330.1660**	165.5866			**358.1609**	179.5841			E	2307.0638	**1154.0355**	2290.0373	1145.5223	21
4	417.1980	209.1026			**445.1929**	223.1001			S	2178.0212	**1089.5142**	2160.9947	1081.0010	20
5	**548.2385**	274.6229			**576.2334**	288.6203			M	2090.9892	**1045.9982**	2073.9626	1037.4850	19
6	645.2912	323.1493			673.2862	337.1467			P	1959.9487	**980.4780**	1942.9222	**971.9647**	18
7	702.3127	351.6600			730.3076	365.6574			G	1862.8959	**931.9516**	1845.8694	923.4383	17
8	865.3760	433.1917			893.3709	**447.1891**			Y	1805.8745	**903.4409**	1788.8479	894.9276	16
9	936.4131	468.7102			964.4081	**482.7077**			A	1642.8111	**821.9092**	1625.7846	813.3959	15
10	993.4346	497.2209			1021.4295	511.2184			G	1571.7740	**786.3907**	1554.7475	777.8774	14
11	1140.5030	570.7551			1168.4979	584.7526			F	1514.7526	757.8799	1497.7260	749.3666	13
12	1255.5300	628.2686			1283.5249	642.2661			D	**1367.6842**	684.3457	1350.6576	675.8324	12
13	1352.5827	676.7950			1380.5776	**690.7925**			P	**1252.6572**	**626.8322**	1235.6307	618.3190	11
14	1465.6668	**733.3370**			1493.6617	747.3345			L	**1155.6045**	578.3059	1138.5779	569.7926	10
15	1522.6883	761.8478			1550.6832	775.8452			G	**1042.5204**	521.7638	1025.4938	513.2506	9
16	1669.7567	835.3820			1697.7516	849.3794			F	985.4989	493.2531	968.4724	484.7398	8
17	1756.7887	878.8980			1784.7836	**892.8954**			S	**838.4305**	419.7189	**821.4040**	411.2056	7
18	1871.8156	936.4115			1899.8106	950.4089			D	**751.3985**	376.2029	734.3719	367.6896	6
19	1999.9106	1000.4589	1982.8841	991.9457	2027.9055	1014.4564	2010.8790	1005.9431	K	**636.3715**	**318.6894**	619.3450	310.1761	5
20	2146.9790	1073.9931	2129.9525	1065.4799	2174.9739	1087.9906	2157.9474	1079.4773	F	**508.2766**	254.6419	491.2500	**246.1287**	4
21	2262.0060	1131.5066	2244.9794	1122.9933	2290.0009	1145.5041	2272.9743	1136.9908	D	**361.2082**	181.1077	344.1816	172.5944	3
22	2361.0744	1181.0408	2344.0478	1172.5276	2389.0693	1195.0383	2372.0427	1186.5250	V	**246.1812**	123.5942	**229.1547**	115.0810	2
23									K	**147.1128**	74.0600	130.0863	65.5468	1

APPENDIX C

CO-AUTHORS PERMISSION FOR USE OF THE PUBLISHED ARTICLE AS CHAPTER 5

Appendix C

The co-authors of the article "Structural and functional changes of PSI-LHCI supercomplexes of *Chlamydomonas reinhardtii* cells grown under high salt conditions" published in Planta Journal (2010: 231 (4): 913-922) have granted permission for the use of article as a chapter in this dissertation.